Aus dem Institut für Physiologische Chemie der Medizinischen Fakultät der Martin-Luther-Universität Halle-Wittenberg
(Prof. Dr. Guido Posern)

Structural and functional characterization of free thiol groups in von Willebrand factor

Dissertation
Zur Erlangung des akademischen Grades
Doktor rerum medicarum (Dr. rer. medic.)

vorgelegt
der Medizinischen Fakultät
der Martin-Luther-Universität Halle-Wittenberg

von Barbara Alicja Solecka
geboren am 28.11.1984 in Szprotawa

Gutachter: 1. Prof. Dr. Rüdiger Horstkorte
2. Prof. Dr. Stephan Hinderlich
3. Prof. Dr. John Pasi

Eröffnungsdatum: 06.11.2012
Verteidigungsdatum: 17.06.2013

Abstract

The present thesis focuses on the structure and function of Willebrand factor (VWF), a blood glycoprotein involved in the primary haemostasis process. Aim of this work was identification of the function, amount and distribution of free thiol groups in plasmatic VWF. The function of free thiol groups in VWF under high physiological shear stress conditions, as well as the effect on the key interactions involved in VWF-mediated platelet adhesion ought to be investigated. Further aim was the determination of distribution of unpaired cysteine residues in VWF multimers and the exact localisation of unpaired cysteine residues within a VWF monomer, as well as the identification of possible differences in free thiol group content between in-solution and collagen type III bound VWF.

For this purpose, plasma derived VWF was derivatized with N-ethylmaleimide (NEM), to block all unpaired cysteine residues accessible on the surface of VWF in solution. The derivatization was followed by detailed structural and functional analysis using multimer analysis (MMA) and Fourier transform infrared spectroscopy (FTIR). Functional differences between the NEM-derivatized sample and the control sample were detected using an *in vitro* flow chamber system, which measures VWF-mediated platelet adhesion to collagen. The interactions with collagen type III and the platelet glycoprotein (GP) Ib receptor were investigated using surface plasmon resonance (SPR). To analyse the amount and distribution of the unpaired cysteine residues, VWF was derivatized with biotin-linked maleimide reagent. Subsequently, the derivatized cysteine residues were analyzed quantitatively by an ELISA and qualitatively by MMA with streptavidin detection. Finally the exact localization of free thiol groups was detected using matrix-assisted laser desorption/ionization mass spectrometry (MALDI-MS) after enrichment and purification of derivatized peptides.

The blockade of free thiol groups in plasma derived VWF caused substantial decrease in VWF activity with respect to mediation of platelet adhesion under physiological shear stress conditions. The decrease in platelet adhesion in the flow chamber assay was a combined effect of VWF-collagen type III and VWF-platelet GPIb receptor interaction inhibition. Free thiol groups were identified in *N*-terminal TIL and D3 domains, D4 domain and the highest amount was identified in *C*-terminal C-domains. From a total of nineteen free thiol groups, the accessibility of four was reduced after VWF binding to collagen type III, indicating new disulfide bond formation upon binding to collagen. In summary, the results suggest a significant regulatory function of free thiol groups on VWF activity in primary haemostasis.

Solecka, Barbara: “Structural and functional characterization of free thiol groups in von Willebrand factor”
Halle (Saale), Univ., Med. Fak., Diss., 80 Seiten, 2012

Referat

Die vorliegende Arbeit befasst sich mit der Funktion des von Willebrand Faktors (VWF) in der primären Hämostase. Ziel dieser Arbeit war die Identifizierung der Funktion, Mengenbestimmung und Verteilung der freien Sulfhydrylgruppen des plasmatischen VWFs. Die Funktion der freien Sulfhydrylgruppen unter sehr hohen arteriellen Scherraten, insbesondere die Interaktionen, die die Adhäsion der Thrombozyten an Kollagen III vermitteln, sollten untersucht werden. Ein weiteres Ziel dieser Arbeit war sowohl die Bestimmung der Verteilung der freien Sulfhydrylgruppen innerhalb von VWF Multimeren als auch die Ermittlung deren genauer Position im VWF Monomer. Weiterhin wurden die Unterschiede in der Zugänglichkeit freier Sulfhydrylgruppen zwischen gelöstem und Kollagen III-gebundenem VWF untersucht.

Zu diesem Zweck wurde der plasmatische VWF mit N-Ethylmaleinimid (NEM) derivatisiert, um alle freie und zugängliche Sulfhydrylgruppen zu blockieren. Die Struktur des derivatisierten VWFs wurde mittels Multimeren Analyse (MMA) und Fourier-Transformations-Infrarotspektroskopie (FTIR) detailliert untersucht. Funktionelle Unterschiede zwischen derivatisiertem und Kontroll-VWF wurden mit Hilfe eines *in vitro*-Flusskammersystem untersucht. Die Interaktionen zwischen VWF und sowohl Kollagen III als auch Thrombozyten-GPIb Rezeptor wurden mit Surface Plasmon Resonance (SPR) gemessen. Um die Menge und Verteilung der freien Sulfhydrylgruppen zu untersuchen wurde VWF mit Biotin-gekoppeltem Maleinimid Reagenz derivatisiert und sowohl qualitativ mittels MMA als auch quantitativ im ELISA untersucht. Die genaue Position der derivatisierten Sulfhydrylgruppen wurde nach der Anreicherung mittels Matrix-unterstützter Laser-Desorption/Ionisation (MALDI-MS) Massenspektrometrie untersucht.

Die Blockierung der freien Sulfhydrylgruppen in plasmatischem-VWF verursachte eine signifikante Abnahme der VWF Aktivität bezüglich der Vermittlung der Thrombozytenadhäsion an Kollagen III. Die beobachtete Aktivitätsabnahme war ein kombinierter Effekt von sowohl verminderter Bindung an Kollagen III, als auch der Inhibierung der VWF-Thrombozyten GPIb Rezeptor Interaktion. Die freien Sulfhydrylgruppen wurden in der *N*-terminalen TIL und D3 Domänen, D4 Domäne und in der größten Menge in den *C*-terminalen C-Domänen identifiziert. Vier der freien Sulfhydrylgruppen der VWF C-Domäne wurden im Kollagen III-gebundenem VWF in reduzierter Menge gefunden, was auf die Bildung neuer Disulfidbrücken hindeutet. Zusammenfassend, deuten die Ergebnisse dieser Arbeit darauf hin, dass freie Sulfhydrylgruppen auf der Oberfläche des plasmatischen VWF eine wichtige Funktion in der primären Hämostase erfüllen.

Solecka, Barbara: “Structural and functional characterization of free thiol groups in von Willebrand factor”
Halle (Saale), Univ., Med. Fak., Diss., 80 Seiten, 2012

Table of contents

List of abbreviations III

1 Introduction 1

1.1 Synthesis and structure of von Willebrand factor (VWF) 1

1.1.1 Synthesis and domain structure 1

1.1.1 Structure of VWF monomer determined by disulfide bonding 2

1.1.3 Processing and secretion 4

1.2 Physiological function of VWF 7

1.2.1 Binding of coagulation factor VIII (FVIII) 7

1.2.2 Mediation of platelet adhesion to injured endothelium 7

1.2.2 Self-association 9

1.2.3 Von Willebrand disease (VWD) 10

1.3 Redox regulation of primary haemostasis 11

1.3.1 Classification of disulfide bonds 11

1.3.2 Redox regulation in platelet function 12

2 Research objective 14

3 Materials and methods 15

3.1 Materials 15

3.1.1 Chemicals 15

3.1.2 Antibodies and conjugates 15

3.1.3 Buffer and solutions 16

3.1.4 Calibrator and controls 17

3.1.5 Biological material 17

3.1.6 Chromatography columns 18

3.1.7 Chromatography media 18

3.1.8 Proteolytic enzymes and inhibitors 18

3.1.9 Equipment 18

2.1.10 Software and server 19

3.2 Methods 20

3.2.1 NEM/MPB derivatization of VWF 20
3.2.3 VWF:Ag determination 20
3.2.4 Inspection of VWF structure after NEM-derivatization 20
3.2.5 Generation of VWF A1-domain fragments by limited proteolytic digestion 22
3.2.6 VWF-collagen type III binding, investigated by SPR 22
3.2.7 VWF-platelet GOF-GPIb receptor binding, investigated by SPR 24
3.2.8 Flow chamber assay-based experiments 24
3.2.9 Quantification and qualitative analysis of MPB incorporation into VWF 26
3.2.10 MPB labelling for MALDI-MS analysis 26
3.2.11 Digestion, purification and enrichment of MPB-labelled peptides 27
3.2.12 MALDI-MS analysis 27
4 Results 28
4.1 Effect of free thiol group derivatization on VWF structure and function 28
4.1.1 Structural analysis of the NEM-derivative of VWF 28
4.1.2 Effect of thiol group derivatization on VWF function under flow 30
4.1.3 Effect of thiol group derivatization on VWF A1-domain 36
4.2 Quantification and identification of free thiol groups in VWF 41
4.2.1 Quantification and visualisation of unpaired cysteine residues in VWF 41
4.2.2 MALDI-MS analysis of MPB derivatization products 42
4.2.3 Analysis of MPB labelled domains and peptides in VWF 45
4.3 Disulfide bond configuration and distribution of free thiol groups in VWF 55
5 Discussion 59
6 Summary 68
7 Zusammenfassung 70
8 Theses 79
Curriculum vitae ..... A
Selbstständigkeitserklärung ..... B
Acknowledgement C

List of abbreviations

ACN	Acetonitrile
ADAMTS-13	A disintegrin-like and metalloprotease with thrombospodin type 1 motif
AU	Absorbance units
CMFDA	5-chloromethylfluorescein diacetate
CK	Cystine knot
CV	Column volume
DC	Dendritic cell
DTT	Dithiothreitol
ELISA	Enzyme linked immunosorbent assay
ER	Endoplasmic reticulum
FPLC	Fast protein liquid chromatography
FTIR	Fourier transform infrared spectroscopy
FVIII	Procoagulant factor VIII
GPIbα	Glycoprotein Ibα
GSH	Glutathione
HAC	Heparin affinity chromatography
Hct	Hematocrit
HGT	High gelling temperature
HMW	High molecular weight
IAA	Iodoacetamide

IEC	Ion exchange chromatography
IMW	Intermediate molecular weight
IU	International units
LGT	Low gelling temperature
LMW	Low molecular weight
mAb	Monoclonal antibody
MIDAS	Metal ion dependent adhesion site
MMA	Multimer analysis
MPB	Maleimide-PEO2-biotin
NEM	N-ethylmaleimide
NIBSC	National institute for biological standards and control
MWCO	Molecular weight cut-off
pAb	Polyclonal antibody
PBS	Phosphate buffered saline
pd	Plasma-derived
PDI	Protein disulfide isomerase
RBC	Red blood cell
RU	Response units
SEC	Size exclusion chromatography
SPR	Surface plasmon resonance
TBS	Tris-buffered saline
TIL	Trypsin inhibitor like
TSP1	Thrombospondin 1

ULVWF	Ultra large von Willebrand factor
VWD	Von Willebrand disease
VWF	Von Willebrand factor
VWF:Ag	VWF antigen
VWF:CB	VWF collagen binding
VWF:RCo	VWF ristocetin cofactor activity
WPB	Weibel–Palade body
wt	Wild type

1 Introduction

The integrity of vascular walls and maintenance of the non-thrombotic state are assured by a physiological process called haemostasis. Haemostasis is tightly regulated, and it requires the combined activity of vascular-, platelet-, and plasmatic factors. The first step of this process leads to formation of a haemostatic plug through platelet aggregation at the site of vessel injury, and is called primary haemostasis. During the second step, known as secondary haemostasis, the primary haemostatic plug is strengthened by the formation of a fibrin net with involvement of the coagulation cascade. The objectives of this thesis are focused on the protein named von Willebrand factor (VWF), which is essential in the process of primary haemostasis at high arterial shear rates. VWF is a large, multimeric blood glycoprotein. It is named after Erik von Willebrand, a Finnish physician who studied inherited bleeding disorders affecting a family from the Åland Islands in 1924. All members of the family were suffering from mild or severe bleeding, suggesting autosomal dominant transmission. Von Willebrand distinguished the condition from other known congenital bleeding disorders including haemophilia A, but he was not able to determine whether this serious bleeding tendency was caused by a defect in platelets, blood plasma or the vasculature (Sadler, 1998). Research over the last decades on von Willebrand disease (VWD) clarified the pathophysiology of this disorder, which is caused by qualitative or quantitative abnormalities in a protein now called VWF.

1.1 Synthesis and structure of von Willebrand factor (VWF)

1.1.1 Synthesis and domain structure

VWF is synthesized by endothelial cells and megakaryocytes. The primary translation product consists of 2813 amino acids and includes a signal peptide of 22 residues, a large propeptide of 741 residues and the mature subunit of 2050 residues with a size of about 250 kDa. The VWF monomer is composed of four types of repeating functional domains according to the universal protein resource database (UniProt) (Fig. 1): Four trypsin inhibitory like (TIL) domains, four VWF D-domains, three VWF A-domains, three VWF C-domains and a *C*-terminal cystine knot-like domain (CK). VWF type-A domains are fulfilling important function by binding to the extracellular matrix (ECM) and platelet glycoprotein (GP) Ib. All three A domains have well defined structures determined by X-ray crystallography (Huizinga *et al.,* 1997; Emsley *et al.,* 1998; Zhang *et al.,* 2009); they exhibit a so-called dinucleotide-binding fold or Rossman fold structure, composed of a central β-sheet flanked by α-helices on both sites (Colombatti *et al.,* 1993; Huizinga *et al.,* 1997). Many proteins contain VWF type A-domains, including the α-subunits of leukocyte integrins, which, contrary to VWF, contain a Metal Ion Dependent Adhesion Site (MIDAS) motif (Bienkowska *et al.,* 1997).

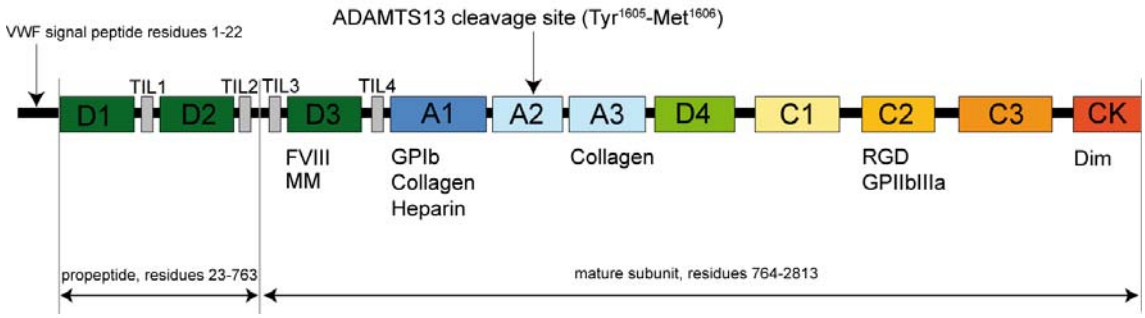

Fig. 1. Domain structure of VWF according to the universal protein resource database (UniProt). The VWF domain structure divided into signal peptide, propeptide and VWF mature subunit. The important binding sites are assigned to respective domains. Domains which are responsible for dimerization and multimerization are labelled with Dim and MM respectively. The ADAMTS-13 cleavage site is annotated.

1.1.1 Structure of VWF monomer determined by disulfide bonding

The average cysteine content of human proteins is 2.26 % (Miseta and Csutora, 2000). Therefore the much higher cysteine content of 8.3 % in VWF mature subunit may indicate structural and functional importance. Actually, the correct disulfide arrangement within one VWF monomer determines FVIII binding (Foster *et al.,* 1987), platelet GPIb receptor binding (Cruz *et al.,* 1993) and correct folding of the A2 domain (Luken *et al.,* 2010). Some cysteine residue mutants were shown to exhibit faster clearance (Schooten *et al.,* 2005). The disulfide pairing in the VWF molecule based on the experimental and theoretical homology data is summarized in Fig. 2 (Marti *et al.,* 1987; Katsumi *et al.,* 2000; Purvis *et al.,* 2007; Zhou *et al.,* 2012). The CK domain, responsible for *C*-terminal dimerization has a well defined structure and disulfide pairing pattern, which was studied by X-ray crystallography of transforming growth factor-β2 (TGF-β2), which also contains this motif (Daopin *et al.,* 1992; Schlunegger and Grutter, 1992). The architecture and disulfide bond pairing in the residual VWF D-, TIL- and VWF C-domains has been analyzed on the basis of homologous domains in a recent publication (Zhou *et al.,* 2012); the findings are based on homology of the TIL-domain of *Apis mellifera* chymotrypsin/cathepsin G inhibitor-1 (AMCI-1) (Cierpicki *et al.,* 2000) and C-domain of crossveinless 2 (Zhang *et al.,* 2008). Additionally, Zhou *et al.* (2012) found homology in large, cysteine rich regions between the original three C-domains (C1, C3, C5), which were designated C-like domains (C2, C4, C6). The C-domain structures are schematically depicted in Fig. 2 and Fig. 3A. Additionally to determined by homology disulfide bonds in the C- and C-like domains, there are several cysteines in the C1 and C2 domain without defined disulfide pairing (red boxes Fig. 33A); most likely forming an additional loop connecting C1 and C2 domains, similarly, cysteines located between C2 and C3 domains are most likely also disulfide-connected (Zhou *et al.,* 2012). Each VWF type A-domain contains an intramolecular disulfide bond, VWF-A1 and VWF-A3 domain loop structure is stabilized by these bonds, contrary to the A2 domain loop, which contains a rare vicinal disulfide bond on the C-terminal end of the loop.

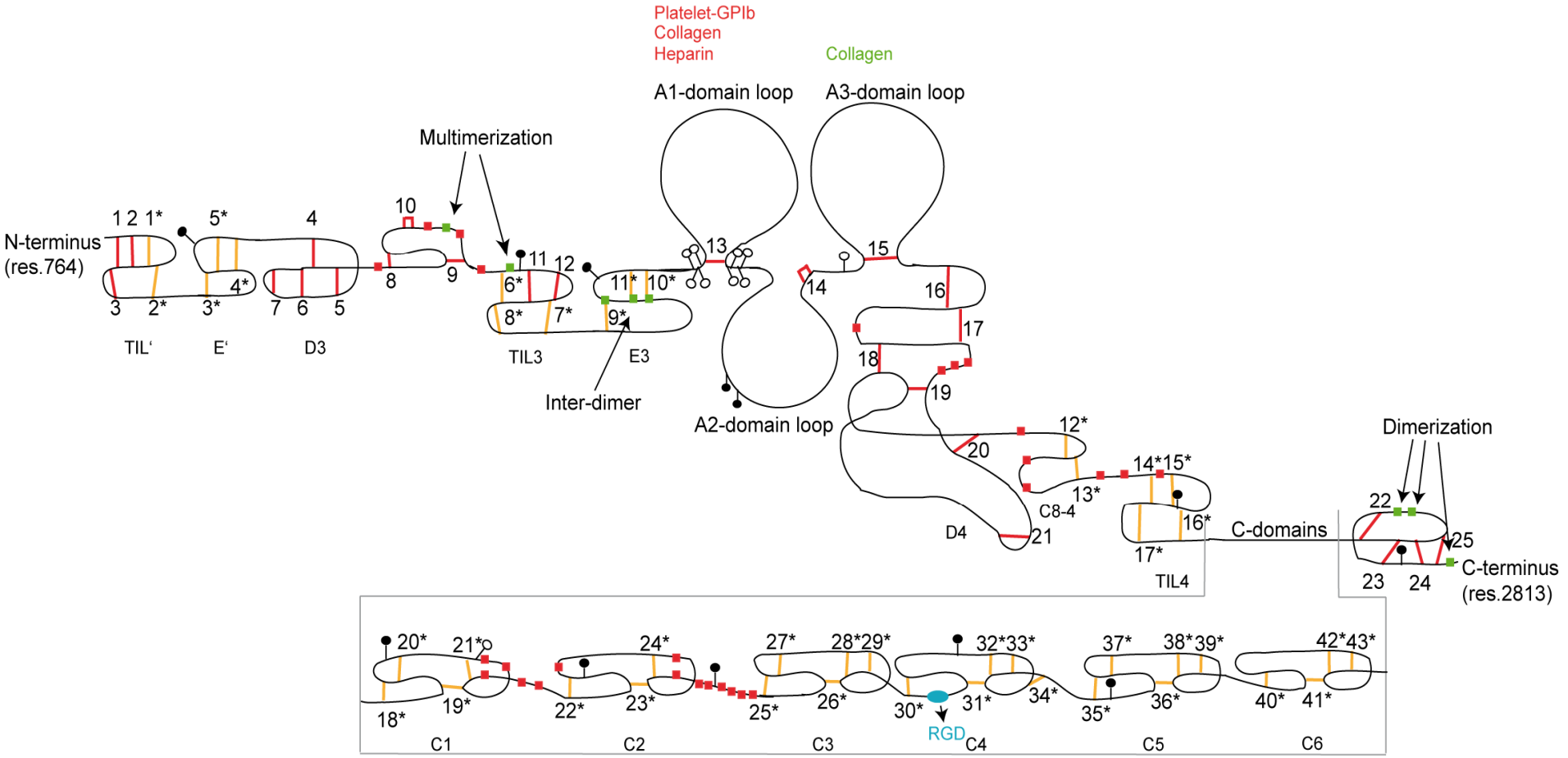

Fig. 2. Disulfide-pairing in VWF monomer. The black line represents the amino acid sequence of the VWF mature subunit. Red and orange lines represent disulfide bonds between two cysteine residues. Chemically determined disulfides are red, and disulfides determined by homology of conserved cysteine residues are orange. Cysteine residues involved in intermolecular di- and multimerization are shown as green rectangles, cysteine residues, whose pairing is not explicitly determined are shown as red rectangles. Closed and open lollipops represent *N*-linked and *O*-linked oligosaccharide side chains respectively. Domain annotation (below the given domain) is according to homology data of Zhou *et al.* (2012). Each disulfide bond is numbered (chemically determined: 1-25; determined by sequence homology: 1*-43*). Cysteine residues depicted on the diagram as single rectangle or involved in disulfide bond are listed in Tab. 1.

Tab. 1. Cysteine residues depicted in Fig. 2 and disulfide bond pairing in VWF. Cysteine residue numbers depicted in Fig. 2 as green and red rectangles are listed; cysteine residues involved in disulfide bonds in Fig. 2 are denoted under specification of the disulfide bond number.

Intermolecular multimerization (green rectangles)	Cys^{1099}, Cys^{1142}, Cys^{1222}, Cys^{1225}, Cys^{1227} Cys^{2771}, Cys^{2773}, Cys^{2811}
Pairing not explicitly determined (red rectangles)	Cys^{1046}, Cys^{1097}, Cys^{1101}, Cys^{1126}, Cys^{1919}, Cys^{1942}, Cys^{1946}, Cys^{1948}, Cys^{2131}, Cys^{2168}, Cys^{2174}, Cys^{2190}, Cys^{2199}, Cys^{2212}, Cys^{2304}, Cys^{2307}, Cys^{2325}, Cys^{2327}, Cys^{2332}, Cys^{2362}, Cys^{2375}, Cys^{2394}, Cys^{2396}, Cys^{2398} Cys^{2405}, Cys^{2418}, Cys^{2420}, Cys^{2425}
Chemically determined disulfide bonds	**1**-Cys^{767}-Cys^{808}, **2**-Cys^{776}-Cys^{804}, **3**-Cys^{810}-Cys^{821}, **4**-Cys^{867}-Cys^{995}, **5**-Cys^{889}-Cys^{1031}, **6**-Cys^{898}-Cys^{993}, **7**-Cys^{914}-Cys^{921}, **8**-Cys^{1060}-Cys^{1084}, **9**-Cys^{1071}-Cys^{1111}, **10**-Cys^{1089}-Cys^{1091}, **11**-Cys^{1149}-Cys^{1169}, **12**-Cys^{1153}-Cys^{1165}, **13**-Cys^{1272}-Cys^{1458}, **14**-Cys^{1669}-Cys^{1670}, **15**-Cys^{1686}-Cys^{1872}, **16**-Cys^{1879}-Cys^{1904}, **17**-Cys^{1899}-$Cys^{1940/1942}$, **18**-Cys^{1927}-Cys^{2088}, **19**-Cys^{1950}-Cys^{2085}, **20**-Cys^{1972}-Cys^{2123}, **21**-Cys^{1993}-Cys^{2001}, **22**-Cys^{2724}-Cys^{2774}, **23**-Cys^{2739}-Cys^{2788}, **24**-Cys^{2750}-Cys^{2804}, **25**-Cys^{2754}-Cys^{2806}
Disulfide bonds determined by sequence homology	**1***-Cys^{788}-Cys^{799}, **2***-Cys^{792}-Cys^{827}, **3***-Cys^{829}-Cys^{851}, **4***-Cys^{846}-Cys^{863}, **5***-Cys^{849}-Cys^{858}, **6***-Cys^{1130}-Cys^{1173}, **7***-Cys^{1157}-Cys^{1196}, **8***-Cys^{1177}-Cys^{1190}, **9***-Cys^{1199}-Cys^{1227}, **10***-Cys^{1222}-Cys^{1237}, **11***-Cys^{1225}-Cys^{1234}, **12***-Cys^{2139}-Cys^{2163}, **13***-Cys^{2150}-Cys^{2184}, **14***-Cys^{2203}-Cys^{2235}, **15***-Cys^{2216}-Cys^{2227}, **16***-Cys^{2220}-Cys^{2254}, **17***-Cys^{2237}-Cys^{2248}, **18***-Cys^{2257}-Cys^{2283}, **19***-Cys^{2278}-Cys^{2319}, **20***-Cys^{2281}-Cys^{2291}, **21***-Cys^{2296}-Cys^{2320}, **22***-Cys^{2340}-Cys^{2360}, **23***-Cys^{2354}-Cys^{2388}, **24***-Cys^{2367}-Cys^{2389}, **25***-Cys^{2431}-Cys^{2453}, **26***-Cys^{2448}-Cys^{2490}, **27***-Cys^{2451}-Cys^{2468}, **28***-Cys^{2473}-Cys^{2491}, **29***-Cys^{2477}-Cys^{2494}, **30***-Cys^{2499}-Cys^{2533}, **31***-Cys^{2528}-Cys^{2570}, **32***-Cys^{2549}-Cys^{2571}, **33***-Cys^{2557}-Cys^{2574}, **34***-Cys^{2565}-Cys^{2576}, **35***-Cys^{2582}-Cys^{2605}, **36***-Cys^{2600}-Cys^{2640}, **37***-Cys^{2603}-Cys^{2619}, **38***-Cys^{2624}-Cys^{2641}, **39***-Cys^{2627}-Cys^{2644}, **40***-Cys^{2649}-Cys^{2676}, **41***-Cys^{2671}-Cys^{2715}, **42***-Cys^{2693}-Cys^{2716}, **43***-Cys^{2701}-Cys2719
Disulfide bonds chemically determined, but contrary to homology data (not depicted)	Cys^{1126}-Cys^{1130}, Cys^{1206}-Cys^{1199}, Cys^{1234}-Cys^{1237}

1.1.3 Processing and secretion

After synthesis, the pro-VWF (mature subunit + propeptide) molecules are transported into the endoplasmic reticulum (ER) and dimerize through disulfide bonds near their carboxyl termini. After dimerization in the ER, VWF dimers are transported to the Golgi to form large multimers via *N*-terminal disulfide bonds (Sadler, 1998). The formation of disulfide bonds between multimers requires acidic pH and the presence of the VWF propeptide (Mayadas and Wagner, 1989). In the Golgi, proteolytic removal of the propeptide and extensive glycosylation also takes place (12 *N*-linked and 10 *O*-linked oligosaccharides). Interestingly, disulfide bonds

forming dimers are very stable in opposite to disulfides forming multimers, which are extremely unstable and are rapidly reduced in the presence of low concentrations of reducing agents like dithiothreitol (DTT) or glutathione (GSH) (Ruggeri and Zimmerman, 1980; Li *et al.,* 2008). About 95 % of synthesized VWF molecules are constitutively secreted basolaterally to the subendothelial matrix and apically to the vascular lumen. The remainder is stored either in α-granules of platelets or in characteristic organelles of endothelial cells called Weibel-Palade bodies (WPB) (Schmugge *et al.,* 2003). WPBs are large cigar-shaped secretory organelles, composed almost entirely of VWF, where the multimerization process continues and VWF multimers are released upon simulation (Metcalf *et al.,* 2008). VWF multimers found in storage organelles are therefore rich in ultra-large (ULVWF) forms in contrast to plasma VWF multimers. Those large multimers are hyperactive in binding platelets, resulting in spontaneous platelets aggregation. Therefore, once the ULVWF multimers are released into plasma, they are rapidly cleaved by a specific protease named ADAMTS-13 (a disintegrin-like and metalloprotease with thrombospodin type 1 motif) (Dong, 2005). This metalloprotease cleaves the Tyr^{1605}–Met^{1606} bond in the VWF A2-domain in healthy individuals. Lack of ADAMTS-13 or impaired function of this enzyme leads to a life-threatening disease called thrombotic thrombocytopenic purpura (TTP). Multimers circulating in blood are not sensitive to ADAMTS-13 cleavage until the scissile bond is exposed by conformational transition of VWF caused by shear stress and/or binding to vascular endothelium. *In vitro,* VWF multimers are cleaved either when rheological forces are applied or in the presence of denaturants (Tsai, 1996). In consequence of VWF cleavage on EC surface after release, VWF circulates in blood as different molecular weight multimers ranging from low (≤ 5-mers, LMW) to intermediate (6- to 10-mers, IMW) and high (> 10-mers, HMW) species. The normal ranges for each category of multimers equal for LMW: 28-45 %; for IMW: 34-45 % and for HMW: 20-36 % (Veyradier *et al.,* 2001). The smallest form of VWF found in blood plasma is a dimer; the structure of plasmatic VWF is depicted in Fig. 3 and the characteristic multimeric pattern is shown in Fig. 4. Additionally, another mechanism may be involved in reducing the VWF multimer size. VWF could be reduced *in vitro* by another plasma protein, thrombospondin-1 (TSP1). The concentration of TSP1 in human plasma is 0.02 μg/ml; additionally platelet α-granules contain TSP1 and release it after activation. Actually, TTP patients have lower TSP1/VWF molar ratio than healthy individuals (Xie *et al.,* 2000; Xie *et al.,* 2001). Although the VWF reduction by TSP1 occurs *in vitro*, mice lacking TSP1 posses VWF multimers of higher sizes than TSP1-positive mice, thus indicating more complicated mechanisms *in vivo*, involving an inhibition of ADAMTS-13. However, the elevated TSP1 concentration resulting from platelet activation and lysis reduces multimer size of VWF released from platelet α-granules (Pimanda *et al.,* 2004).

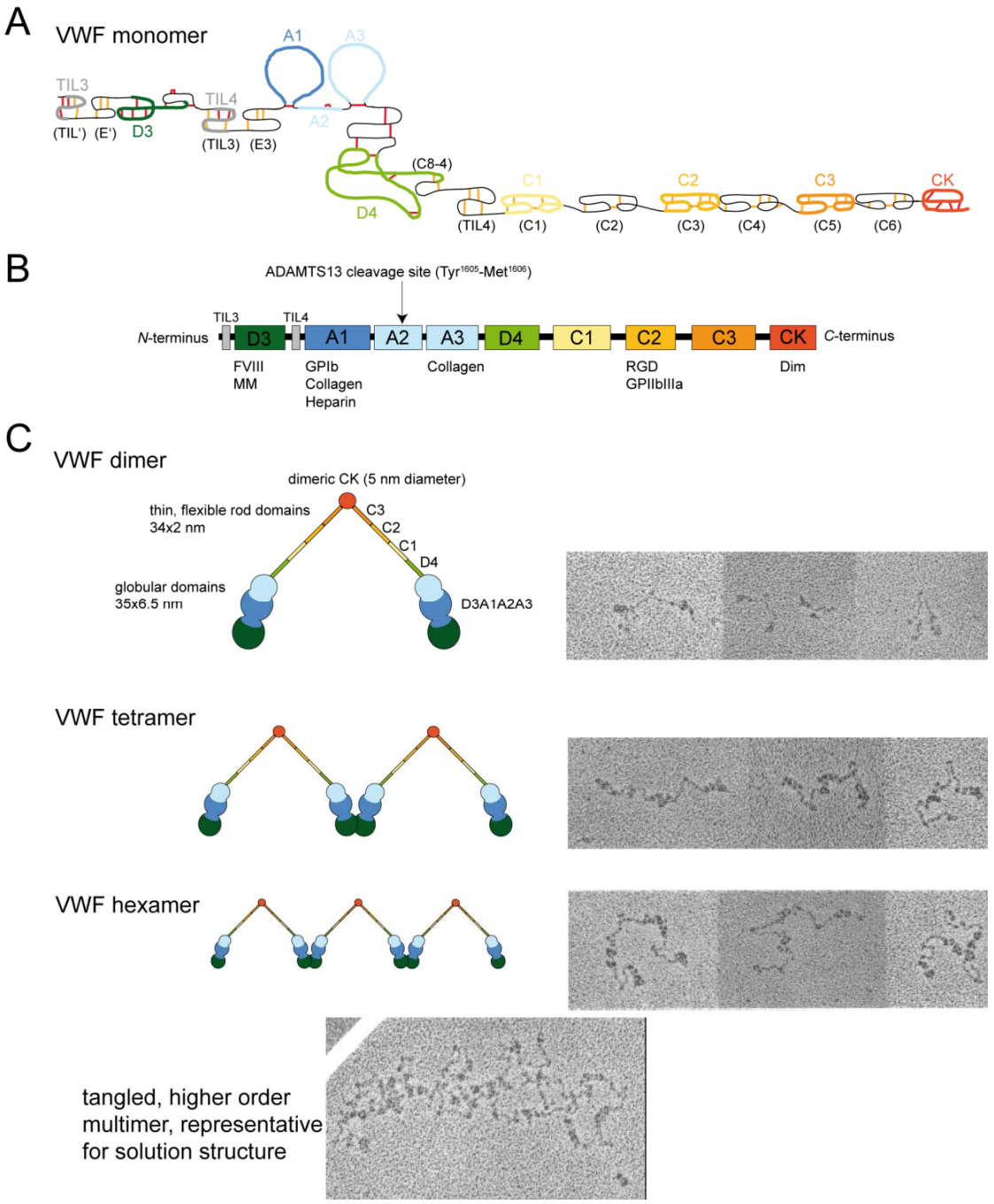

Fig. 3. Domain composition and structure of VWF in solution. (A) The VWF structure resulting from disulfide bond pairing in Fig. 2, additionally chain fragments assigned to domains according to UniProt are coloured and labelled with the respective domain name and colour. The domain annotation according to homology data is shown in brackets. (B) The VWF domain structure according to UniProt with the important binding sites is depicted. Domains which are responsible for dimerization and multimerization are labelled with Dim and MM, respectively. The ADAMTS-13 cleavage site is annotated. (C) The structure of the dimer, tetramer, hexamer and higher order multimer is depicted according to Fowler *et al.* 1985 and Sadler 1998; Electron micrographs are adopted from (Fowler *et al.*, 1985).

Aside from regulation of VWF multimer size in blood, preventing spontaneous aggregation of VWF with platelets, cleavage by ADAMTS-13 is also responsible for the characteristic triplet structure of plasma VWF. ADAMTS-13 cleaves within the A2 domain creating asymmetric VWF multimers. Some of the fragments have one extra 140 kDa *N*-

terminal fragment and some lack one *N*-terminal fragment with respect to the corresponding multimer they have been cleaved off (Furlan *et al.,* 1993; Fischer *et al.,* 1998) (Fig. 4).

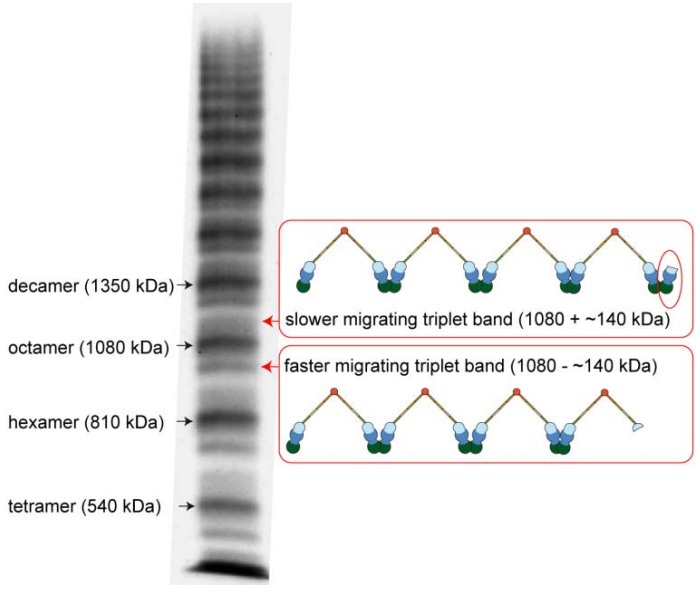

Fig. 4. Characteristic multimeric pattern of plasma VWF visible after non-reducing agarose gel electrophoresis. On the left hand side the characteristic plasma VWF multimer pattern is depicted (top-HMW multimers, bottom-LMW multimers). The structures of octamer satellite bands resulting from ADAMTS-13 cleavage in the A2 domain is depicted on the right hand side of the image.

1.2 Physiological function of VWF

1.2.1 Binding of coagulation factor VIII (FVIII)

The first important function of VWF is the binding of procoagulant factor VIII (FVIII), which is not active or lacks in patients with haemophilia A. FVIII circulates in blood in complex with VWF. VWF protects FVIII from activated protein C-catalyzed inactivation (Koedam *et al.,* 1988) and prevents activation of FVIII by activated factor X (Koedam *et al.,* 1990; Koppelman *et al.,* 1994). As a result, the FVIII half-life in the absence of VWF is drastically shortened, from about 12 h to 2 h.

1.2.2 Mediation of platelet adhesion to injured endothelium

The second important function of VWF is mediation of platelet adhesion to injured endothelium. VWF binds to constituents of connective tissue and platelet surface glycoproteins, thereby mediating platelet adhesion and aggregation at sites of vascular injury, especially under conditions of high fluid shear rates found in the normal arterial circulation. Platelets are anucleated cells involved in the haemostatic repair of damaged vasculature. They are circulating in blood and do not interact with normal vessel wall. When ECM components are exposed, they adhere, activate and aggregate. Distinct mechanisms of platelet adhesion are characteristic for different shear rates. At very low shear rates platelets can directly adhere to exposed ECM and above a threshold shear rate of 500 to 800 s^{-1} in human blood, VWF is essential for platelet

adhesion at the sites of injury. Under this conditions only the interaction between VWF A1-domain and platelet GPIbα has a sufficiently high on-rate to initiate platelet adhesion (Ruggeri, 2002; Ruggeri and Mendolicchio, 2007). In the absence of injury, VWF circulates in blood and does not bind platelets, whereas bound to constituent of extracellular matrix it mediates platelet adhesion via interaction between VWF A1 and platelet GPIb. The mechanism which triggers the transition of VWF from inactive to active has not been identified yet. There are two theoretical models which could explain this process; an "allosteric model" which describes two conformations of VWF: (i) an inactive conformation which does not bind platelets because of a shielding effect caused by the globular 'ball-of-yarn'-structure hiding the GPIbα binding site and (ii) a high affinity state conformation which is induced after binding to connective tissue. Another hypothesis is an "entropic model", which assumes that immobilized VWF restricts the motion of multiple binding sites, and thereby distributes them favourably to bind several GPIbα receptors (Sadler, 1998).

The main VWF-binding ligands in ECM are collagens type I and III in deeper layers of the vessel wall, and microfibrillar collagen type VI in the subendothelial matrix (Sixma *et al.,* 1995; Li *et al.,* 2002). VWF contains two functional binding sites for collagen type III located within its A1 and A3 domain. The major binding site for collagen type III is located within the A3 domain. The function of the A1 domain with respect collagen binding has not yet been fully understood. Controversial results have been published confirming its important function in collagen type III binding (Baronciani *et al.,* 2005) and the ability of A3-independent function (Bonnefoy *et al.,* 2006; Morales *et al.,* 2006), whereas other studies reveal that the A3 domain is absolutely essential in collagen type III-binding (Lankhof *et al.,* 1996). It has been shown, that both domains compete with each other in collagen type III binding, because their binding sites on collagen are overlapping (Pareti *et al.,* 1987). Additionally, VWF binding to collagen could be blocked by a peptide, which binds one of the VWF C-domains (Szanto *et al.,* 2009), suggesting a further regulatory mechanism.

As introduced above, immobilization and/or high shear stress triggers activation of the VWF molecule, which, when activated, is able to bind platelet GPIb receptor. The binding site for the platelet receptor GPIb resides in the A1 domain of VWF (Andrews *et al.,* 1989b). This binding site is cryptic in inactive conformation of VWF and becomes exposed after binding to subendothelial matrix and shear stress exposure. The VWF A1 – GPIbα-binding is most important to promote platelet adhesion, however - because of the fast dissociation rate of this interaction - cannot support irreversible adhesion. The result of this interaction is activation-independent platelet tethering to thrombogenic surfaces, which leads to a slow movement of tethered platelets in the direction of flow. The presence of additional structures signifying a serious lesion is the trigger for irreversible platelet adhesion and aggregation. These additional interactions exhibit a slower rate of bond formation, but the formed bonds are stable. Notable in

this regard is the role of the activated platelet integrin αIIbβ3 (GPIIbIIIa), which binds to the Arg-Gly-Asp (RGD) sequence in VWF, or to collagen and its receptors (Bonnefoy *et al.,* 2006; Ruggeri and Mendolicchio, 2007). The mechanism of platelet adhesion and aggregation is displayed in Fig. 5. Both interactions, VWF-GPIb and VWF-GPIIbIIIa are necessary for stable platelet adhesion to collagen type III under flow conditions. Whereas the GPIb interaction is required for initial platelet adhesion, the GPIIbIIIa interaction is required for firm adhesion which is able to resist high shear stress, and leads to platelet spreading (Lankhof *et al.,* 1995; Savage *et al.*, 2002) and plug formation.

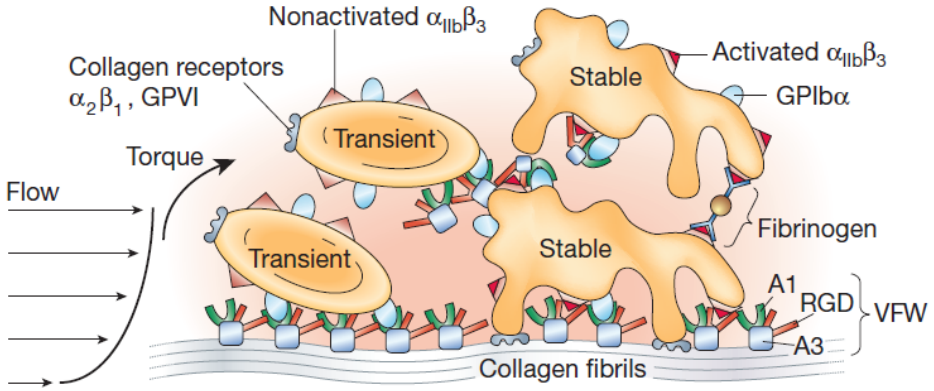

Fig. 5. Mechanism of platelet adhesion and aggregation under high shear stress. Tethering to immobilized VWF allows close contact between circulating platelets and thrombogenic surface or adherent platelets that have been activated. Secondary interactions with collagen in the extracellular matrix (adhesion), or fibrinogen or fibrin bound to activated platelets (aggregation), stabilize these interactions. Figure was obtained from (Ruggeri, 2002).

Immobilized fibrinogen is also a substrate for platelet arrest under flow conditions. In experimental perfusion systems, using whole blood, platelets adhere in a shear-rate limited fashion to purified fibrinogen and fibrin, which are progressively less efficient up to a limit of 1,000 to 2,000 s^{-1} shear rate. Additionally, fibrinogen stabilizes formed clots by supporting platelet aggregation on collagen fibrils. Without fibrinogen, thrombi mediated by VWF grew rapidly at high shear rate but were unstable. In the presence of both, VWF and fibrinogen, thrombi grew more slowly but were found to be stable (Ruggeri and Mendolicchio, 2007). Fibronectin has also supporting role in platelet arrest to collagen I and III under lower shear rate (800-1,300 s^{-1}) conditions. In the study of Houdijk *et al.,* (1985) the combined action of VWF and fibronectin was required for maximal platelet-subendothelium interaction and spreading, whereas fibronectin alone was not able to mediate platelet adhesion.

1.2.2 Self-association

Another interesting attribute of VWF is its self-association, which has been described by several research groups. However, the suggested underlying mechanism, the stability of formed VWF-aggregates and the shear stress requirement to induce this interaction varied from study to study. Perfusion studies with physiological shear stress and VWF concentrations

showed that platelets are not able to adhere to a surface coated with VWF lacking the A1 domain, but when plasma-free blood containing wild type-VWF (wt-VWF) was perfused over this surface, the platelet adhesion could be fully restored. The same surface perfused again with plasma free blood without wt-VWF showed substantial decrease in platelet adhesion (Savage *et al.,* 2002). Indicating that soluble VWF in the perfused blood can rapidly interact with immobilized VWF and mediate the surface capture of platelets, but this association is also rapidly reversible. Static light scattering studies showed that hydrodynamic forces can induce VWF self-association in suspension. After application of very high shear rates (2155 and 6000s^{-1}) VWF formed higher multimer weight multimers compared to non-sheared VWF, this aggregates were stable until dissolution by the addition of SDS (Shankaran *et al.,* 2003). Another study which observed reversible non-covalent interaction described self-association in a static ELISA assay, which involves all VWF domains (Ulrichts *et al.,* 2005). Further study described plasma-derived filamentous network formation which was formed on collagen I after perfusion with VWF concentrations five times higher than physiological and under high shear stress (Barg *et al.,* 2007).

An example of stable, covalent association of VWF multimers to newly released ULVWF multimers attached to endothelial cells is described in the study of Li *et al*., (2008). The stable, covalent association of VWF was further supported by the study of Ganderton *et al*., (2011). This group analyzed the *C*-terminal region of VWF, and identified multiple cysteine residues, which were reduced to different level. After analysis of the cysteine pairing in homologous *C*-domain of crossveinless 2, Ganderton *et al*. developed a model of lateral self-association of VWF mediated by new disulfide forming between *C*-domains of different multimers.

Different study revealed that plasma VWF contains free thiol groups in the D3 and C-domain and that these thiol groups are forming disulfide bonds after applications of very high physiological (50 dynes/cm^2) or pathological shear stress (100 dynes/cm^2) in a cone-and-plate viscometer, whereas it was not differentiated whether new disulfide bonds were formed intra- or inter-molecular. Moreover, the blockade of this shear induced thiol disulfide exchange in the VWF molecule with thiol reactive maleimide reagent inhibited VWF binding to platelets (Choi *et al.,* 2007).

1.2.3 Von Willebrand disease (VWD)

VWD is a heterogeneous bleeding disorder with symptoms ranging from mild episodes - like gum bleeding - to life-threatening visceral bleeding. It is the most common congenital bleeding disorder, with a prevalence ranging between 1 per 10000 individuals to 1.3 % depending on the type (Kessler, 2007). The International Society on Thrombosis and Haemostasis classified VWD into three major categories: Type 1, caused by quantitative deficiency of functionally normal VWF, with an autosomal dominant inheritance and relatively

mild symptoms. Type 2, caused by qualitative abnormalities in VWF structure. This type is independent on VWF quantity and can be inherited either dominant or recessive. Type 2 VWD is further divided into four variants (2A, 2B, 2M, and 2N) based upon details in the phenotype. In VWD 2A the lack of HMW multimers (>10) parallels with a decrease in platelet adhesion. In classical type 2A the lack of large multimers is caused by increased susceptibility to ADAMTS-13 cleavage. VWD type 2B is characterized by higher affinity of VWF multimers to GPIb and subsequent faster VWF proteolysis by ADAMTS-13. Type 2M is characterized by the presence of all multimers, but the triplet structure shows a decrease or even absence of flanking subbands and it is overlaid with amorphous material (Budde *et al.,* 2006). Most type 2M mutations are located in the A1 domain of VWF, which causes defective binding to platelet-GPIbα receptor, whereas type 2N mutations affect the VWF FVIII-binding and subsequently reduce FVIII stabilization in blood. Type 3, complete deficiency of VWF, is inherited in recessive manner. This most severe subtype is caused by the absence of plasmatic, tissue and cellular VWF because of a frame shift, a deletion and/or a nonsense mutation in the *VWF* gene on chromosome 12.

1.3 Redox regulation of primary haemostasis

The process of primary haemostasis is tightly regulated and part of the regulatory mechanism involves thiol-disulfide exchange reactions. Those reactions are mediated by oxidoreductases present in plasma as well as on the platelet-surface (Essex, 2009). Targets of such oxidoreductases are so-called allosteric disulfide bonds, which are 'labile', i.e. very susceptible to any kind of reduction. Changes in the redox state of such disulfide bonds provoke structural changes within the protein, often stabilizing the active protein conformation.

1.3.1 Classification of disulfide bonds

Disulfide bonds can be classified into three groups, so called structural, catalytic and allosteric disulfide bonds. Apart from the distinct function in protein, each group displays a typical disulfide bond configuration defined by the central three torsion angles (χ_2, χ_3 and $\chi_{2'}$). Those three fundamental disulfide bond configurations formed by the bond are spiral, hook and staple (Fig. 6). The analysis of all five torsion angles (χ_1, χ_2, χ_3, $\chi_{2'}$, $\chi_{1'}$) defined by the bond yields 20 subtypes of disulfide bond configuration; if the χ_3 angle is negative bond is left hand (LH), if positive bond is right hand (RH); the χ_1 and $\chi_{1'}$ define the +, - or +/- signs in front of bond designation. Additionally each bond can be characterized by the dihedral strain energy (DSE). DSE describes the strain energy of the bond and is high for bonds held in an energetically unfavourable conformation. Structural disulfides, being the most common group, stabilize the tertiary and quaternary structure of the proteins and are stable because of the characteristic spiral (most common –LHSpiral) conformation and low DSE. Two other groups, namely catalytic and allosteric disulfide bonds, are known to alternate between oxidized and

reduced state in mature protein. The DSE of those bonds is higher when compared to the structural disulfides, so they are easily reduced, and they exhibit rare hook (nearly all are +/-RHHook) and staple (nearly all are –RHStaple) conformation respectively. Additionally, the allosteric disulfide bonds are characterized by a short distance between C_α of cysteines forming the bond; whereas the catalytic disulfides most often occur within the CGXC motif (Schmidt *et al.,* 2006; Azimi *et al.,* 2011).

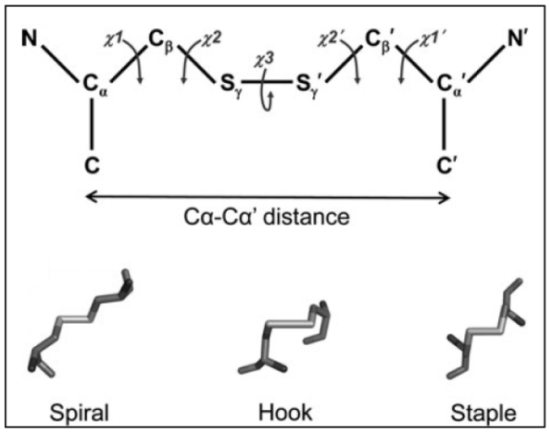

Fig. 6. Configuration of the three types of disulfide bonds. Three fundamental disulfide bond configurations based on the χ_2, χ_3 and $\chi_{2'}$ torsional angle analysis. Figure obtained from (Azimi *et al.,* 2011).

1.3.2 Redox regulation in platelet function

Platelet function is regulated in part by thiol-disulfide balance. For example, reduced glutathione and cysteine inhibit platelet aggregation induced by several agonists while dithiothreitol and β-mercaptoethanol promote aggregation (Thomas *et al.,* 1986). The platelet plasma membrane contains protein disulfide isomerase (PDI) (Chen *et al.,* 1995; Essex *et al.,* 1995), an oxidoreductase responsible for formation, reduction and isomerization of disulfide bonds. PDI contains two active sites with closely spaced cysteines in a consensus sequence CGHC. Activated platelets expose 440 % more reduced thiols than resting platelets on the outer surface of their plasma membrane. Among proteins exposing those reduced thiols on the platelet membrane are active site disulfides in PDI and platelet GPIb receptor. Moreover, those two proteins were found in close proximity on plasma membrane, indicating that PDI regulates GPIb receptor function (Burgess *et al.,* 2000). Another platelet receptor, which is regulated by thiol-disulfide exchange, is the αIIbβ3 integrin (Yan and Smith, 2000). Additionally, endothelial cells secrete PDI which is required for thrombus formation *in vivo* (Jasuja *et al.,* 2010). Among adhesive proteins which are either secreted from platelet α-granules or circulating in plasma, several expose free thiol groups; among them are thrombospondin-1 (TSP1), vitronectin, fibronectin and VWF (Essex, 2009). Those proteins can potentially be also involved in redox reactions, low molecular weight thiols present in plasma (e.g. glutathione) regulate these

processes by converting redox sensitive disulfide bonds to thiols and by providing an appropriate redox potential.

Interestingly, the rare vicinal cysteines in CGXC consensus sequence are also present in the VWF, each VWF D-domain and VWF C-domain contains one CGXC motif. Though the oxidoreductase activity of this sites in VWF mature subunit has never been directly proven, the VWF pro-peptide consisting of D1- and D2-domain have been shown to catalyze the multimerization of VWF. Moreover, the vicinal cysteines have been shown to play an important role in this regard, as the disruption of this consensus sequence (CGLC) by inserting an additional glycine (CGGLC) resulted in abrogation of the VWF multimerization process (Mayadas and Wagner, 1992).

2 Research objective

VWF contains unusually high amount of cysteine. Disulfide bonds significantly contribute to the correct conformation of VWF, which in turn is a prerequisite for proper VWF function. Disulfide pairing stabilizes the VWF structure on the level of a single monomer as well as its complex multimeric structure. Beside proteolytic cleavage, the size distribution of VWF multimers is partly controlled by thiol-disulfide exchange reactions in plasma. The fact that plasma VWF exposes unpaired cysteine thiols on its surface and the differential susceptibility of VWF disulfide bonds to reduction suggests a regulatory role in addition to the structural function. In fact the thiol-disulfide exchange is one of the regulators of primary haemostasis process. The unpaired thiol groups identified on the surface of plasmatic VWF have been largely assigned to facilitate the so-called self-association, a process, which has been shown to result in covalently linked, ultralarge VWF networks under certain conditions. However, the differentiation whether the function of free thiol groups is limited to the self-association or modulates VWF activity under physiological conditions is not clear

Objective of the present study was to investigate, whether free thiol groups of plasma VWF regulate the physiological VWF function under normal arterial shear stress conditions, and to elucidate, which mechanisms are involved in this regulation. For this purpose plasma derived VWF was derivatized with the thiol blocking reagent N-ethylmaleimide and its function was investigated with respect to the physiological activity; i.e. the ability to mediate platelet adhesion to collagen type III under physiological flow conditions as well as binding to collagen type III and the platelet GPIb-receptor. Furthermore, similar studies were performed using VWF fragments comprising the VWF-A1 domain. In order to determine the amount and the location of the derivatized cysteine residues, studies with biotin-linked maleimide were performed. The domain incorporation as well as detailed analysis of derivatized peptides was performed using MALDI-MS.

3 Materials and methods

3.1 Materials

3.1.1 Chemicals

Product	**Manufacturer**
Agarose HGT	FMC Bioproducts, Rockland, ME, USA
Agarose LGT Type VII	Sigma-Aldrich Chemie, Steinheim, Germany
Biacore Amine Coupling Kit: 0,2 M *N*-Hydroxysuccinimide (NHS), 0,5 M 1-Ethyl-3-(3-dimethylaminopropyl) carbodiimide hydrochloride (EDC), 1 M Ethanolamine hydrochloride-NaOH, pH 8,5	GE Healthcare Bio-Sciences AB, Uppsala, Sweden
BioRad Protein Assay (dye reagent, 5x concentrate)	Bio-Rad Laboratories, Hercules, USA
CMFDA Green (5-chlormethylfluorescein diacetate dye)	Molecular Probes, Inc., Eugene, USA
Heparin (Clexane®, Enoxaparin sodium)	Aventis Pharma, Frankfurt, Germany
N-ethylmaleimide	E3876, Sigma-Aldrich, Steinheim, Germany
Maleimide-PEO2-biotin	21901, Thermo Fisher Scientific, Bonn, Germany
Pasteurized, homogenized, UHT (Ultra-high temperature processed) milk, 1.5 % fat	REWE-Handelsgruppe GmbH, Köln, Germany
Sigma Fast OPD tablet set (peroxidase substrate)	Sigma-Aldrich Chemie, Steinheim, Germany
SuperSignal West Pico Chemiluminescent Substrate	Pierce, Rockford, Il, USA
UDP-α-D-Galactose, disodium salt	Calbiochem/Merck, Darmstadt, Germany

All other chemical products were obtained from Sigma-Aldrich Chemie (Steinheim, Germany) and Roth (Karlsruhe, Germany) in high-purity quality. Disposables were purchased from Falcon (Heidelberg, Germany), Eppendorf (Hamburg, Germany) and Nunc (Wiesbaden, Germany).

3.1.2 Antibodies and conjugates

Specification	**Manufacturer**
Monoclonal Mouse Anti-Human Von Willebrand Factor (clone RFF-VIII R/1)	Acris Antibodies, Hiddenhausen, Germany
Monoclonal Mouse Anti-Human Von Willebrand Factor (clone 82D6A3)	Kind gift from Dr. H. Deckmyn

NeutrAvidin-HRP conjugate	31001, Thermo Fisher Scientific, Bonn, Germany
Polyclonal Rabbit Anti-Human Von Willebrand Factor Proxidase Conjugate	DakoCytomation, Glostrup, Denmark
Polyclonal Rabbit Anti-Human Von Willebrand Factor	DakoCytomation, Glostrup, Denmark

3.1.3 Buffer and solutions

Buffer or solution	**Components in final concentration, pH**
Acetate buffer	10 mM sodium acetate, pH 4.0
Agarose gel electrophoresis running buffer	250 mM Tris, 1.925 M glycine, 0.5 % (w/v) sodium dodecyl sulphate (SDS)
Agarose gel electrophoresis sample buffer	10 mM Tris-HCl, pH 8.0, 10 mM disodium EDTA, 15 % (v/v) glycerine, 2 % (w/v) SDS 0.003 % (v/v) bromphenol blue
Agarose gel electrophoresis separation gel buffer	375 mM Tris-HCl, pH 8.8
Agarose gel electrophoresis stacking gel buffer	125 mM Tris-HCl, pH 6.8
Biacore EDTA regeneration solution	10 mM HEPES, 150 mM NaCl, 350 mM EDTA, 0.005% Tween 20; pH 8.3
Biacore nickel solution	500 µM $NiCl_2$ in Biacore running buffer (HBS-EP) for VWF-GOF GPIb interaction
Biacore running buffer (HBS-EP) for VWF-collagen type III interaction	3.4 mM EDTA, 10 mM HEPES, 150 mM NaCl, 0.005 % tween 20; pH 7.4
Biacore running buffer (HBS-EP) for VWF-GOF GPIb interaction	50 µM EDTA, 10 mM HEPES, 150 mM NaCl, 0.005 % tween 20; pH 7.4
Biacore surface regeneration solution A for VWF-collagen type III interaction	1 mM EDTA, 1 M NaCl, 0.1 M sodium citrate, pH 5.0
Biacore surface regeneration solution B for VWF-collagen type III interaction	10 mM taurodeoxycholic acid, 100 mM Tris, pH 9.0
Biacore surface regeneration solution C for VWF-collagen type III interaction	0.1 M H_3PO_4
Biacore surface regeneration solution for VWF-GOF GPIb interaction	1 M $MgCl_2$, 1 M KSCN
Blotting buffer	200 mM Na_2HPO_4, 50 mM NaH_2PO_4, 0.2 % (w/v) SDS, pH 7.4
Dispase I digestion buffer	10 mM Tris, 150 mM NaCl, 0.2 mM $CaCl_2$,

	pH 7.4
ELISA blocking buffer	0.1 % (w/v) BSA, 0.1 % (v/v) tween 20 in PBS
ELISA coating buffer (carbonate/bicarbonate buffer)	7.5 mM Na_2CO_3, 17 mM $NaHCO_3$, pH 9.6
ELISA stop solution	1 M HCl
ELISA washing solution	0.1 % tween 20 in PBS
Fixation solution	4 % (w/v) paraformaldehyde in PBS
PBS (Phosphate-buffered saline)	136 mM NaCl, 2.7 mM KCl, 15 mM Na_2HPO_4 x 2 H_2O, 1.8 mM KH_2PO_4, pH 7.4
Platelet buffer	145 mM NaCl, 10 mM HCO_3^--free N-2-hydroxyethylpiperazine-N'-2-ethanesulfonic acid (HEPES), 10 mM glucose, 0.2 mM Na_2HPO_4, 5 mM KCl, 2 mM $MgCl_2$, 0.3 % (w/v) bovine serum albumin (BSA), pH 7.4
Trypsin digestion buffer	10 mM Tris HCl, 150 mM NaCl, pH 7.4
Trypsin digestion buffer (MALDI-MS)	25 mM NH_4HCO_3, pH 8.0

3.1.4 Calibrator and controls

Product	**Manufacturer**
Albumin From Bovine Serum (2 mg/ml)	Sigma-Aldrich Chemie GmbH, Steinheim, Germany
Control Plasma Normal, LOT 1P41000	Haemochrom Diagnostica GmbH, Essen, Germany
1st International Standard von Willebrand Factor, Concentrate, NIBSC code 00/514	NIBSC, Hertfordshire, UK

3.1.5 Biological material

Product	**Manufacturer**
Human serum albumin	Sigma-Aldrich Chemie GmbH, Steinheim, Germany
Leukocyte-depleted thrombocyte concentrates	Haema, Blood and Plasma Donation Centre Berlin, Germany
Pepsin-digested collagen type III from human placental villi	Southern Biotechnology, Birmingham, US
Plasma-derived VWF/FVIII (pdVWF) Wilate	Octapharma Pharmazeutika Produktionsges.m.b.H, Vienna, Austria

Red blood cells, concentrate	Haema, Blood and Plasma Donation Centre Berlin, Germany

3.1.6 Chromatography columns

Specification, commercial product name	**Manufacturer**
HiTrap™ Heparin HP, 5 ml column volume (CV)	GE Healthcare Europe, Munich, Germany
NAP 5 columns, Sephadex G-25, 0.5 ml CV	GE Healthcare Europe, Munich, Germany
PD-10 desalting columns Sephadex™ G-25 Medium, 13.5 ml CV	GE Healthcare Europe, Munich, Germany
ZipTip C18 Pipette Tips	Millipore GmbH, Schwalbach/Ts., Germany

3.1.7 Chromatography media

Commercial product name	**Manufacturer**
Fractogel EMD TMAE (M)	Merck, Darmstadt, Germany
Streptavidin Sepharose	GE Healthcare Europe, Munich, Germany

3.1.8 Proteolytic enzymes and inhibitors

Specification, commercial product name	**Manufacturer**
Trypsin (MALDI-MS)	T1426, Sigma-Aldrich Chemie GmbH, Steinheim, Germany
Trypsin	T8003, Sigma-Aldrich Chemie GmbH, Steinheim, Germany
Dispase I	D4818, Sigma-Aldrich Chemie GmbH, Steinheim, Germany
S. aureus V8 Protease	20195, Thermo Fisher Scientific, Bonn, Germany
Soybean trypsin inhibitor	T9003, Sigma-Aldrich

3.1.9 Equipment

Instrument	**Manufacturer**
ÄKTA FPLC	GE Healthcare Europe, Munich, Germany
Biacore sensor chip CM5	GE Healthcare Bio-Sciences AB, Uppsala, Sweden
Biacore sensor chip NTA	GE Healthcare Bio-Sciences AB, Uppsala, Sweden
Biacore T100 and Biacore 2000	GE Healthcare Bio-Sciences AB, Uppsala, Sweden

Blotting power supply PowerPac 200	BioRad, Hercules, USA
Chemiluminescence and fluorescence imaging system, Fujifilm LAS-1000	Fuji Photo Film, Japan
Disposable 5 ml polypropylene columns	Pierce, Rockford, US
Electrophoresis EPH electrodes	GE Healthcare Europe, Munich, Germany
Electrophoresis power supply EPS 3501 XL	GE Healthcare Europe, Munich, Germany
Electrophoresis unit Multiphor II	GE Healthcare Europe, Munich, Germany
Filter for electrophoresis 22x6cm Filter paper model 583 GelDryer	BioRad, Hercules, USA
Flow chambers, µ-slide VI flow	ibidi GmbH, Munich, Germany
Fluorescence microscope	Carl Zeiss MicroImaging, Göttingen, Germany
FLUOstar OPTIMA microplate reader	BMG LABTECH, Jena, Germany
Fold back clips, 51 mm	Roth GmbH & Co. KG, Karlsruhe, Germany
FPLC pump	Smartline pump 1000, Knauer, Berlin, Germany
Gel bond film, agarose gel support medium 12.7 cm x 16.5 cm	Lonza, Rockland USA
Glass microfibre filters	Whatman, Middlesex, UK
Hoefer TE Transphor electrophoresis unit	GE Healthcare Europe, Munich, Germany
Ibidi pump system	ibidi, Munich, Germany
Primo R Benchtop centrifuge	Heraeus, Hanau, Germany
Spacer PVC: 20 x 140 x 1.5 mm, 20 x 300 x 1.5 mm	W. Max Wirth Kunstoff-Erzeugnisse, Braunschweig, Germany
Spectrometer type Specord 40	Analytik Jena, Jena, Germany
Thermostatic circulator MultiTemp III 230 VAC	GE Healthcare Europe, Munich, Germany
Tensor 27 FT-IR spectrometer	Bruker Optics, Ettlingen, Germany
Ultraflex II TOF/TOF mass spectrometer	Bruker Daltonics, Bremen, Germany
Automated Micro Viscometer	Anton Paar, Graz, Austria

2.1.10 Software and server

Commercial name	**Producer**
Adobe Photoshop CS3	Adobe corp., San Jose, USA
Adobe Illustrator CS3	Adobe corp., San Jose, USA
Biaevaluation software	GE Healthcare Bio-Sciences, Uppsala, Sweden
Image Gauge V3.3	Fuji Film Science, Japan
I-TASSER server	http://zhanglab.ccmb.med.umich.edu/I-TASSER/

Prism 5 for Windows 5.01	GraphPad Software Inc., San Diego, USA
Protein Prospector server	http://prospector.ucsf.edu/prospector/mshome.htm
RasWin Molecular Graphics 2.7.5	Bernstein + Sons, P.O. Box 177, Bellport, NY, USA
Matrix science server	http://www.matrixscience.com/
mMass 5.0.0	Martin Strohalm; http://www.mmass.org/
UNICORN 5.1	GE Healthcare Bio-Sciences, Uppsala, Sweden

3.2 Methods

3.2.1 NEM/MPB derivatization of VWF

The experiments were performed using VWF/FVIII concentrate Wilate. 100 mM NEM/MPB stock solution was prepared directly before use. The derivatization was performed in 20 mM Tris-HCl pH 7.0 using 1 mM NEM/MPB per 30 µg/ml VWF:Ag and 10 mM NEM/MPB per 30 µg/ml VWF:Ag or using buffer only for a control sample. Incubation was performed at 37 °C for 60 minutes. Termination of the reaction and separation of NEM was performed on PD-10 desalting columns. The PD10 column was equilibrated with 3 column volumes (CV) buffer followed by application of 2 ml derivatized sample onto the column. After washing with 0.5 ml buffer, protein fraction containing VWF was eluted with 3.5 ml buffer. Samples were aliquoted and stored at -80°C until analysis.

3.2.3 VWF:Ag determination

Concentration of VWF:Ag was determined by a sandwich ELISA. The microtiter plate was incubated with a polyclonal rabbit anti-human VWF antibody diluted 1:500 in coating buffer (4 °C, O/N). After blocking with ELISA blocking buffer (37 °C, 1 h), the plate was incubated with samples containing VWF:Ag and VWF standard diluted in blocking buffer (37 °C, 2 h). For detection, plates were incubated with a polyclonal rabbit anti-human VWF peroxidase-coupled antibody, diluted 1:2,000 in blocking buffer, for 2 h at 37 °C. Every incubation step was followed by three times washing with ELISA washing solution. As a substrate, Sigma Fast OPD tablet set was used, and after 15 min incubation colour development was stopped with 1 M HCl. Absorbance reading was performed in a FLUOstar OPTIMA microplate reader at 492 nm wavelengths.

3.2.4 Inspection of VWF structure after NEM-derivatization

VWF multimer analysis (MMA) before and after NEM separation was performed as described by Budde et al., (2006), using SDS-agarose gel electrophoresis in a discontinuous buffer system. Separating gels were composed of LGT agarose in separation gel buffer, whereas 1.2 % (w/v) agarose as low resolution gels for the illustration of the multimer composition, and

1.6 % (w/v) agarose as high resolution gels for the illustration of the triplet structure were utilized. The stacking gel was composed of 0.8 % (w/v) HGT agarose in stacking gel buffer. The separation gel was poured between two glass plates separated by spacers, (12.5 cm x 22 cm x 1.5 mm width x length x height). After polymerisation, about 2.5 cm x 22 cm of the separation gel was cropped, replaced by stacking gel and left for polymerization. Subsequently 8 to 10 slots were punched. A volume of 20 µl sample diluted to 0.5 µg/ml VWF:Ag was applied per slot. On the top and bottom of the gel filter paper was placed with one end dipped in buffer to assure current flow. Electrophoresis was performed in a Multiphor II electrophoresis unit at 65 V for 1 h at 15 °C. After the sample moved out of the slots, electrophoresis was stopped and the slots were filled with stacking gel to assure better current flow. Afterwards the electrophoresis was carried on at 55 V for 18 h at 15 °C. For better separation of the VWF sub-bands a final electrophoresis step was conducted with 120 V for 1 h at 15 °C. Separated VWF multimers were blotted onto nitrocellulose membranes in a tank blot Hoefer TE Transphor electrophoresis unit. Electrobloting was performed at 1.5 A for 4 h at 15 °C. Prior to blotting procedure, the trimmed membrane, filter papers and gels were incubated in blotting buffer. Subsequently, membranes were blocked with 100 % UHT milk for 30 min, followed by incubation with a polyclonal rabbit anti-human VWF peroxidase-coupled antibody diluted 1:2,000 in UHT milk (4 °C, O/N). SuperSignal West Pico chemiluminescent substrate was poured onto the membrane and rubbed in by rolling movement with a plastic tube. The chemiluminescence signal was visualized utilizing the imaging system Fujifilm LAS-1000.

Fourier transform infrared spectroscopy (FTIR) analysis of VWF was performed in Tensor 27 FTIR spectrometer using the AquaSpec sample cell at 21 °C. The NEM derivatized- and control sample were rebuffered into 20 mM Tris-HCl pH 7.4 buffer and concentrated to 2 mg/ml using 100K molecular cut off centrifugal filter devices. The samples were repeatedly measured against the ultrafiltrate. The IR spectra were recorded with a resolution of 4 cm^{-1} in a range from 3100 cm^{-1} to 950 cm^{-1}. The evaluation was performed using OPUS 6.0 software. The spectra were vector normalized in the amide I and II region (1720-1480 cm^{-1}). A mean spectrum was generated for each sample. To calculate the internal variation within one sample, differential spectra were formed by subtraction of the single spectra from the mean spectrum; subsequently the differential spectra were integrated in amide I region showing the difference peaks (1700-1550 cm^{-1}). Internal variation within one sample and the difference (conformational change difference, ΔK) between the derivatized and the control sample was calculated for the amide I region of the spectrum using a formula:

$$\Delta K = \frac{\int (amide\ I\ of\ tested\ sample - amide\ I\ of\ control\ sample)}{2 \times \int amide\ I\ of\ control\ samle} \times 100\ \%$$

3.2.5 Generation of VWF A1-domain fragments by limited proteolytic digestion

The 39/34-kDa monomeric VWF A1-domain fragment encompassing residues Leu-1243 to Gly-1481 (DA1) was prepared by dispase I digestion as described previously (Andrews *et al.,* 1989b). Briefly, the VWF was incubated with dispase I in dispase digestion buffer using 1:0.3 VWF:dispase weight ratio for 6 h at RT. The digestion was terminated by addition of EDTA to final concentration of 10 mM. The cleavage products were injected on the heparin column, equilibrated with the dispase digestion buffer. After extensive washing with 200 mM NaCl in digestion buffer, the DA1 fragment was eluted with 500 mM NaCl. The dimeric VWF A1-domain fragment (TA1) was obtained by trypsin digestion using 1:20 VWF:trypsin weight ratio for 1 h at 37 °C in 10 mM Tris, 150 mM NaCl pH 7.4 buffer. The digestion was terminated by addition of soybean trypsin inhibitor and the cleavage products were injected on the heparin column equilibrated with the trypsin digestion buffer and after extensive washing with 200 mM NaCl in digestion buffer, the TA1 fragment was eluted using stepwise salt gradient at about 250-300 mM NaCl concentration. The tryptic TA1 (130 kDa) fragment, is a homodimer of residue sequence Val-1036 to Lys-1491 (Fujimura *et al.,* 1991). Both fragments were concentrated using centrifugal filter devices and desalted with NAP5 columns. The purity of the obtained fragments was verified by SDS-PAGE with Coomassie staining. Concentration of the fragments was determined using the Bradford assay. The sequence of the fragments was confirmed by MALDI-MS analysis after in-gel trypsin digestion. NEM derivatization of the TA1 fragment was performed in 20 mM Tris-HCl pH 6.8 using 1 mM NEM per 70 µg/ml or using buffer only for a control sample. Incubation was performed at 37 °C for 60 minutes. Termination of the reaction and separation of NEM was performed on PD-10 desalting columns.

3.2.6 VWF-collagen type III binding, investigated by SPR

Real-time collagen binding assay was performed in Biacore 2000 and Biacore T100 systems. Human pepsin-digested collagen type III was covalently bound to the surface of a CM5 sensor chip using the amine coupling kit. The surface was activated by injection of 35 µl NHS/EDC in a 1:1 mixture at a 5 µl/min flow rate. Subsequently the ligand (collagen type III) was injected at a 2 µl/min flow rate, whereas collagen was dialyzed against acetate buffer prior to injection and diluted to 100 µg/ml. This step was manually stopped when a desired level of response units (RU) was achieved. Finally, free NHS-ester binding sites on the surface were saturated with 35 µl of 1 M ethanolamine at a flow rate of 5 ml/min. Biacore sensor chip CM5 is composed of four flow cells. One of the flow cells (FC1) served as reference flow cell and the activation with NHS/EDC was followed directly by inactivation with ethanolamine. For binding level studies, collagen type III coating level of ~3000 response units (RU) was used, in contrast to kinetic studies, where a low coating level of ~1200 RUs was utilised. HBS-EP was used as biacore running buffer. All experiments were conducted using 20 µl/min flow rate.

Regeneration was carried out as described before (Romijn *et al.,* 2003), three regeneration solutions (A, B and C) were injected one after another for 60 seconds at a 10 µl/min flow rate. For binding studies all samples were re-buffered in biacore running buffer using PD-10 columns. To estimate the influence of NEM derivatization on the binding level, 1 IU/ml of each sample was injected for 120 sec over the collagen type III coated surfaces in triplicate in a random order. Each injection was followed by regeneration. The relative response 40 seconds after injection end in the dissociation phase is defined as the binding level. For kinetic studies, the analyte was injected for 250 second followed by 800 seconds dissociation in random order. For full length VWF, an internal 0.5 IU/ml VWF binding control was injected every 10 cycles to monitor surface binding capacity. After each measurement the baseline was controlled. Binding data was evaluated with the 1:1 Langmuir binding model after reference cell subtraction, buffer injection was evaluated as a 0 analyte concentration. The regeneration of the collagen type III surface was not complete, resulting in increase of the baseline level from cycle to cycle and decreased internal control binding. Therefore, the R_{max} parameter was fitted locally. Because the aim of this experiment was the comparison between samples and not estimation of the absolute kinetic data of the complex and multivalent interaction between VWF and collagen type III, the 1:1 Langmuir model was used to avoid complex binding models and simplify the analysis. For the DA1 fragment a 1:1 Langmuir binding model, and for the TA1 a bivalent binding model was applied. Non-specific binding was eliminated by subtraction of the reference flow cell.

Following constants are calculated using the fitting models: The association rate constant (k_a), describing the rate of complex formation, i.e. the number of Ligand-Analyte (LA) complexes formed per second in a 1 M solution of L (ligand) and A (analyte), whereas L is representative for collagen type III, and A for VWF. The k_a is expressed in $M^{-1}s^{-1}$ and is typically in the range of 1×10^3 to 1×10^7 for biological systems. The dissociation rate constant (k_d) reflects the stability of the complex, i.e. the fraction of complexes that decay per second. The unit of k_d is s^{-1}, and values generally range from 1×10^{-1} to 1×10^{-6} in biological systems. A k_d of 0.01 s^{-1} implies that 1 % of the complexes decay per second. An equilibrium dissociation constant (K_D) reflects the ratio of both rate constants ($K_D = k_d/k_a$). A bivalent binding model gives rise to two sets of rate constants, first for the initial binding of the analyte with its first binding site to the ligand molecule, reported in this thesis. The second binding will give stabilization on the ligand-analyte complex without extra response but with shifting the equilibrium constant. Additionally a χ^2 parameter is calculated, giving a statistical approximation of how closely the model aligns to the experimental data, whereas χ^2 values lower than about 10 indicate good correlation between mathematical simulation and experimental sensorgrams with normal noise levels (www.sprpages.nl).

3.2.7 VWF-platelet GOF-GPIb receptor binding, investigated by SPR

GPIb binding assay was performed using biacore 2000 instrument. Recombinant gain-of-function (GOF) GPIb fragment carrying His-tag was immobilized onto nitrilotriacetic acid (NTA)-chip to a level of 1000 RU. Since the interaction between His-Tag and NTA is not covalent, and the GPIb fragment dissociated gradually, the immobilization was stabilized by additional covalent amine coupling according to (de Mol and Fisher, 2010). Briefly, the new NTA-chip was first regenerated with the regeneration solution containing EDTA, subsequently the NTA was activated by the injection of nickel solution (20 µl at 20 µl/min) to give a baseline rise of ~40 RU. For activation of the dextran surface a volume of 35 µl at a 5 µl/min flow rate was injected. This was followed by the injection of the His-tagged GOF-GPIb fragment at a 2 µl/min flow rate. Subsequently, 35 µl of 1 M ethanolamine was injected at a 5 µl/min flow rate, followed by injection of EDTA regeneration solution to wash out nickel. By this procedure, GOF-GPIb was covalently coupled to the NTA-chip. The reference flow cell was activated with NHS/EDC and inactivated with ethanolamine. The analyte was injected for 250 seconds what was followed by 800 seconds dissociation. The order of sample type injection was random. Obtained binding sensorgrams were fitted with the 1:1 Langmuir binding model. Non-specific binding was eliminated by subtraction of the reference flow cell; buffer injection was evaluated as a 0 analyte concentration

3.2.8 Flow chamber assay-based experiments

Commercially available ibidi flow chambers were used for perfusion studies. For all flow chamber experiments, µ-slides were prepared as follows: Each channel of the flow chamber was coated with 80 µl of 0.1 mg/ml human pepsin-digested collagen type III (4 °C, O/N), washed with PBS, saturated with 1 % HSA in PBS for 1 h at room temperature (RT) and rinsed with PBS. Perfusion studies were performed using a combination of the ibidi pump system and an FPLC pump at a physiological shear rate of 1700 s^{-1}. This system assures unidirectional flow over the flow chamber channel. The appropriate air pressure was adjusted according to each sample prior to perfusion studies dependent on its viscosity. Prior to the assay, the perfusion mixture viscosity was measured using a falling ball viscometer. Before analysis, the pump system and tubings were saturated with 3 % BSA in PBS and washed with 20 mM Tris-HCl; pH 7.4.

For VWF-mediated platelet adhesion studies, isolated and fluorescence labelled platelets mixed with red blood cells (RBC) to a hemoatocrit (Hct) of 33 % were perfused over collagen type III-coated flow chambers at 1700 s^{-1} shear rate for 5 min as described previously (Fuchs *et al.,* 2010). The VWF sample was spiked to the perfusion mixture just prior to perfusion. Platelets and RBCs were prepared as follows: Freshly prepared concentrates of leukocyte-depleted thrombocytes were incubated with 200 µM UDP-α-D-Gal and cell tracker

green CMFDA for 30 minutes at 37 °C. Platelets were isolated using Sepharose 2B columns as described previously (Vollmar *et al.,* 2003). Briefly, 7 ml Sepharose 2B were washed with 50 mL of 0.9 % NaCl in a disposable filter (glass microfibre filters), poured into a column (disposable 5 ml polypropylene columns) and equilibrated with 5 CV of platelet buffer. Platelets were collected in clouded drops and diluted to 2.5 x 10^8 platelets/ml with platelet buffer. For determination of platelet count, a photometric method was used utilizing a spectrometer type Specord 40 (Walkowiak *et al.,* 1997). The absorbance of collected platelets was read at 800 nm wavelength, and the amount of platelets was calculated using the following equation:

$$N\left[\frac{10^8}{ml}\right] = \left\{\left[\frac{6.23}{\left(2.016 - K \times \lambda \times \frac{A}{800}\right)}\right] - 3.09\right\} \times dilution\ factor$$

N = platelet count; λ = wavelength; K = cuvette layer thickness; A = absorbance at 800 nm

A volume of 60 ml of freshly prepared red blood cell concentrate was washed with 0.9 % NaCl using a Primo R Benchtop centrifuge for 15 min at 4 °C and 1500 x *g*, until the supernatant was clear, and utilized at 40 % Hct. Subsequently, to a mixture of RBCs and fluorescently labelled platelets in platelet buffer, 1 IU/ml VWF was spiked just prior to perfusion. Perfusion was conducted for 5 minutes using 1700 s^{-1} shear rate. Subsequently, bound platelets were fixed with 4 % paraformaldehyde in PBS. Images of CMFDA-labelled platelets bound to the channel surface were taken using a fluorescence microscope equipped with AxioCam and AxioVision 4.6 software. Thirty images of each channel were taken at randomly chosen positions along the centre of a flow chamber channel with an exposure time of 900 ms at 400 x magnification. Percentage of the platelets coverage was determined using the AutMess software module. Statistical analysis was performed using GraphPad Prism 5 for Windows 5.01. Comparison was done using the student's *t*-test with a significance level of 95 %.

For VWF-collagen type III-binding VWF samples were mixed with RBCs to a haematocrit of 40 % and a final VWF:Ag concentration of 1 IU/ml. Samples were perfused over collagen type III-coated flow chamber at a shear rate 1700 s^{-1} for 1 and 5 minutes, unbound VWF was washed out by 1 minute perfusion with 20 mM Tris-HCl pH 7.4. The remaining buffer was aspirated from each channel and replaced by 80 µl 2 % SDS solution; flow chambers were then incubated for 30 minutes at 60 °C and detached proteins were aspirated from the channel. For VWF:Ag ELISA, samples were diluted 1:200 with blocking buffer. The VWF:Ag ELISA was performed as described above, with the exception that VWF standard was diluted with blocking buffer containing 0.001 % SDS.

For A1 domain fragment-mediated platelet adhesion the perfusion was performed as described for full length VWF, with the exception that samples were not spiked to the perfusion mixture but bound to collagen type III under static conditions prior to perfusion. The binding was performed at RT for 2 h. For the binding samples were re-buffered in PBS and applied in equal molar concentrations of 190 nM, which was 51.3 µg/ml for full length VWF (MW of 270 kDa); 5.7 µg/ml for the dispase generated monomeric A1 fragment (MW of 30 kDa); 22.8 µg/ml for trypsin generated dimeric A1 fragment (MW of 130 kDa). Subsequently each channel was rinsed with buffer to wash out unbound sample prior to platelet perfusion.

3.2.9 Quantification and qualitative analysis of MPB incorporation into VWF

To investigate which domain possesses unpaired thiol groups, MPB-labelled VWF was digested with *Staphylococcus aureus* (*S. aureus*) V8 protease. *S. aureus* V8 protease digestion was performed O/N at 37 °C under non-reducing conditions at a 1:80 enzyme to protein weight ratio in Tris-HCI, pH 7.8. The digested protein was separated by SDS-PAGE and blotted onto nitrocellulose membrane. Blotted fragments were visualized by Ponceau S staining. Blots were subsequently blocked with skimmed UHT milk for 30 minutes at RT, and incubated with either polyclonal rabbit anti-human VWF antibody (anti-VWF pAb) coupled with HRP or with NeutrAvidin-HRP conjugate for 2 hours at RT, the proteins were visualized using chemiluminescent substrate. Identification of V8 protease digestion products was verified by in-gel trypsin digestion of the three major proteolytic bands followed by MALDI-MS analysis.

The amount of incorporated MPB was quantified essentially as described previously (Xie *et al.,* 2001). MaxiSorp plates, coated with anti-VWF pAb, were incubated with MPB derivatized samples diluted to 3 mIU/ml and 6 mIU/ml. Subsequently the biotin label was detected by incubation with NeutrAvidin-HRP, and simultaneously the VWF:Ag amount in the samples was quantified by anti-VWF pAb HRP conjugate.

For the examination of the distribution of MPB label within VWF multimers, MMA was performed as described; additionally, parallel to the incubation with anti-VWF pAb coupled with HRP, the nitrocellulose membrane with resolved VWF multimers of the same sample was incubated with NeutrAvidin-HRP.

3.2.10 MPB labelling for MALDI-MS analysis

Three differentially prepared samples were derivatized with MPB. The first was incubated with 10 mM MPB per 30 µg/ml VWF:Ag in 20 mM Tris-HCl, pH 7.0, the second with 10 mM MPB per 30 µg/ml VWF:Ag in 20 mM Tris-HCl/2 % SDS, pH 7.0. The third VWF sample was first bound to collagen type III coated slide, prepared as for flow chamber assay; after 2 h binding, flow chamber channels were rinsed with buffer and incubated with 10 mM

MPB in 20 mM Tris-HCl/2 % SDS, pH 7.0 for 30 min at 60 °C. The derivatization was stopped in all three samples by the addition of 20 mM GSH.

3.2.11 Digestion, purification and enrichment of MPB-labelled peptides

All VWF samples were resolved on reducing SDS-PAGE, stained with colloidal Coomassie and the 250 kDa VWF band was excised. The Coomassie stain was removed from gel slices by incubation in 50 % Ethanol at 4 °C O/N. The gel slices were lyophilized and subsequently reduced with 100 mM DTT in 100 mM ammonium carbonate buffer for 30 min at RT. After aspiration of reducing solution, gel slices were dehydrated by incubation in 50 % and subsequently 100 % acetonitrile (ACN) for 15 min each. The reduced disulfide bonds were blocked with 55 mM iodoacetamid (IAA) solution for 20 min at RT in the darkness. Gel slices were repeatedly dehydrated with ACN and subsequently lyophilized. Dry gel slices were incubated 30 min in 12.5 µg/ml proteomic grade trypsin in 25 mM ammonium carbonate buffer on ice. Rehydrated gel slices were then incubated at 37 °C O/N, when needed 25 mM ammonium carbonate buffer was added to cover the slices completely with liquid. Tryptic peptides were released from gel slices as follows: After aspiration of the supernatant, gel slices were incubated 40 min with 60 % ACN/0.1 % TFA at 300 rpm and subsequently incubated in ultrasonic bath for 5 min. After aspiration of the supernatant the step was repeated and again the supernatant was aspirated. All three supernatant fractions were pooled. The enrichment on streptavidin sepharose beads was performed as described previously (Dorum *et al.,* 2010) with several modifications. Briefly, peptides released from gel matrix were lyophilized and diluted in PBS/0.1 % SDS, pH 7.4 buffer. Subsequently washed streptavidin sepharose beads were added. The mixture was incubated at RT for 1.5 h, under constant rotation. Streptavidin sepharose beads, with attached MPB labelled peptides were washed three times with PBS/0.1 % SDS followed by three times washing with 20 % ACN. Bound peptides were eluted from streptavidin sepharose beads by 30 min incubation with 70 % ACN/2 % TFA/0.2 mM biotin solution at RT. The eluate was mixed with α-cyano-4-hydroxycinnamic acid matrix (CHCA) solution in 50 % ACN/0.1 % TFA and spotted on the target plate.

3.2.12 MALDI-MS analysis

Identification of limited *S.aureus*-, dispase- and trypsin-digestion products was performed by in-gel digestion as described for MPB labelled peptides, except that tryptic peptides were purified using ZipTip C18 Pipette Tips directly after digestion according to manufacturer's instructions. Finally all peptides were subjected to matrix-assisted laser desorption ionization-time of flight mass spectrometry (MALDI-TOF-MS) in the reflector mode using (CHCA) as matrix. The spectra were analyzed using mMass software (Strohalm *et al.,* 2010).

4 Results

4.1 Effect of free thiol group derivatization on VWF structure and function

First intention of the present study was the determination of the physiological function of unpaired cysteine residues in the VWF molecule. This was accomplished by blocking all reactive and accessible thiol groups in the native VWF molecule with N-ethylmaleimide followed by inspection of the derivatized molecule in VWF activity assays. The experimental setup of this part of the study is presented in Fig. 7.

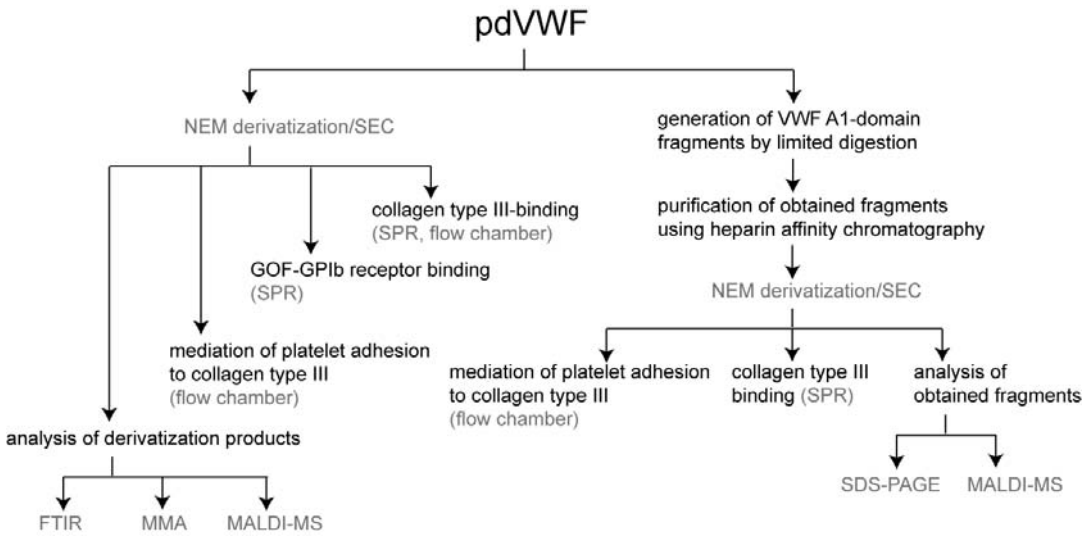

Fig. 7. Analysis of the function of unpaired cysteine residues in VWF. Pd: plasma derived.

N-ethylmaleimide (NEM) is an organic compound, widely used for covalent modification of cysteine residues in proteins. At pH 6.5-7.5, NEM is specific towards free thiol groups (Rogers *et al.,* 2006; Hill *et al.,* 2009). Maleimide groups react with sulfhydryls by nucleophilic attack of the thiolate anion on one of the carbons of the double bond (Fig. 8). Covalent thioether bonds are irreversible and prevent disulfide bond formation.

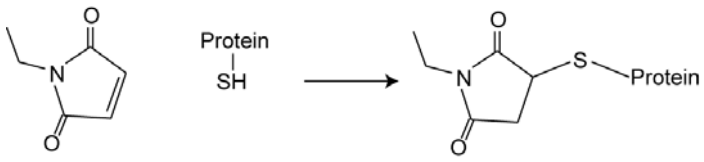

Fig. 8. Structure of N-ethylmaleimide and the schematic reaction with protein free thiol group.

4.1.1 Structural analysis of the NEM-derivative of VWF

To assure that derivatization did not provoke denaturation or aggregation as well as to control the secondary structure of the protein, structural analysis was performed. The multimer structure of VWF was not impaired by the derivatization (Fig. 9). All multimer sizes were

present for each sample in comparable amounts, both for the sample prior to and after purification by SEC. The attachment of NEM did not provoke an increase or decrease in VWF multimer size. The triplet structure of individual multimers also remained intact.

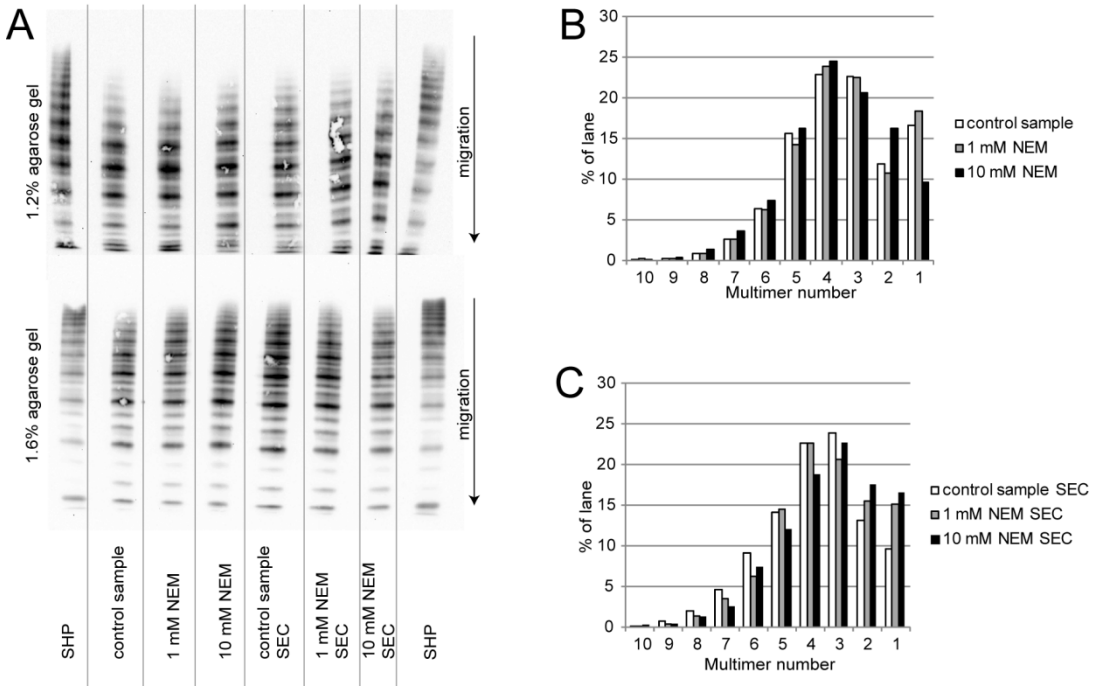

Fig. 9. Effect of NEM derivatization on VWF multimer structure. The NEM derivatization was performed using 1mM or 10mM NEM per 30 µg/ml VWF. Excess of reagent was removed by size exclusion chromatography on PD-10 columns (SEC). Multimer analysis was performed before and after NEM removal. (A) The upper gel (1.2% agarose) shows intact multimer structure of derivatized samples, the bottom gel (1.6%) shows intact triplet structure of derivatized samples. SHP is standard human plasma. The migration direction is from the top to the bottom of the gel. (B), (C) Densitometric evaluation of 1.2 % gel (A, upper gel) of the sample before (B) and after NEM removal (C). The smallest multimer is the dimer (No. 1).

Moreover, the possible effect of NEM-derivatization on VWF structure was evaluated by FTIR spectroscopy. This technique measures the infrared radiation absorbed by organic molecules converted into energy of molecular vibrations. The evaluation of FTIR spectra was performed solely for the amide I band region (1700-1600 cm^{-1}), as it is most sensitive region for protein secondary structure elements. Approximately 80 % of amide I signal results from C=O stretch vibrations of the peptide linkages, whose frequency depends on the hydrogen-bonding and coupling along the protein chain. Different secondary structure elements exhibit different frequencies within the amide I band; e.g. 1638-1640 cm^{-1} region corresponds to a native β-sheet, 1650-1653 cm^{-1} to α-helix, 1660-1667 and 1682-1687 cm^{-1} to β-turns and finally 1626-1628 and 1690 cm^{-1} are representative for intermolecular antiparallel β-sheet, which is observed after protein aggregation (Lacey *et al.*, 1998; Kong and Yu, 2007). The derivatization had no impact on the secondary structure elements of VWF, i.e. the FTIR spectra of NEM-derivatized (n=6,

internal variation of 0.22 %) and non-derivatized (n=5, internal variation of 0.46 %) VWF were identical. The observed difference of 0.48 % (Fig. 10) is related to inter-assay variability.

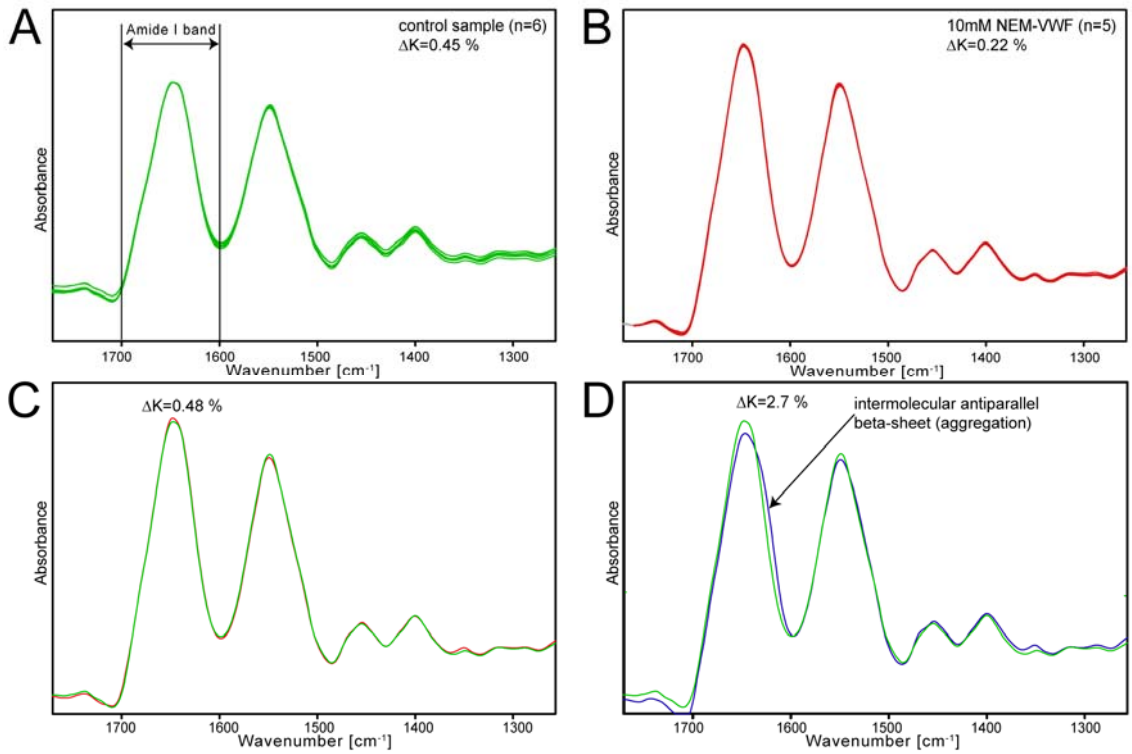

Fig. 10. Effect of NEM derivatization on VWF secondary structure elements measured by FTIR. The NEM-derivatized (red spectrum) and control (green spectrum) sample, rebuffered into 20 mM Tris-HCl, pH 7.4 and concentrated to 2 mg/ml using 100K molecular cut off centrifugal filter devices, were repeatedly measured against the ultrafiltrate, additionally heat denatured (5 min, 90 °C) sample (blue spectrum) was measured. Spectra (A) and (B) show repeated measurement of control- and NEM-derivatized sample respectively. (C) Superimposed mean spectra of the control and NEM-derivatized sample. (D) Superimposed mean spectra of the control and heat denatured sample.

4.1.2 Effect of thiol group derivatization on VWF function under flow

To investigate the physiological significance of unpaired cysteine residues in VWF, an *in vitro* flow chamber system was utilized. In this assay reconstituted blood is perfused over a collagen type III surface to mimic the shear forces found in human arterial circulation. Flow perfusion experiments were conducted at 1700 s^{-1} shear rate, which in this setup corresponds to a shear stress of approx. 50 dyne/cm^2. Under these conditions, VWF is mandatory to mediate platelet adhesion to injured endothelium. In the flow chamber system injured endothelium is mimicked by collagen type III. VWF samples were spiked into perfusion mixture just prior to perfusion. An end point platelet surface coverage of four independent experiments is shown in Fig. 11A. Representative end point pictures for each sample after 5 minutes perfusion is shown in Fig. 11B. The derivatization of VWF sulfhydryl groups with 1 mM NEM reduced the ability to mediate platelet adhesion from 25 % to a level of 13 %. A higher degree of derivatization did not further reduce the platelet coverage. The collagen type III bound platelet aggregates after perfusion with NEM pre-treated samples were rarely distributed, whereas perfusion with the

control sample produced uniformly covered surface. Reduction of platelet binding could be provoked by inhibition of one or both of the two main steps of this process; the initial VWF binding to collagen type III or/and the VWF GPIb binding sites exposure, which allows platelet rolling and adhesion to VWF.

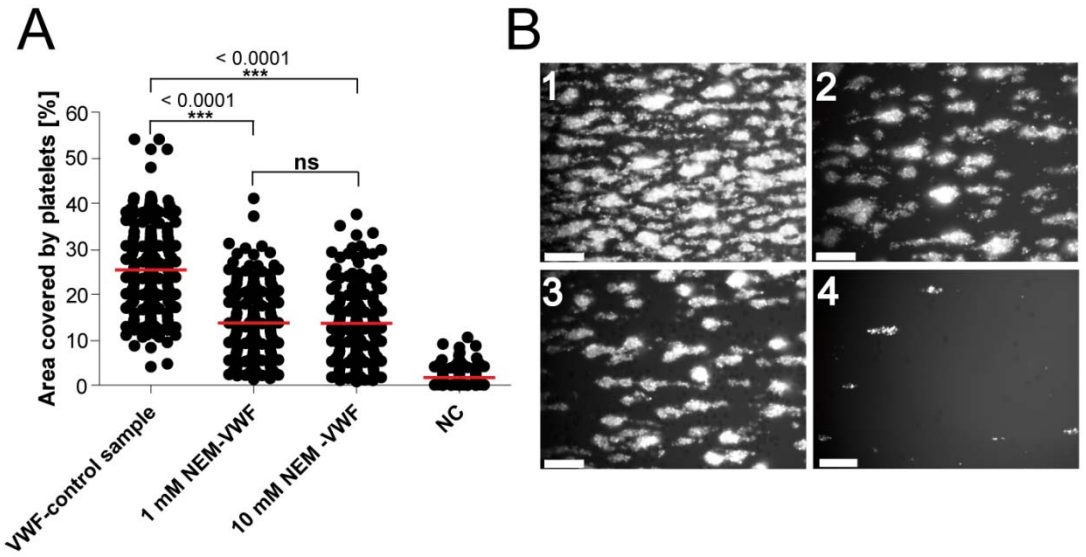

Fig. 11. Free thiol groups of VWF are involved in VWF mediated platelet adhesion to collagen type III under physiological flow conditions. VWF samples were spiked into reconstituted blood and perfused over collagen type III coated surface. After 5 minutes perfusion the area covered by adhered platelets was quantified. (A) Percentage of platelet surface coverage. Quantification of platelet surface coverage from four independent flow chamber experiments each performed in duplicate. Randomly chosen images of the flow-channels were analyzed for percentage of platelet coverage. NC: negative control. Results of statistical analysis utilizing the student's *t*-test with a significance level of 95 % are indicated on top of the graph. Red horizontal bars represent mean values. The significance levels are marked by asterisks and p-values for the *t*-test are indicated. Ns: not significant. (B) Representative images of fluorescence labelled platelets bound to collagen type III; 1-control sample, 2- 1 mM NEM-VWF, 3- 10 mM NEM-VWF, 4- negative control. Scale bar- 50 µm.

The flow chamber model allows also the investigation of VWF-binding to collagen type III under physiological shear stress conditions. For this purpose a mixture of RBCs and VWF was perfused over a collagen type III surface. The amount of collagen-bound VWF was quantified using a VWF:Ag assay either after 1 minute or 5 minutes perfusion (Fig. 12). After one minute perfusion, about 60 ng VWF of control sample bound to collagen type III, and about 10 ng less VWF bound after perfusion with both samples derivatized with NEM. After five minutes perfusion the difference between control sample and 1 mM NEM sample became insignificant, but the amount of collagen-bound VWF using the sample derivatized with 10 mM NEM was 20 ng lower than for both other samples.

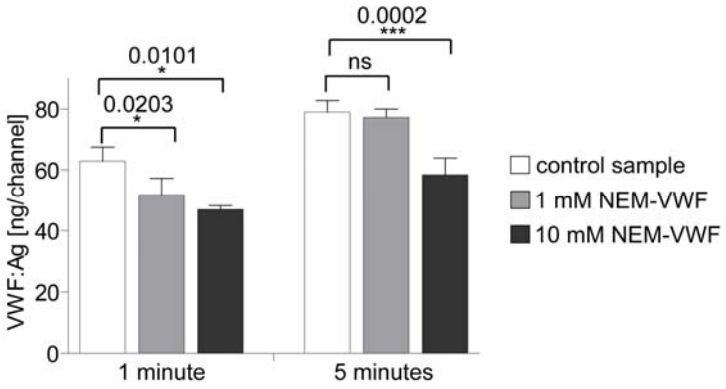

Fig. 12. Free thiol groups of VWF are involved in VWF-collagen type III interaction under physiological flow conditions. VWF samples were spiked into perfusion mixture composed of erythrocytes and platelet buffer just prior to perfusion. After 1 or 5 minutes of perfusion, unbound proteins were washed out from each channel. Bound VWF, detached with 2% SDS and incubation at 60°C for 30 min, was quantified using VWF:Ag ELISA. Results of statistical analysis utilizing the student's *t*-test with a significance level of 95 % are indicated on top of the graph. The significance levels are marked by asterisks and p-values for the *t*-test are indicated. Ns: not significant. N=3.

To investigate the kinetics of this inhibition mechanism, the same interaction was tested using SPR (Fig. 13). Using this technique it is possible to estimate association and dissociation rate constants for the interaction between an immobilized ligand (collagen type III) and perfused analyte (VWF). The aim of this experiment was the comparison between samples and not estimation of the absolute kinetic data of this complex and multivalent interaction. Therefore the 1:1 Langmuir binding model was used for evaluation of the binding data for the sake of simplification. The binding sensorgrams with mathematical correlations are shown in Fig. 13. The kinetic and affinity constants are summarized in Tab. 2. An estimated K_D of 3.0 nM determined for the control sample was similar to the previously reported K_D of 3.3 nM (Romijn *et al.,* 2003). NEM derivatization decreased VWF-collagen type III binding affinity. The decrease was very small and statistically insignificant for the 1 mM NEM treated sample. However, the 10 mM NEM pre-treated sample bound to collagen type III with a 65 % lower affinity. Higher dissociation affinity constant is for this interaction an effect of lower association rate. The 10 mM NEM pre-treated sample binds 1.9 times slower to collagen type III comparing to the control sample.

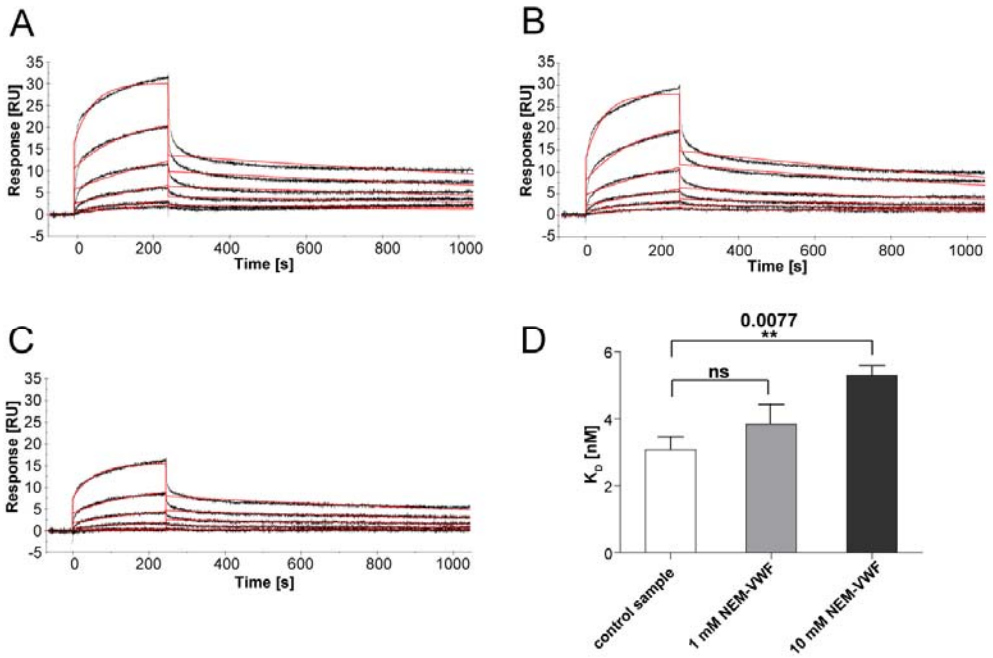

Fig. 13. Determination of kinetic and affinity constants of VWF-collagen type III interaction and influence of free thiol groups on this interaction. Collagen type III was coupled to CM5 chip via amine coupling to a level of 1200 RU. VWF samples in HBS-EP buffer were perfused using a flow rate of 20 µl/min. (A), (B) and (C) depicts representative binding sensorgrams (black curves) with a fitted 1:1 Langmuir binding model (red lines); (A)-control sample; (B) Sample derivatized with 1 mM NEM; (C) Sample derivatized with 10 mM NEM. Samples were applied in five 1:3 dilution steps, with the highest analyte concentration of 185 nM. Sample concentrations were calculated considering the molecular mass of a VWF monomer (270 kDa); χ^2 values for individual fits ranged between 1.7 and 2.2 for the control sample, between 0.5 and 1.6 for the 1 mM NEM-VWF sample and between 0.2 and 0.6 for the 10 mM NEM-VWF sample. (D) Affinity constants as means of 3 independent experiments. Results of statistical analysis utilizing the student's *t*-test with a significance level of 95 % are indicated on top of the graph. The significance levels are marked by asterisks and p-values for the *t*-test are indicated. Ns: not significant.

Tab. 2. Kinetic and affinity constants for VWF-collagen type III interaction studied by SPR. Values represent means ± SD of 3 independent experiments.

Analyte	k_a [M^{-1} s^{-1}] * 10^5	k_d [s^{-1}] * 10^{-4}	K_D [nM]
VWF control sample	2.1 ± 1.0	6.4 ± 1.8	3.0 ± 0.8
1 mM NEM-VWF	1.7 ± 0.4	6.3 ± 1.7	3.8 ± 0.6
10 mM NEM-VWF	1.1 ± 0.3	5.9 ± 0.9	5.2 ± 0.5

Since VWF contains two domains able to bind collagen type III it was reasonable to resolve, inhibition of which VWF domain was responsible for the lowered collagen type III affinity of VWF, i.e. which domain was inhibited by NEM derivatization. Inhibition studies were performed using SPR and the final binding level was used as read out. To selectively inhibit the VWF-A3 collagen type III interaction, inhibitory anti-A3 antibody (82D6A3) was used. To inhibit VWF-A1 collagen type III interaction sample was spiked with heparin

(CLEXANE®). Samples were pre-incubated five minutes with inhibitory agents, followed by measuring the binding level by SPR (Fig. 14).

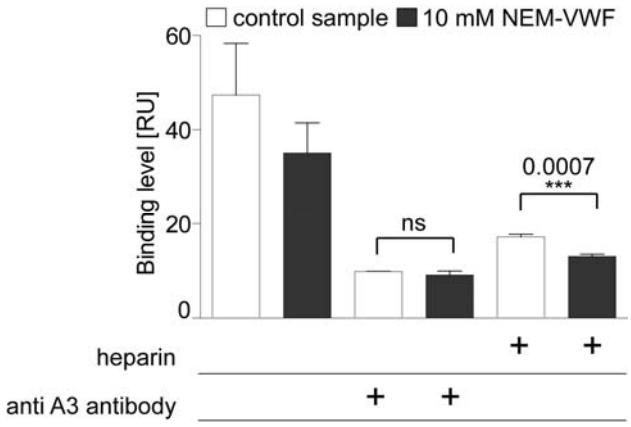

Fig. 14. Selective inhibition of VWF-collagen type III binding domains in SPR. 1 IU/ml VWF sample (control sample or 10 mM NEM-VWF) were incubated 5 min at RT with either 200 µM heparin (CLEXANE®) or 2.5 µg/ml inhibitory anti-A3 Ab (82D6A3). Each sample was injected for 120 sec over collagen type III-coated surface in triplicate in random order. The binding level expresses the relative response 40 seconds after injection end in the dissociation phase. Results of statistical analysis utilizing the student's *t*-test with a significance level of 95 % are indicated on top of the graph. The significance levels are marked by asterisks and P-values for the *t*-test are indicated. Ns: not significant.

Both, anti-A3 Ab and heparin significantly inhibited VWF-collagen type III interaction (Fig. 14). Inhibition of the VWF A3 or A1 domain in the control sample decreased collagen type III-binding from 42 RU to 10 RU or 17 RU, respectively. The difference between the control sample and the NEM derivatized sample was 12 RU. After inhibition of the A3 domain both samples bound to collagen type III to approximately the same level, the difference between both samples (0.7 RU) was not statistically significant. Heparin had overall lower inhibitory potential than the anti-A3 Ab, and interestingly it inhibited both samples to different levels. The 4 RU difference between control and the NEM derivatized sample was statistically significant. These results indicate that the inhibitory effect of NEM on the VWF-collagen type III interaction may result from the inhibition of the A3 domain, because this effect persists even after inhibition of the A1 domain mediated collagen type III binding, but not after inhibition of the A3 domain.

Circulating VWF does not bind platelets. The interaction with platelet GPIb receptor requires VWF binding to subendothelial matrix. Additionally, several agents like snake venom ristocetin or botrocetin 'activate' VWF and are widely used to determine VWF activity in clinical laboratories. Another possibility to measure VWF activity is the use of a gain-of function GPIb receptor fragment, which binds VWF without physiological activation or modulators. In the present study use of GOF-GPIb was considered less artificial and therefore more physiological reliable than using chemical modulators. The VWF GOF-GPIb interaction was measured by SPR. For the evaluation the 1:1 Langmuir binding model was used for

simplicity, though the actual interaction is more complex because of the multimeric nature of VWF. The binding sensorgrams with fitted 1:1 binding model as well as kinetic rates and constants for this interaction are summarized in Tab. 3 and Fig. 15.

Tab. 3 Kinetic and affinity constants for VWF-GP1b-GOF interaction studied by SPR. Values represent means ± SD of three independent experiments.

Analyte	k_a [M^{-1} s^{-1}] * 10^5	k_d [s^{-1}] * 10^{-4}	K_D [nM]
VWF control sample	1.3 ± 0.2	6.0 ± 1.0	4.8 ± 1.3
1 mM NEM-VWF	1.1 ± 0.1	4.0 ± 0.7	3.7 ± 0.9
10 mM NEM-VWF	0.4 ± 0.1	6.8 ± 1.4	16.2 ± 6.0

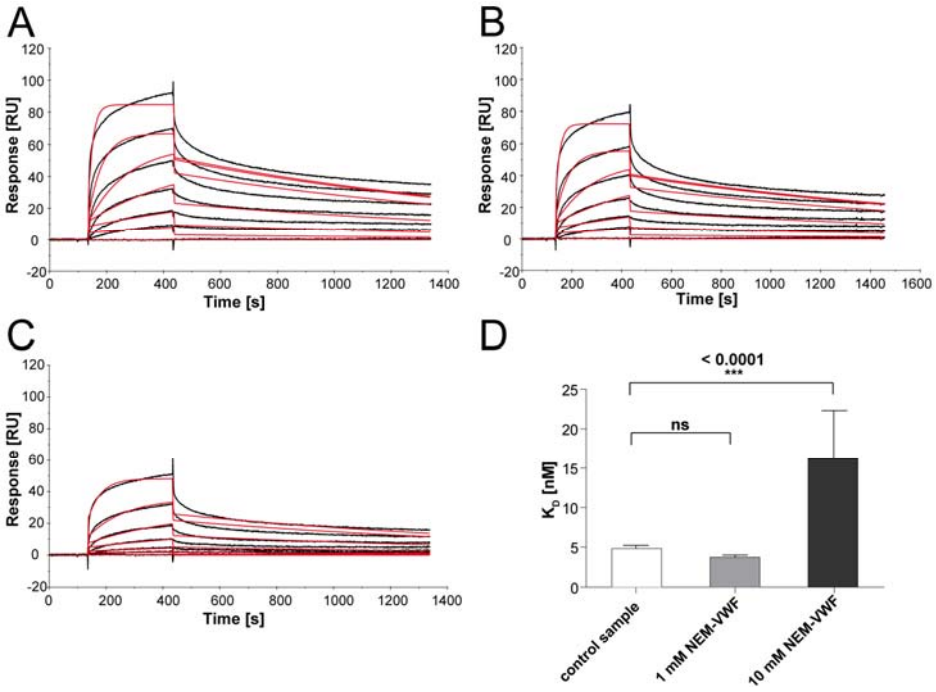

Fig. 15. Free thiol groups of VWF are involved in VWF-platelet GPIb receptor interaction. GOF-GPIb was immobilized on a NTA Chip via His-Tag. VWF samples in HBS-EP buffer were perfused using a flow rate of 20 µl/min. (A), (B) and (C) show representative binding sensorgrams (black curves) with a fitted 1:1 Langmuir binding model (red lines); (A) control sample; (B) Sample derivatized with 1 mM NEM; (C) Sample derivatized with 10 mM NEM. Samples were applied in five 1:3 dilution steps, with the highest analyte concentration of 500 nM. Sample concentrations were calculated considering the molecular mass of a VWF monomer (270 kDa); χ^2 values for individual fits ranged between 10 and 12 for the control sample, between 8 and 11 for the 1 mM NEM-VWF sample and between 2 and 3 for the 10 mM NEM-VWF sample. (D) Kinetic and affinity constants as a mean of 3 independent experiments. Results of statistical analysis utilizing the student's *t*-test with a significance level of 95 % are indicated on top of the graph. The significance levels are marked by asterisks and p-values for the *t*-test are indicated above. Ns: not significant.

The control and the 1 mM NEM-VWF samples bound to the GOF-GPIb receptor with similar affinities of 4.8 nM and 3.7 nM respectively, the difference between both affinities was

not statistically significant (Fig. 15D). A higher level of derivatization caused a strong decrease of the affinity, resulting in dissociation affinity constant of 16.2 nM. This decrease was mainly caused by the association rate k_a, which was 3.2 times lower than for the control sample, however the stability of formed complexes was also impaired, reflected by an increase in k_d from 6.0 s^{-1} to 6.8 s^{-1} (Tab. 3).

4.1.3 Effect of thiol group derivatization on VWF A1-domain

Each VWF monomer contains one binding site for the platelet GPIb receptor in its A1 domain. The A1 domain forms an intramolecular disulfide loop. The loop itself contains no cysteine residues in contrast to the adjacent *N*-terminal sequence, which is rich in cysteine residues. The A1 domain exists in VWF molecule also as an intermolecular dimer connected to another VWF monomer by one to three disulfide bridges (Azuma *et al.,* 1991) formed by one to three cysteine residues (Cys^{1222}, Cys^{1225} or Cys^{1227}) (Azuma *et al.,* 1993). Since the monomeric fragment obtained by dispase digestion and the recombinant A1 fragment (residues 1238-1471) are able to bind the GPIb receptor in the absence of a modulator (Andrews *et al.,* 1989b; Cruz *et al.,* 1993) and the dimeric A1 fragments obtained by limited trypsin digestion (residues 1211-1491) requires modulators or collagen to bind the GP1b receptor (Bonnefoy *et al.,* 2006; Morales *et al.,* 2006), it is possible that the regulatory mechanism switching the A1 conformation from inactive to active requires the dimeric structure of A1 domain and is located *N*-terminal to the A1 domain loop. The preliminary limited trypsin digestions indicated incorporation of the biotin-linked maleimide into the A1 domain neighbouring sequence. The purpose of the following experiments therefore aimed to investigate whether the derivatization of cysteine residues in the sequence neighbouring the A1 loop has an impact on the physiological function of the domain.

Two fragments containing the A1 domain were generated. The first, smaller fragment was obtained by limited dispase digestion. This fragment, with a molecular weight of approx. 34 kDa unreduced and approx. 37 kDa reduced contained only the disulfide-bonded A1 domain loop and no other cysteine residue, and is abbreviated ‘DA1’. The second fragment (abbr. ‘TA1’) was obtained by limited trypsin digestion and is a dimer with a molecular weight of 130 kDa unreduced and approx. 75 kDa reduced. This fragment contains an adjacent *N*-terminal sequence additionally to the A1 loop. The sequences of both fragments are summarized in Fig. 17. Both fragments were generated under non-denaturing, physiological pH conditions to retain their functionality, purified using heparin affinity chromatography and analyzed by SDS-PAGE. The DA1-fragment migrated as a closely spaced double-band, both in the unreduced (Fig. 16A, lane 2) and reduced state (Fig. 16A, lane 1). Both bands had the same amino acid sequence which was confirmed by MALDI-MS and differed most likely with respect to their glycosylation (Andrews *et al.,* 1989b). The reduction of the disulfide loop in the DA1 fragment

resulted in a decreased electrophoretic mobility of the fragment. SDS-PAGE analysis of the TA1 fragment revealed the presence of an additional approx. 31 kDa double-band on both non-reducing and reducing gels, which was not recognized by the anti-A1 antibody (Fig. 16B). This band was further analyzed using MALDI-MS and identified as the *N*-terminus of VWF (Fig. 17). Again both bands did not differ in the sequence but most likely differed with respect to their glycosylation. As only the A1 domain contains a heparin binding site in the VWF molecule it is unlikely that the 31 kDa fragment alone could be enriched by heparin affinity chromatography. The only reasonable explanation for the presence of this fragment in the heparin sepharose eluate is the was non-covalent association with the TA1 fragment during the digestion and purification procedure and subsequent dissociation of the two fragments due to denaturation of the sample for SDS-PAGE analysis. The non-covalent association of the *N*-terminus and A1 domain of VWF has been described previously (Ulrichts *et al.*, 2006) and is depicted in Fig. 16D.

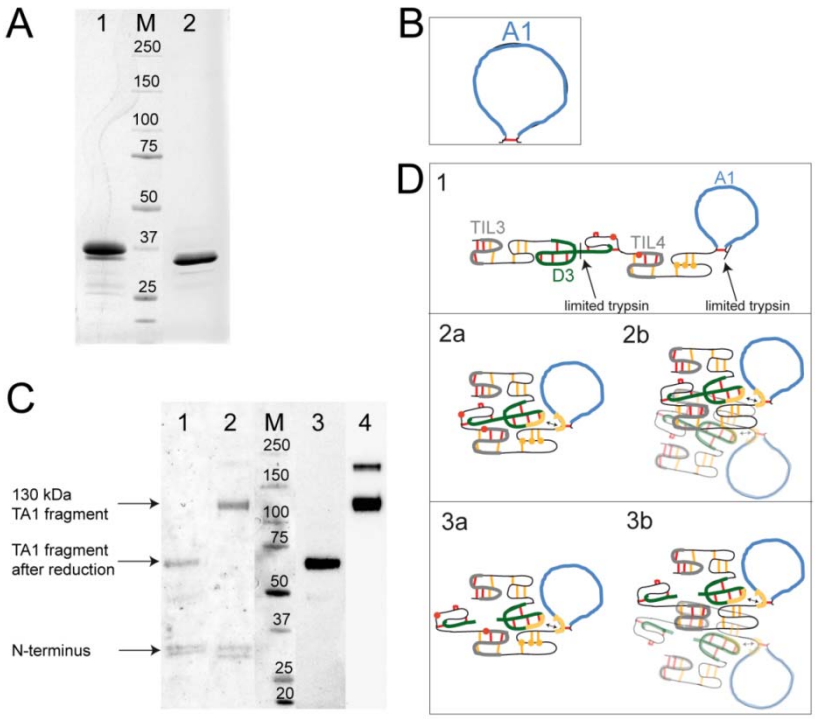

Fig. 16. Characterization of VWF-A1-domain fragments by SDS-PAGE and Western blot. (A) Purified DA1 fragment was analyzed under reducing (lane 1) and non-reducing conditions (lane 2) by SDS-PAGE and Coomassie staining. (B) Schematic illustration of DA1 fragment. (C) Purified TA1 fragment was analyzed under non-reducing (lanes 2 and 4) and reducing conditions (lanes 1 and 3) by SDS-PAGE and Western blot. The blotted TA1 fragment was detected by Ponceau S stain (lanes 1 and 2), and anti-A1 mAb RFF_VII R/1 (lanes 3 and 4). M stands for molecular weight marker; molecular weights are expressed in kDa. (D) Illustration of the TA1 fragment origination and association with protein *N*-terminus; 1- *N*-terminal VWF domains encompassing two limited trypsin cleavage sites, 2a- possible solution structure, resulting from non covalent association of D3 and A1 domains described by Ulrichts *et al.*, (2006), interacting patches are marked orange and with bidirectional arrow. 2b- 2a dimer, 3a- 2a structure after trypsin cleavage, 3b- 3a dimer (possible TA1 fragment structure). Red dots represent cysteine residues responsible for *N*-terminal multimerization; orange dots represent cysteine residues responsible for intermolecular dimer formation.

Fig. 17. Sequences of fragments, obtained by limited trypsin (TA1, *N*-Terminus); and dispase (DA1) digestion. Both A1 domain fragments were purified by heparin affinity chromatography, resolved on SDS-PAGE and analysed by MALDI-MS. Peptides, which were found in the spectrum are underlined. The A1 domain sequence is highlighted in grey. Cysteine residues involved in the intramolecular disulfide loop are orange and marked with black arrowheads. Cysteine residues forming intermolecular dimer are blue and marked with black arrowheads, the residual cysteine residues are red. Cysteines involved in *N*-terminal multimerization are green and marked with black arrowheads.

To investigate whether the blockade of free cysteine residues in the sequence neighbouring the A1 domain affects its interaction with collagen type III and/or platelet-GPIb receptor, the TA1 domain fragment was derivatized with NEM and collagen binding using SPR as well as platelet binding using the flow chamber was investigated. The DA1 fragment was used in the experiments as a control. The collagen type III binding assay revealed no difference between the NEM-treated TA1 fragment and the untreated fragment. The affinity constants for both interactions were almost identical with a K_D of 6.2 nM and 6.3 nM for the TA1 and the NEM-TA1 sample, respectively (Fig. 18A, B and D). Since the sample is a dimer, the sensorgrams were evaluated using the bivalent analyte binding model. The monomeric DA1 fragment bound with about 55-times lower affinity to collagen type III, yielding a K_D of 341 nM (Fig. 18C, D). These results indicate that for the VWF collagen type III binding mediated by the A1 domain the dimeric structure of the A1 domain is essential and that the free sulfhydryl groups present in the *N*-terminal neighbouring sequence of the A1 domain are not required for this interaction. The outcome of this experiment confirm the observation from the inhibition experiments, that the A1 domain of VWF is not involved in the NEM-induced inhibition of the VWF- collagen type III interaction (see Fig. 14).

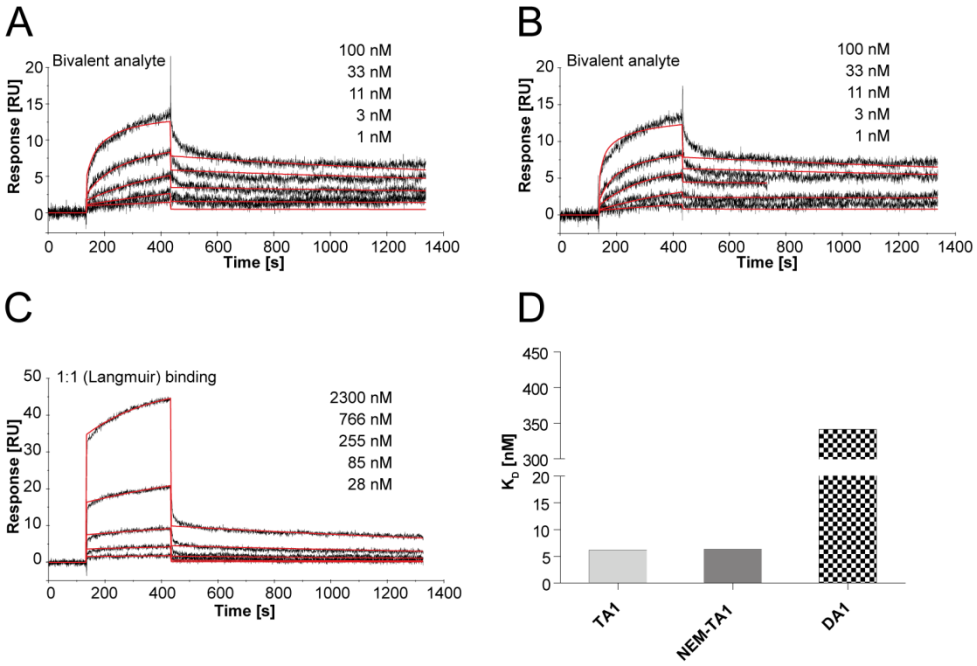

Fig. 18. Binding of VWF-A1 domain fragments to collagen type III measured by SPR. Collagen type III was coupled to CM5 Chip via amine coupling to a level of approx. 4000 RU. Samples in HBS-EP buffer were perfused using a 20 µl/min flow rate. (A), (B) and (C) depicts representative binding sensorgrams (black curves) fitted with either bivalent binding model (A, B) or 1:1 Langmuir binding model (C), (red lines). (A) TA1; (B) NEM-TA1; (C) DA1. Samples were diluted in five 1:3 steps. Concentrations are indicated on each sensorgram. Sample concentrations were calculated using the molecular mass of: A, B- the 130 kDa TA1 dimer, C- 35 kDa DA1 monomer; χ^2 values for individual fits for all samples were < 1. (D) Affinity constants as a mean of 2 independent experiments. Note the discontinued y-axis.

For flow chamber experiments investigating the A1 domain-fragment mediated platelet adhesion collagen type III coated slides were incubated with the samples under static conditions to produce a surface saturated with each sample. This procedure was chosen, because the monomeric A1 domain binds and activates platelets in solution, as in contrast to full length VWF it does not need to be activated by binding on collagen type III. Additionally a control full length VWF and a 10 mM NEM sample were tested using the same experimental procedure. Under these saturating conditions, both samples, VWF and 10 mM NEM bound to collagen type III to the same extent (Fig. 19C). As expected, full length VWF produced a uniform, almost completely platelet-covered surface (Fig. 19B picture 1), which yielded a value of 68 % coverage. The 10 mM NEM-VWF sample mediated as well highly covered surface, however surface coverage was significantly lower (57 %) compared to the non-derivatized sample. This experiment generated very important data, namely that in the collagen type III-bound VWF unpaired cysteine residues play an important role in platelet arrest. The data obtained using the TA1 fragments was contraire to the data obtained with full length VWF, in this case, the NEM derivatization of the A1 domain resulted in significantly higher mediation of platelet adhesion (36 %) when compared to unmodified TA1 fragment (24 %). The monomeric DA1 fragment was not as effective as the TA1 fragment, resulting in only 16 % platelet surface coverage. One

reason for this might be the faster dissociation of this fragment from the collagen type III surface, as soon as the high shear stress was applied, but often only platelet rolling instead of stabile association on the collagen type III surface was observed. This would indicate that the DA1 coating is stable, the interaction with the GPIb receptor occurs, but platelets are not activated to the same extent as for the dimeric domain.

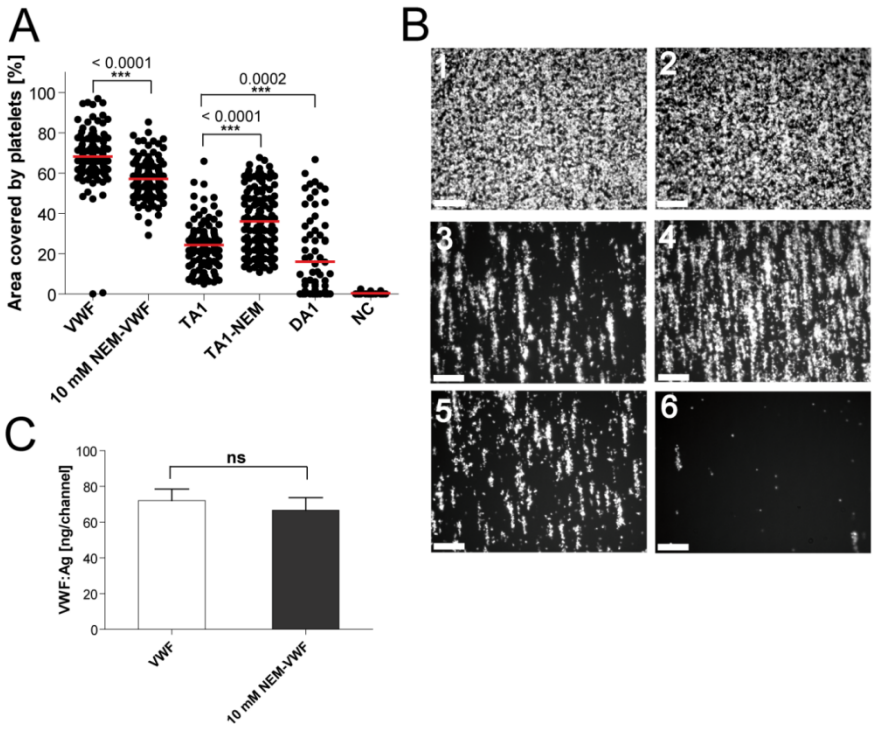

Fig. 19. Effect of free thiol group blocking with NEM on VWF-A1 domain mediated platelet adhesion to collagen type III. Purified A1 domains (DA1, TA1 and NEM derivatized TA1) and full length VWF were bound to collagen type III pre-coated slide surface. After 5 minutes perfusion with reconstituted blood the area covered by adhered platelets was quantified. (A) Percentage of platelet surface coverage. Quantification of platelet surface coverage from three independent flow chamber experiments each performed in duplicate. Randomly chosen images of the flow-channels were analysed for percentage of platelet coverage. Results of statistical analysis utilizing the student's *t*-test with a significance level of 95 % are indicated on top of the graph. Red horizontal bars represent mean values. The significance levels are marked by asterisks and p-values for the *t*-test are indicated above. Ns: not significant. (B) Representative images of fluorescently labelled platelets bound to collagen type III pre-incubated with: 1-VWF, 2-10 mM NEM-VWF, 3-TA1, 4- NEM-TA1, 5-DA1, 6-NC. Scale bar-50 µm. (C) VWF, bound to collagen type III under static conditions, detached with 2% SDS and 30 min incubation at 60°C, was quantified in VWF:Ag. Ns: not significant. N=3

4.2 Quantification and identification of free thiol groups in VWF

The second aspect of this study was the quantification and identification of unpaired cysteine residues in the VWF molecule and thereby clarification of the mechanism causing the observed modulation of VWF activity by NEM-derivatization. Identification and quantification of the free thiol groups was accomplished by using biotin-linked maleimide derivatization, providing the possibility to detect and enrich the protein or peptide-attached label. Fig. 20 gives an overview of steps and methods applied in this part of the study.

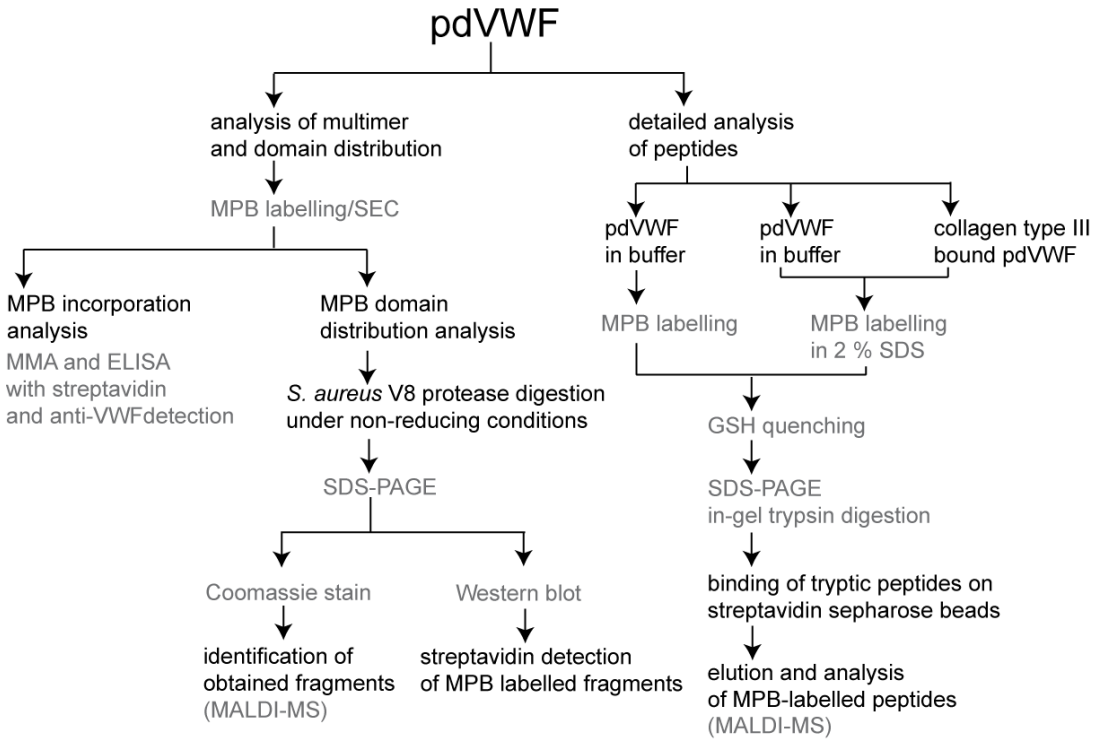

Fig. 20. Quantitation and identification of free thiol groups in VWF. Pd: plasma derived.

4.2.1 Quantification and visualisation of unpaired cysteine residues in VWF

The MPB labelling, using conditions specified for NEM-derivatization, yielded 16.6 % and 34.5 % MPB incorporation after derivatization with 1 mM and 10 mM MPB respectively (Fig. 21A). The applied ELISA method allowed quantification of the percentage of MPB label incorporated into the VWF molecule, meaning that 16.6 % and 34.5 % of all multimers captured on the microtitre plate incorporated MPB label. To investigate, whether all multimers incorporated the MPB label to the same extent, multimer analysis (MMA) of the 10 mM MPB derivatized sample was performed with both, anti-VWF detection and streptavidin detection. The result clearly showed that the MPB incorporation increases with decreasing multimeric size of VWF (Fig. 21C and D). This can be explained by the fact, that high molecular weight multimers presumably adopt coiled and globular structure in solution and thereby do not expose all unpaired cysteine residues on the surface, or rather, not all unpaired cysteine residues are accessible for the MPB modification. To investigate, if the MPB incorporation into VWF is

saturable, the same ELISA assay was performed with samples derivatized with 0.5-100 mM MPB (Fig. 21B). To simplify the analysis, the MPB label was not separated using SEC, instead the reaction was quenched with GSH. The analysis showed that the highest MPB incorporation level of about 80 % is reached at 50 mM MPB while higher concentrations do not result in an increase of the extent of modification. Furthermore, the incorporation level in both ELISA assays was compared, with the purpose to determine, whether the way of stopping the MPB reaction influences the incorporation level. As shown in Fig. 21A this is not the case, as no significant differences between both incorporation levels were found.

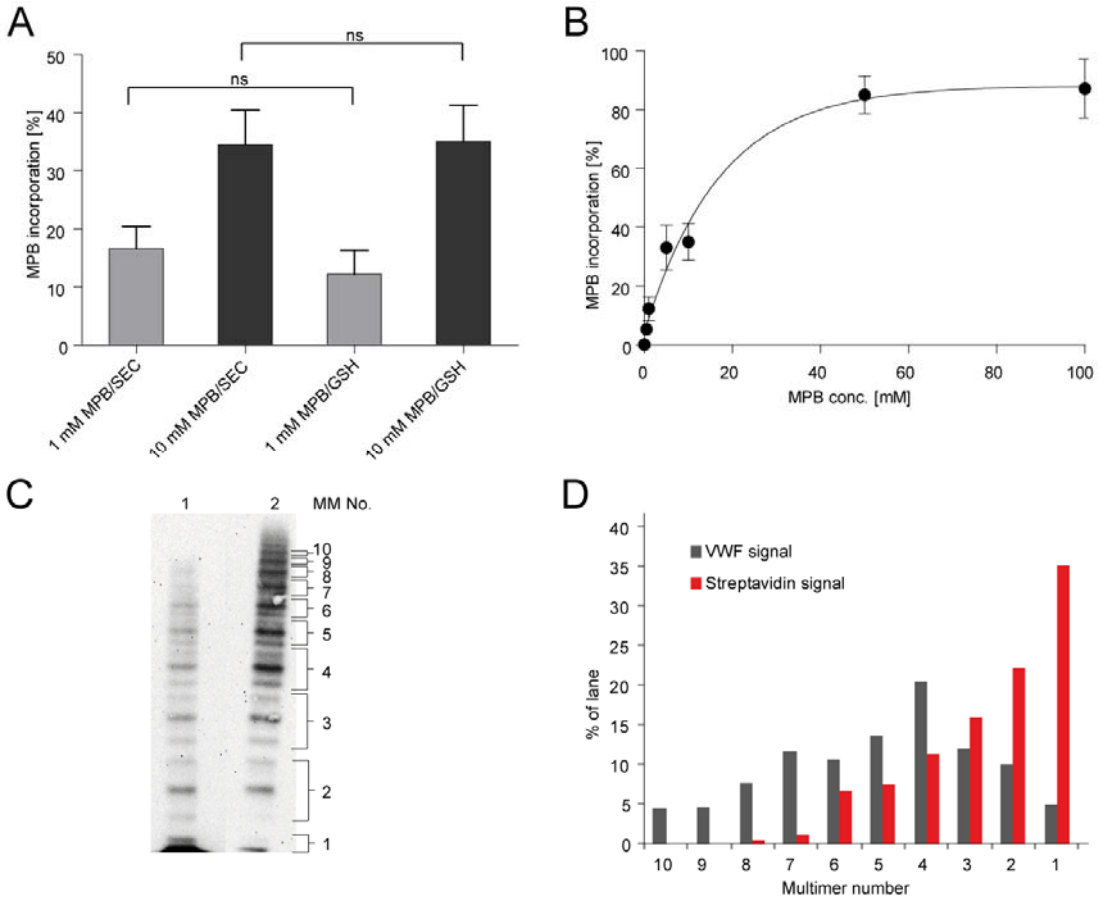

Fig. 21. Amount and location of MPB label incorporation into VWF. (A) The MPB derivatization was performed using 1 mM or 10 mM MPB per 30 µg/ml VWF. Excess of reagent was removed by size exclusion chromatography on PD-10 columns (SEC), or reaction was stopped by the addition of 2 or 20 mM of GSH respectively (GSH). Samples were captured onto microtitre plates with polyclonal anti-VWF antibodies. Bound VWF was detected with anti-VWF-HRP and MPB label with streptavidin-HRP. Ns.-not significant in *t*-test, n=4. (B) The MPB derivatization was performed using 0.5-100 mM MPB per 30 µg/ml VWF and the reaction was quenched with 1-200 mM GSH respectively. The ELISA assay was performed as in (A). (C) MMA of the 10 mM MPB derivatized sample, 1-detected with streptavidin-HRP, 2-detected with anti-VWF-HRP. (D) Densitometric analysis of MMA shown in C.

4.2.2 MALDI-MS analysis of MPB derivatization products

MPB incorporation was analyzed mass spectrometrically as well. As the interpretation of mass spectrometric data obtained from measurements of derivatized peptide mixtures is

challenging, exemplary experiments using a sample decapeptide were performed. To understand and interpret the data obtained with VWF correctly, a synthetic decapeptide with two reduced cysteine residues was analysed after MPB attachment. The molecular weight of the non-derivatized decapeptide is 1154.2 Da in the reduced state. The attachment of two MPB molecules theoretically raises the molecular weight of the peptide to 2204.6 Da, assuming a molecular weight of 525.2 Da for the MPB molecule (Fig. 22A). The spectrum of all obtained derivatization products is shown in Fig. 23A. In fact, one of the obtained derivatization products had a molecular weight of 2204.7 Da and it was assigned to a peptide with two derivatized cysteine residues. As shown in Fig. 23A two additional products were obtained with molecular masses 18 Da and 2 x 18 Da higher than the 2204.7 Da peptide. Those peaks were assigned to the derivatization products containing one or two hydrolyzed maleimide rings respectively. The hydrolysis of the maleimide ring has been described by Majima et al., (1995) and is depicted in Fig. 22C.

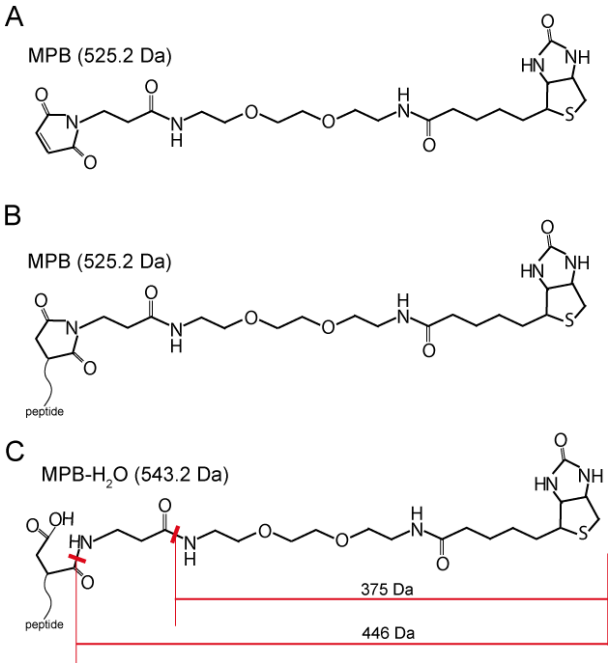

Fig. 22. Structure of Maleimide-PEO2-biotin and possible fragmentation mode. (A) The structure of unmodified reagent. (B) Product of the reaction between MPB and a peptide containing free SH group. (C) Further modification of the product shown in (B), which is hydrolysis and opening of the maleimide ring. Red thick bars represent proposed breakage positions during MALDI-MS/MS. The mass of resulting fragments is indicated.

For each of the three derivatization products MALDI-MS/MS spectra were generated and the obtained fragment ions were analyzed (Fig. 23B, C, D). Fig. 23B shows the ions obtained after fragmentation of the 2204.7 Da product; b and y ions which could be assigned to the peptide sequence are marked black, W marks the tryptophan immonium ion. Analysis of the fragment ion spectrum of the single-hydrolyzed derivatization product (Fig. 23C) revealed the presence of an additional very strong signal at 1776.3 Da. After analysis of this mass and evaluation of the structure of the hydrolyzed MPB reagent; this mass could be assigned to the product of MPB

decomposition resulting in the 446 Da loss from the parent mass (2222.7 Da), schematically presented on the Fig. 22C. Such fragmentation is reasonable on account of the fact, that MPB reagent contains in its structure amide bonds which break down upon peptide fragmentation by MS/MS. Furthermore, the water molecule added during the MPB hydrolysis process was also split off from the molecule (2204.7 Da), and the resulting molecule lost again 446 Da resulting in a 1759.2 Da fragment (note red bidirectional arrows marking the distance in the Fig. 23C insert). Additionally, two fragments resulting from the complete loss of the reagent mass (543.2) with masses of 1679.0 and 1661.4 were identified. The analysis of the fragment ion spectrum of the double-hydrolyzed derivatization product (Fig. 23D) confirmed this fragmentation mode. As this molecule contains two apparently ‘labile’ hydrolyzed maleimide groups, the parent ion (2240.7) first loses 446 Da, and the originated molecule loses again 446 Da. The loss of one or two water molecules again results in fragments following the same fragmentation scheme, which is visible on the spectrum as a series of 18 Da spaced peptides, which loose 446 Da (note red bidirectional arrows marking the distance on the Fig. 23D, insert). Whereas the characteristic distances from the parent ion (446 Da, 543 Da) arise only in the samples with hydrolyzed maleimide ring, small fragments (270.0 Da, 375.0 Da and 446.0 Da) resulting from the same fragmentation are visible in all MPB label containing spectra (Fig. 23B, C, D; red marked masses). While it is plausible from the MPB structure that fragments of 375 Da and 446 Da are generated in an MS/MS experiment, the occurrence of a 270 Da fragment is not instantly clear. It might represent a cysteine residue to which the remainder of the MPB moiety after a loss of 375 Da remains attached.

In summary, mass spectrometric analysis of the MPB-derivatized model-peptide considerably simplifies the interpretation of the complex data obtained by analysis of VWF peptides. Moreover the presence of the characteristic fragmentation mode allows rapid identification and confirmation of MPB attachment.

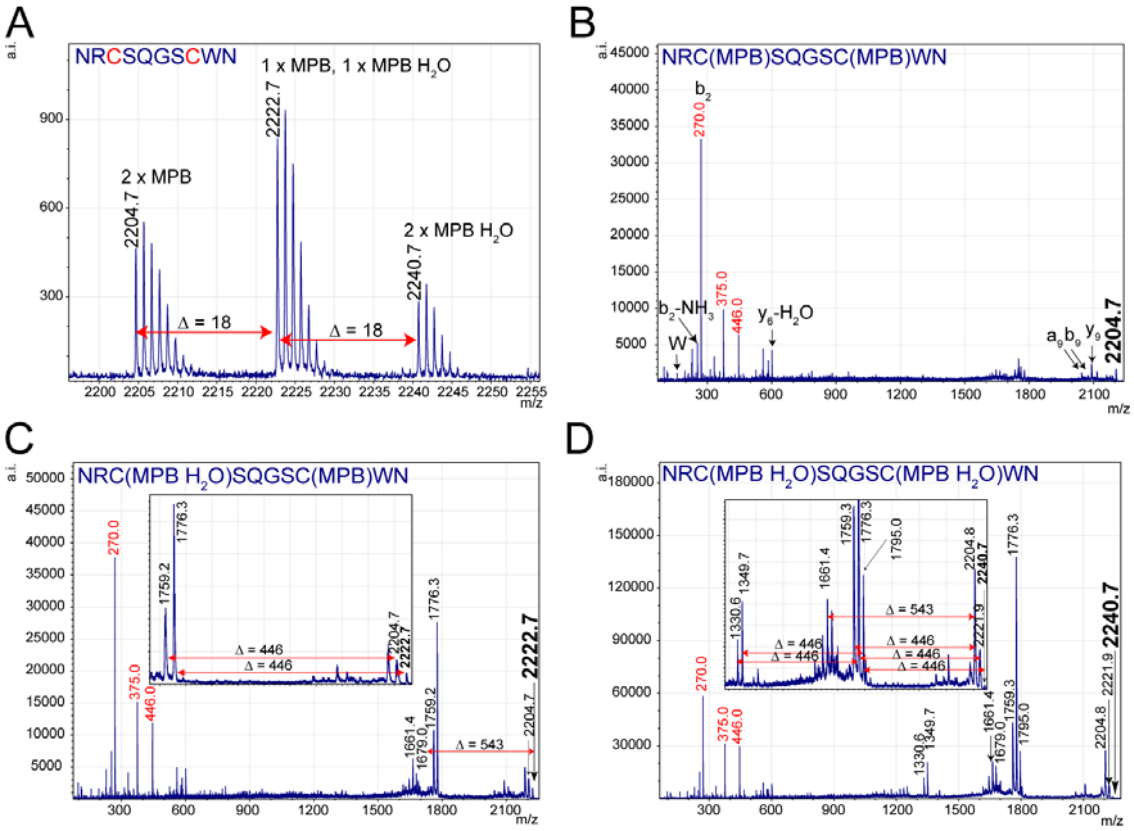

Fig. 23. MALDI-MS analysis of the MPB derivatized synthetic peptide. (A**)** All obtained derivatization products of the synthetic peptide. **(**B**)** Fragment spectrum of the non-hydrolyzed derivatization product. **(**C**)** Fragment spectrum of the single hydrolyzed derivatization product. **(**D**)** Fragment spectrum of the double hydrolyzed derivatization product. The sequence of the peptide and the position of modified cysteine residue are indicated on top of each spectrum. Distance between significant masses is marked with red bidirectional arrows. Red marked masses represent MPB fragmentation products.

4.2.3 Analysis of MPB labelled domains and peptides in VWF

First, the distribution of free sulfhydryl groups within VWF domains was investigated. This was accomplished using *S.aureus* V8 protease by taking advantage of the fact, that this protease has only two specified cleavage sites within the native VWF molecule located between Glu^{1673}-Gly^{1674} and between Glu^{2128}-Glu^{2129} (Bockenstedt *et al.,* 1986; Fretto *et al.,* 1986; Girma *et al.,* 1986; Pareti *et al.,* 1987). Furthermore, application of this protease is advantageous, because it separates VWF *C*-terminal domains, which has been shown to posses free cysteine thiols (Choi *et al.,* 2007). The second, independent experimental setup was the mass spectrometric analysis of the VWF sample derivatized with 10 mM MPB. A detailed, mass spectrometric analysis of unpaired cysteine residues could be performed after enrichment of MPB-labelled peptides. Without enrichment, both NEM- and MPB-labelled peptides were not detectable in the spectra after trypsin digestion. In addition to evaluation of peptides resulting from derivatization of VWF in buffer solution, the redox-state of cysteine residues on the VWF molecule bound to collagen type III was tested. The change in the redox state of the cysteine residues in VWF bound to collagen is interesting since it reflects the possible thiol-disulfide reorganisation accompanying the conformational transition from soluble to immobilized. To

solubilise the collagen type III bound VWF and make all possible cysteine residues accessible, 2 % SDS solution was added during the MPB derivatization. Finally, a control sample in solution containing 2 % SDS was also derivatized and analyzed.

S.aureus V8 protease cleavage products were separated on SDS-PAGE under reducing conditions. Reduced cleavage products were detected either by Coomassie staining or by Western blotting and subsequent streptavidin detection (Fig. 24). The sequences of three major cleavage fragments were additionally confirmed by MS analysis. As previously described by (Fretto *et al.,* 1986), the 170 kDa fragment was identified as an *N*-terminal fragment encompassing TIL3-D4 domains; the 110 kDa fragment was identified as a *C*-terminal fragment encompassing C1-CK domains and a part of D4 domain. The 50 kDa fragment was identified as a *C*-terminal part of 170 kDa fragment encompassing A3 and D4 domains. The exact sequences of the fragments are given in Fig. 30. Strong MPB signals were detected in the 170 kDa and 110 kDa fragments. These results indicate that both the *N*- and the *C*- terminus of the protein contain free cysteine residues. A very faint signal was also detected in the 50 kDa band, which suggests that some cysteine residues were also derivatized in the A3/D4 domain fragment.

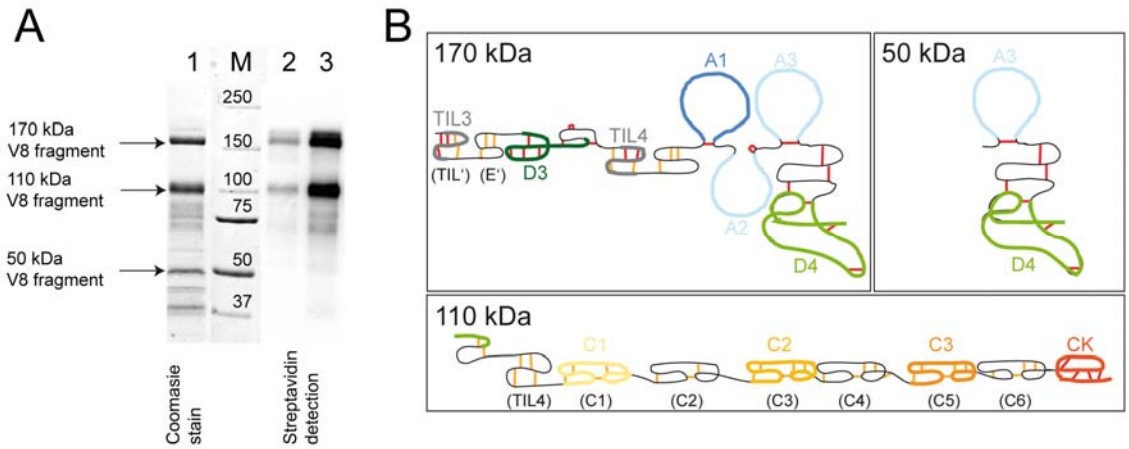

Fig. 24. Incorporation of MPB into *S.aureus* V8 protease fragments. VWF samples derivatized with 1 mM (lane 2) and 10 mM MPB (lane 3) were digested under non-reducing conditions in Tris-HCl buffer, pH 7.8 O/N at 37°C with V8 protease. (A) Cleavage products were separated on reducing 8-16 % SDS-PAGE and stained with Coomassie (lane 1) or blotted on nitrocellulose membrane and detected with streptavidin-HRP conjugate (lanes 2 and 3). M stands for molecular weight marker; molecular weights are expressed in kDa. (B) Illustration of cleavage products.

The majority of the enriched, MPB containing peptides derived from the sample derivatized in buffer could be assigned to MPB-derivatized VWF peptide masses. The spectrum of the eluate is shown in Fig. 25A and a list of assigned peptide sequences is presented in Tab. 4. Most of the peptide-attached MPB label was in the hydrolyzed state, which is reasonable considering the fact that after labelling long processing of the sample is conducted partly at alkaline pH (trypsin digestion). Under these high pH conditions the maleimide ring has been shown to hydrolyze rapidly (Majima *et al.,* 1995). For several peptides, especially for peaks

with high intensity, a small non-hydrolyzed version of the same peptide was found. Surprisingly three peptides were found with strong signals originating from both peptides with non-hydrolyzed and hydrolyzed MPB label. In these cases the non-hydrolyzed peak was more intense than the hydrolyzed version of the same peptide. This was observed to be the case for peptides, in which the MPB label was attached to the cysteine residue placed *C*-terminal of the trypsin cleavage site (peptides marked with arrows Fig. 25A). Six out of the peptides identified in this experiment have previously been described to contain unpaired cysteine residue (Choi *et al.,* 2007; Ganderton *et al.,* 2011) (peptides in Tab. 4 marked with one asterisk). Seven peptides were further characterized by MALDI-MS/MS to confirm the assigned sequence. Those peptides are marked in the Tab. 4 with two asterisks. The MS/MS fragment ion spectrum of the most intensive peptide in the eluate with the mass of 1717.8 Da is shown in Fig. 25B. In this particular case the label was not attached to a cysteine residue, but to the α-amino group of the protein *N*-terminus. Maleimide groups have been shown to be reactive towards amino groups at alkaline pH, therefore the derivatization presented in this study was performed at pH 7.0. Though it is possible that the α-amino group is a target for the nucleophilic attack of the maleimide reagent because of the low pK_a value of 9.2, compared with the γ-amino group of lysine residue which has a pK_a of 10.8 (Stryer, 1990). The prominent presence of this peptide may also indicate the high accessibility of protein *N*-terminus in the coiled VWF structure, and it is most probable that the same process occurs during the derivatization with NEM. In Fig. 27, interpreted fragment ion spectra of six peptides with cysteine-attached MPB label are presented. As expected for all spectra with fragment ions derived from a peptide with attached hydrolyzed MPB label, the characteristic losses of 446 and 543 Da (note the red bidirectional arrows) as well as the 270 Da, 375 Da and 446 Da peaks are observed.

In summary, the application of MPB for derivatization enabled the identification of exact position of the free thiol groups in VWF. The enrichment by streptavidin immunoprecipitation was highly specific as the majority of eluted peptide masses could be assigned to derivatized peptides. Moreover, the characteristic fragmentation spectra confirmed the presence of the label.

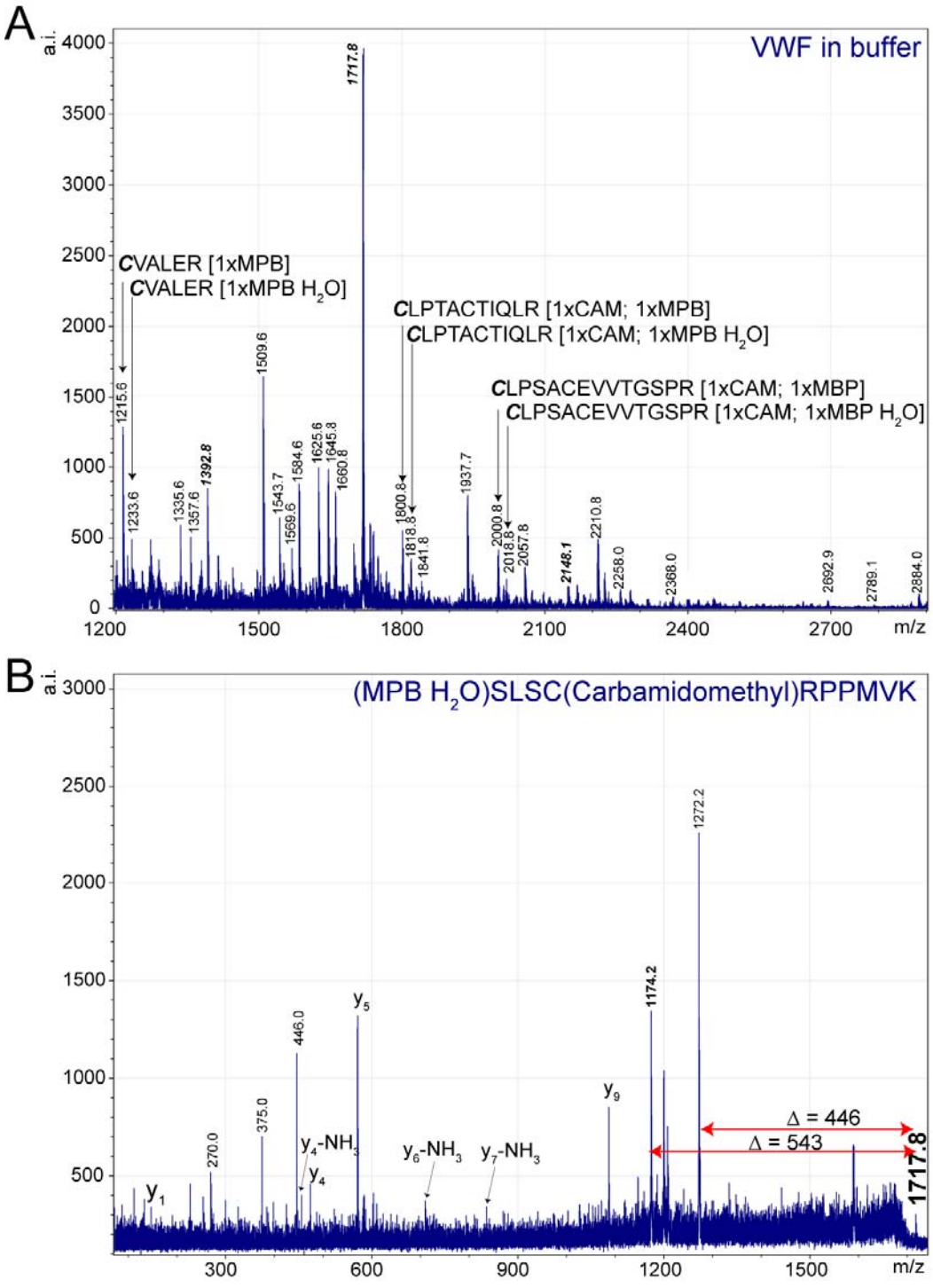

Fig. 25. Identification of unpaired cysteine residues in VWF accessible for MPB derivatization in buffer. VWF was labelled with biotin-linked maleimide (MPB) in Tris-HCl buffer and resolved on SDS-PAGE. After in-gel trypsin digestion of ~270 kDa VWF band, MPB linked peptides were purified and enriched on streptavidin sepharose beads. The eluate was analysed using MALDI-MS. (A) MALDI-MS spectrum of all MPB derivatized cysteines in buffer solution. Peptides marked with arrows show characteristic 18 Da distance between non-hydrolyzed and hydrolyzed MPB ring. (B) MS/MS spectrum of the prominent 1717.8 Da peptide, the identified sequence, and modified *N*-terminal α-amino group are indicated on the top of the spectrum. Characteristic 446 and 543 Da distances for the MPB fragmentation are marked with red bidirectional arrows.

The second analyzed VWF sample was derivatized in the presence of 2 % SDS. This spectrum was compared with the in-buffer derivatized sample spectrum. The comparison revealed high level of similarity (Fig. 25A *vs.* Fig. 26A). However, both spectra differed in the relative intensity of the 1717.8 Da-peptide, which was significantly less intense in the sample derivatized in the presence of SDS. This finding confirms the concept of a high accessible *N*-terminal α-amino group present on the surface of coiled VWF protein in buffer solution, which is abrogated after SDS solubilisation. This possibly also implies that uncoiled protein presents more unpaired cysteine residues and therefore the extent of the reaction with the protein *N*-terminus appears to be reduced. Apart from the 1717.8 Da-peptide all peaks had comparable relative intensities. The second difference was the presence of an additional peptide in the spectrum of the SDS-solubilised sample (Fig. 26A; green marked peptide), which is also listed in the Tab. 4. Finally, in the spectrum obtained with the sample derivatized in buffer solution, additional peaks were detected which could not be assigned to MPB-derivatized VWF peptides (1392.8 Da and 2148.1 Da; Fig. 25A; peptides marked in bold italic font). The fragment ion spectra of both peptides revealed the presence of characteristic 446 and 543 Da distances, unfortunately the sequences could not be determined.

Upon VWF binding to extracellular matrix constituents, amongst other to collagen type III, the conformation of VWF changes (Bendetowicz *et al.,* 1999; Ulrichts *et al.,* 2006). After transition from soluble to immobilized state VWF apparently displays a GPIb binding conformation (Hulstein *et al.,* 2005; Kang *et al.,* 2007), which enables platelets in flowing blood to interact with it. Moreover, conformational changes in the A3 domain modulate the interaction between A1 domain and platelet-GPIb receptor (Obert *et al.,* 1999). The following experiment was performed in order to elucidate, whether the conformational change in VWF induced by collagen type III binding involves new disulfide pairing, or if this new conformation is stabilized by new disulfide bonds formed by originally free sulfhydryl groups. To accomplish this, spectra obtained for on-collagen derivatized VWF and for VWF derivatized in-solution were compared (Fig. 25A *vs*. B). Again, identical peptides were found, however relative intensities of some peptides were noticeably lower when compared to intensities of the same peptides in the control spectrum (red marked peptides on Fig. 26A and B). For example, the peptide with a mass of 2210.8 Da originally significantly more intensive than the neighbouring 2258.0 Da peptide in Fig. 25A possesses the same intensity as the 2258.0 Da peptide in control spectrum (Fig. 25B) (note peaks marked with red arrowheads on both spectra). Similarly the 2000.8, 1584.6 and 1335.6 Da peptides have lower relative intensities compared to the respective signals in the control spectrum and the neighbouring peaks in the same spectrum (Fig. 25; note peaks marked with green, blue and black arrowheads on both spectra respectively). Additionally, the intensity of the 1717.8 Da peptide is drastically reduced, which

may also indicate reduced accessibility. These observations were made consistently in two independent experiments.

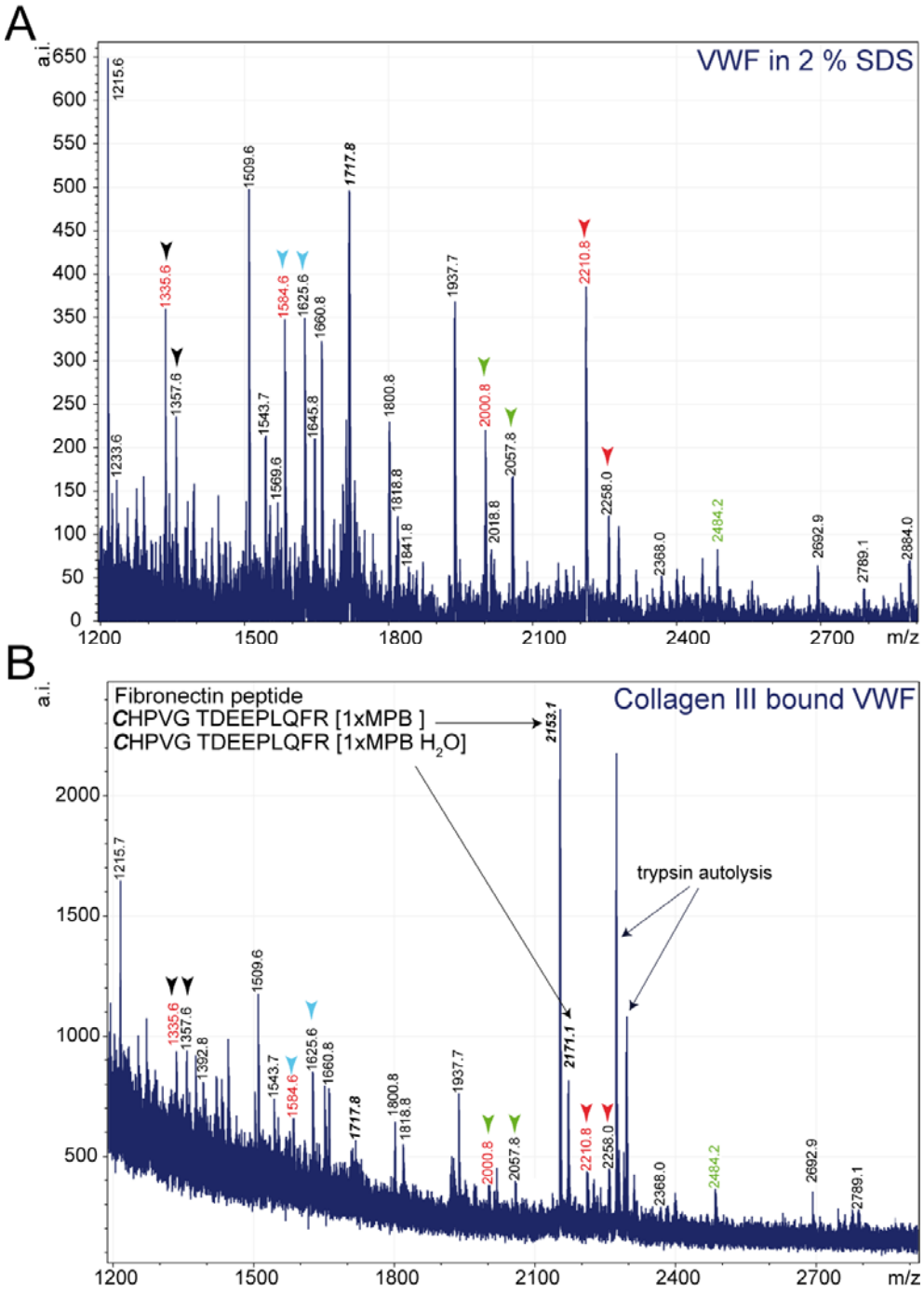

Fig. 26. Identification of unpaired cysteine residues in VWF, and comparison between all sulfhydryl groups as well as sulfhydryl groups accessible after VWF-collagen type III binding. VWF in solution (A) or collagen type III bound VWF (B) was labelled with biotin-linked maleimide (MPB) in Tris-HCl buffer with 2 % SDS. Samples were resolved on SDS-PAGE. After in-gel trypsin digestion of ~270 kDa VWF bands, MPB-linked peptides were purified and enriched on streptavidin sepharose beads. The eluate was analysed using MALDI-MS. (B) Most prominent peaks in spectrum (marked by black arrows) were assigned to fibronectin. (A), (B) Peptide masses which are noticeably less intense in spectrum (B) compared to spectrum (A) are marked in red. The peptide, which is only detectable in samples derivatized in the presence of SDS is marked green (absent in Fig. 25 spectrum A).

Furthermore, the most prominent difference between those two spectra (Fig. 26A, B) is the presence of two peaks in the on-collagen derivatized VWF sample, which both could be assigned to the same fibronectin peptide (Fig. 26B-peaks marked with black arrows). The sequence, position and the fragment ion spectrum of hydrolyzed and non-hydrolyzed form of identified peptide is presented in the Fig. 28 and Tab. 5. The appearance of this peptide in the spectrum again confirms all previous observations: First, the signal for the peptide containing a non-hydrolyzed maleimide ring is more intense than the signal for its hydrolyzed counterpart, because of the fact, that the MPB label is attached to the *N*-terminal cysteine residue, thus adjacent to the cleavage site. Second, in the fragment ion spectrum of the peptide with the hydrolyzed maleimide ring but not with the non-hydrolyzed ring characteristic 446 Da and 543 Da losses are observed (Fig. 28A and B).

Tab. 4. Sequences of peptides labelled with MPB. All masses which could be assigned to MPB-labelled VWF peptides are listed. Peptide sequences marked by two asterisk were confirmed by MS/MS. Free sulfhydryl groups in peptides marked by one asterisk were previously identified (Choi *et al.,* 2007; Ganderton *et al.,* 2011). Cysteine residues modified by MPB are bold and underlined. Cysteine residues in peptides, in which the exact MPB label position was not identified, are shown in italic font.

POSITION	SEQUENCE	REDUCED CYS POSITION	MASS [Da]
764-773	**S**LSCRPPMVK.l [1xCarbamidomethyl; 1xMPB H_2O] **	-	1717.8
764-773	SLS**C**RPPMVK.l [1xMPB H_2O] **	767	1660.8
774-782	k.LV**C**PADNLR.a [1xMPB H_2O]	776	1543.7
821-826	r.**C**VALER.c [1xMPB] **	821	1215.6
913-920	k.G**C**SHPSVK.c [1xMPB H_2O]	914	1357.6
1027-1035	k.VSSQ**C**ADTR.k [1xMPB H_2O] **	1031	1509.6
1053-1061	k.QTMVDSS**C**R.i [1xMPB H_2O]	1060	1569.6
1122-1133	r.TATL*C* PQS*C* EER.n [1xCarbamidomethyl; 1xMPB H_2O]	1126/1130	1937.7
1944-1956	r.WTCPCV**C**TGSSTR.h [2xCarbamidomethyl; 1xMPB H_2O] **	1950	2057.8
2081-2099	k.TYGL*C* GI*C* DENGANDFMLR.d [1xCarbamidomethyl; 1xMPB H_2O]	2086/2089	2692.9
2364-2369	r.KEE**C**KR.v [1xMPB H_2O] **	2367	1335.6
2465-2478	r.VAQ**C**SQKPCEDSCR.s [2xCarbamidomethyl; 1xMPB H_2O] * **	2468	2210.8
2479-2493	r.SGFTYVLHEGE*CC* GR.c [1xCarbamidomethyl; 1xMPB H_2O] *	2490/2491	2258.0
2494-2507	r.**C**LPSACEVVTGSPR.g [1xCarbamidomethyl; 1xMPB]	2494	2000.8
2516-2535	k.SVGSQWASPENP*C* LINE*C* VR.v [1xCarbamidomethyl; 1xMPB H_2O] *	2528/2533	2789.1
2567-2575	k.TSAC**C**PSCR.c [2xCarbamidomethyl; 1xMPB H_2O] *	2571	1584.6
2594-2604	k.TVMIDV**C**TTCR.c [1xCarbamidomethyl; 1xMPB H_2O] *	2600	1841.8
2644-2654	r.**C**LPTACTIQLR.g [1xCarbamidomethyl; 1xMPB]	2644	1800.8
2663-2677	k.RDETLQDG*C* DTHF*C* K.v [1xCarbamidomethyl; 1xMPB H_2O]	2671/2676	2368.0
2711-2730	k.IPGT*CC* DTCEEPECNDITAR.l [3xCarbamidomethyl; 1xMPB H2O] *	2715/2716	2884.0

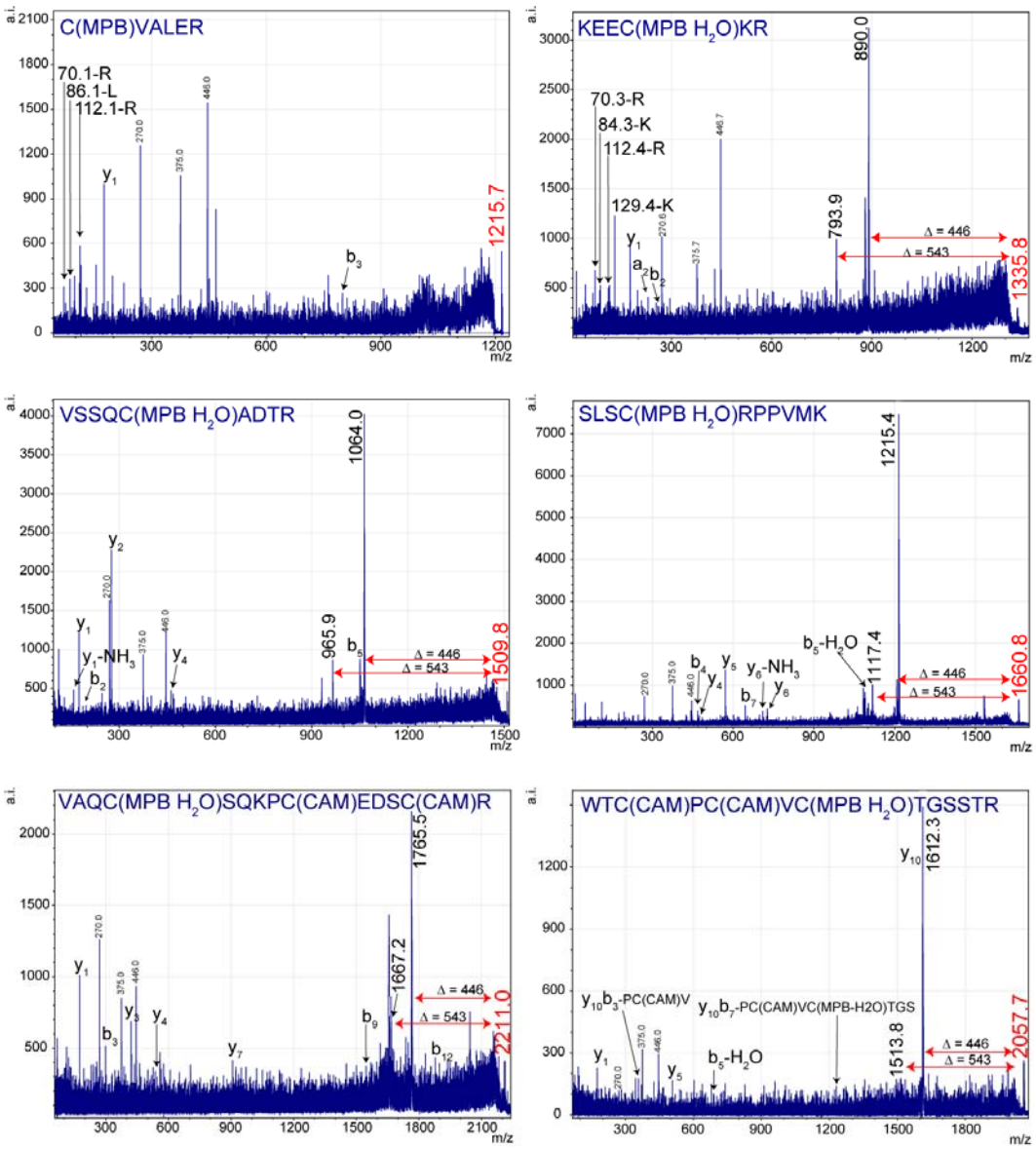

Fig. 27. MALDI-MS/MS spectra of MPB-labelled peptides. The identified sequence and modified cysteine residues are indicated on the top of the spectra. Characteristic 446 and 543 Da distance for the MPB fragmentation is marked with red bidirectional arrows.

Interestingly, the identified fibronectin peptide, though generated with trypsin, is not specifically cleaved at the *C*-terminus. Unexpectedly it is cleaved after serine residue; see Tab. 5). This may just result from an unspecific cleavage, but it may as well indicate the generation of a new potential cleavage site for trypsin at the site of MPB attachment. However, this was observed only in this one case and would therefore require further analysis.

Tab. 5. Sequence and position of the MPB-labelled fibronectin peptide.

POSITION	SEQUENCE	REDUCED CYS POSITION	MASS [Da]
2136-2149	s.CHPVGTDEEPLQFR.v [1xMPB]	2136	2153.1
2136-2149	s.CHPVGTDEEPLQFR.v [1xMPB H_2O]	2136	2171.1

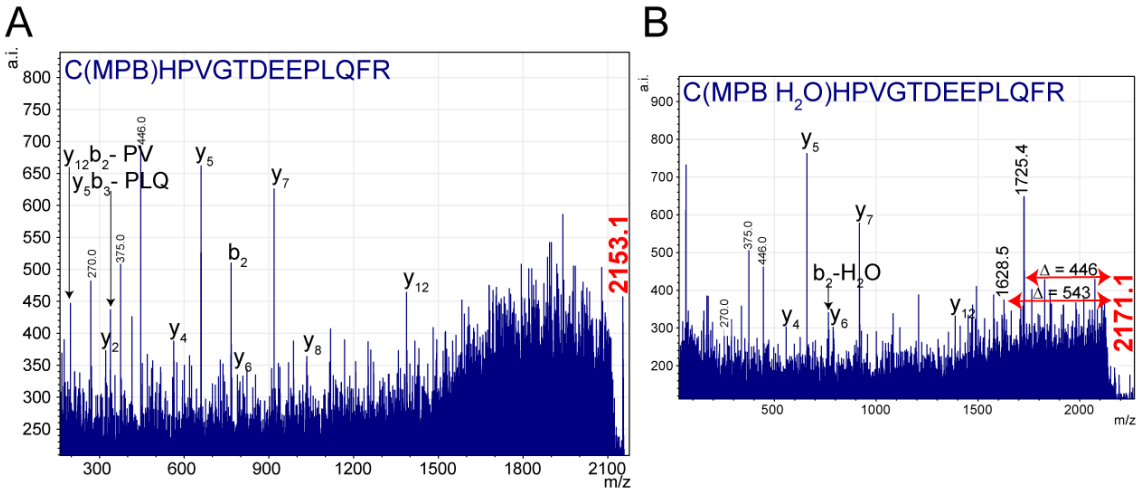

Fig. 28. MALDI-MS/MS spectra of MPB labelled fibronectin peptide. (A) MS/MS spectrum of the peptide containing a non-hydrolyzed MPB ring. (B) MS/MS spectrum of the same peptide containing hydrolyzed MPB ring (note characteristic distances marked by red bidirectional arrows).

In general, this finding indicate an enrichment of fibronectin on the collagen type III surface and that collagen type III-bound fibronectin possesses at least one unpaired cysteine residue. The enrichment of fibronectin - present in a very low amount in the original sample - on the collagen type III surface was also detected in the collagen-bound VWF sample prior to enrichment on streptavidin sepharose beads (Fig. 29). The detected free thiol group of fibronectin is placed within the last (III-15) of a total of fifteen tandem FN-III domain repeats near the fibrin binding site at the protein *C*-terminus. This cysteine residue has previously been described as one of two free cysteine residues in fibronectin buried within the tertiary structure of the domain (Smith *et al.*, 2007; Lemmon *et al.*, 2011).

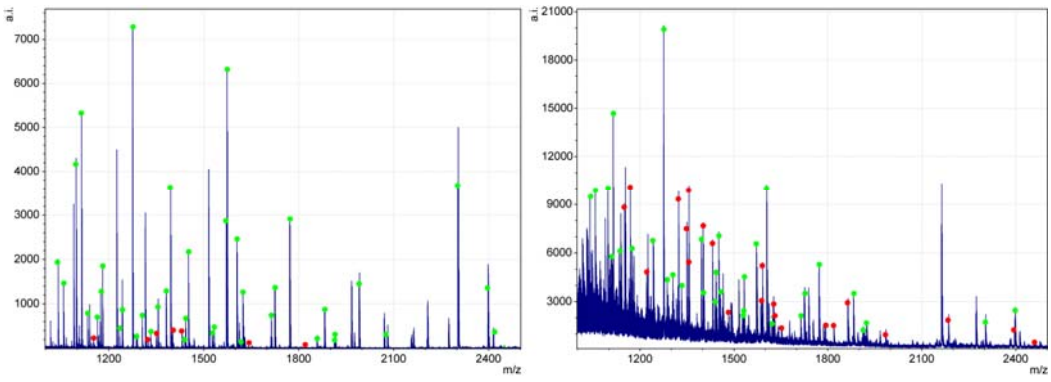

Fig. 29. Intensity of fibronectin signals in samples prior to enrichment on streptavidin sepharose. An in-solution (left hand side spectrum) and collagen type III-bound (right hand side spectrum) VWF sample was labelled with MPB in the presence of 2 % SDS. After SDS-PAGE the 270 kDa band gel slice was digested with trypsin and analyzed with MALDI-MS. Peptides marked with green dots could be assigned to the VWF sequence, peptides marked with red dots could be assigned to the fibronectin sequence.

All unpaired cysteine residues identified in the VWF molecule are summarized in Fig. 30 (marked yellow or underlined). The VWF sequence is presented to indicate the VWF fragments generated by the *S.aureus* V8 protease and thereby facilitating a comparison with streptavidin signal intensities observed on the Western blot (Fig. 24). The strong streptavidin signals in 170 and 110 kDa fragments on the Western blot correlate well with the detection of several free cysteine residues in corresponding sequences by mass spectrometry. The faint streptavidin signal in the 50 kDa band on Western blot could be assigned to two cysteine residues with attached MPB label identified by mass spectrometry.

170 kDa (residues 764-2128)

SLSCRPPMVK LVCPADNLRA EGLECTKTCQ NYDLECMSMG CVSGCLCPPG MVRHENRCVA LERCPCFHQG
KEYAPGETVK IGCNTCVCQD RKWNCTDHVC DATCSTIGMA HYLTFDGLKY LFPGECQYVL VQDYCGSNPG
TFRILVGNKG CSHPSVKCKK RVTILVEGGE IELFDGEVNV KRPMKDETHF EVVESGRYII LLLGKALSVV
WDRHLSISVV LKQTYQEKVC GLCGNFDGIQ NNDLTSSNLQ VEEDPVDFGN SWKVSSQCAD TRKVPLDSSP
ATCHNNIMKQ TMVDSSCRIL TSDVFQDCNK LVDPEPYLDV CIYDTCSCES IGDCACFCDT IAAYAHVCAQ
HGKVVTWRTA TLCPQSCEER NLRENGYECE WRYNSCAPAC QVTCQHPEPL ACPVQCVEGC HAHCPPGKIL
DELLQTCVDP EDCPVCEVAG RRFASGKKVT LNPSDPEHCQ ICHCDVVNLT CEACQEPGGL VVPPTDAPVS
PTTLYVEDIS EPPLHDFYCS RLLDLVFLLD GSSRLSEAEF EVLKAFVVDM MERLRISQKW VRVAVVEYHD
GSHAYIGLKD RKRPSELRRI ASQVKYAGSQ VASTSEVLKY TLFQIFSKID RPEASRITLL LMASQEPQRM
SRNFVRYVQG LKKKKVIVIP VGIGPHANLK QIRLIEKQAP ENKAFVLSSV DELEQQRDEI VSYLCDLAPE
APPPTLPPDM AQVTVGPGLL GVSTLGPKRN SMVLDVAFVL EGSDKIGEAD FNRSKEFMEE VIQRMDVGQD
SIHVTVLQYS YMVTVEYPFS EAQSKGDILQ RVREIRYQGG NRTNTGLALR YLSDHSFLVS QGDREQAPNL
VYMVTGNPAS DEIKRLPGDI QVVPIGVGPN ANVQELERIG WPNAPILIQD FETLPREAPD LVLQRCCSGE
GLQIPTLSPA PDCSQPLDVI LLLDGSSSFP ASYFDEMKSF AKAFISKANI GPRLTQVSVL QYGSITTIDV
PWNVVPEKAH LLSLVDVMQR EGGPSQIGDA LGFAVRYLTS EMHGARPGAS KAVVILVTDV SVDSVDAAAD
AARSNRVTVF PIGIGDRYDA AQLRILAGPA GDSNVVKLQR IEDLPTMVTL GNSFLHKLCS GFVRICMDED
GNEKRPGDVW TLPDQCHTVT CQPDGQTLLK SHRVNCDRGL RPSCPNSQSP VKVEETCGCR WTCPCVCTGS
STRHIVTFDG QNFKLTGSCS YVLFQNKEQD LEVILHNGAC SPGARQGCMK SIEVKHSALS VELHSDMEVT
VNGRLVSVPY VGGNMEVNVY GAIMHEVRFN HLGHIFTFTP QNNEFQLQLS PKTFASKTYG LCGICDENGA
NDFMLRDGTV TTDWKTLVQE WTVQRPGQTC QPILE

50 kDa (residues 1674-2128)

CCSGEGLQIP TLSPAPDCSQ PLDVILLLDG SSSFPASYFD EMKSFAKAFI SKANIGPRLT QVSVLQYGSI
TTIDVPWNVV PEKAHLLSLV DVMQREGGPS QIGDALGFAV RYLTSEMHGA RPGASKAVVI LVTDVSVDSV
DAAADAARSN RVTVFPIGIG DRYDAAQLRI LAGPAGDSNV VKLQRIEDLP TMVTLGNSFL HKLCSGFVRI
CMDEDGNEKR PGDVWTLPDQ CHTVTCQPDG QTLLKSHRVN CDRGLRPSCP NSQSPVKVEE TCGCRWTCPC
VCTGSSTRHI VTFDGQNFKL TGSCSYVLFQ NKEQDLEVIL HNGACSPGAR QGCMKSIEVK HSALSVELHS
DMEVTVNGRL VSVPYVGGNM EVNVYGAIMH EVRFNHLGHI FTFTPQNNEF QLQLSPKTFA SKTYGICGIC
DENGANDFML RDGTVTTDWK TLVQEWTVQR PGQTCQPILE

110 kDa (residues 2129-2813)

EQCLVPDSSH CQVLLLPLFA ECHKVLAPAT FYAICQQDSC HQEQVCEVIA SYAHLCRTNG VCVDWRTPDF
CAMSCPPSLV YNHCEHGCPR HCDGNVSSCG DHPSEGCFCP PDKVMLEGSC VPEEACTQCI GEDGVQHQFL
EAWVPDHQPC QICTCLSGRK VNCTTQPCPT AKAPTCGLCE VARLRQNADQ CCPEYECVCD PVSCDLPPVP
HCERGLQPTL TNPGECRPNF TCACRKEECK RVSPPSCPPH RLPTLRKTQC CDEYECACNC VNSTVSCPLG
YLASTATNDC GCTTTTCLPD KVCVHRSTIY PVGQFWEEGC DVCTCTDMED AVMGLRVAQC SQKPCEDSCR
SGFTYVLHEG ECCGRCLPSA CEVVTGSPRG DSQSSWKSVG SQWASPENPC LINECVRVKE EVFIQQRNVS
CPQLEVPVCP SGFQLSCKTS ACCPSCRCER MEACMLNGTV IGPGKTVMID VCTTCRCMVQ VGVISGFKLE
CRKTTCNPCP LGYKEENNTG ECCGRCLPTA CTIQLRGGQI MTLKRDETLQ DGCDTHFCKV NERGEYFWEK
RVTGCPPFDE HKCLAEGGKI MKIPGTCCDT CEEPECNDIT ARLQYVKVGS CKSEVEVDIH YCQGKCASKA
MYSIDINDVQ DQCSCCSPTR TEPMQVALHC TNGSVVYHEV LNAMECKCSP RKCSK

Fig. 30. Position of unpaired cysteine residues in the VWF sequence illustrated on *S.aureus* V8 protease fragments. The sequence of the three *S.aureus* digestion fragments with highlighted VWF-A1 (light grey) and A3 (dark grey) domains and characteristic CGXC sequences (framed red) is depicted. All cysteine residues are marked red. All identified unpaired cysteine residues are highlighted in yellow. Peptides, where the exact MPB label position was not identified are underlined.

4.3 Disulfide bond configuration and distribution of free thiol groups in VWF

All unpaired cysteine residues identified in VWF in the present study were found to exist in paired state as well. The respective disulfide bonds were previously either chemically confirmed or predicted by homology. Beyond identification of disulfide bonds and their location within the molecule, knowledge of the possible function of the respective disulfide bond may be evaluated. The differentiation, whether a disulfide bond fulfils a structural or functional role, can be partly deducted from its three dimensional configuration. In order to better understand the VWF disulfide pairing and to assess potential function of reduced cysteine residues at a given position in the VWF molecule; the analysis of VWF disulfide configuration was performed. For this purpose, the available X-ray crystallography and homology data was analysed by *in silico* modelling. The three dimensional structure of the VWF TIL- and VWF C-domain was predicted using I-TASSER, an online platform for protein structure and function predictions. The torsional angles forming the disulfide bond in the crystal structure data of VWF were measured using RasWin software, and the corresponding configuration was assigned according to Schmidt *et al.* (2006).

Of all VWF domains, only the most functionally relevant A1, A2 and A3 domains were crystallized so far. Consequently the conformation of present within the structure disulfide bonds can be estimated. In fact the disulfide bond forming the A1 domain loop has a spiral conformation in the crystal structure (Emsley *et al.,* 1998) and its structural importance is confirmed by the fact, that the reduction of this bond results in abrogation of the interaction with platelet GPIb receptor (Cruz *et al.,* 1993). In contrast, the rare disulfide bond formed between two adjacent cysteine residues in the A2 domain exhibits a +/-LHStaple conformation with high dihedral strain energy (DSE) and short Cα distance (Azimi *et al.,* 2011) indicating a regulatory function. Interestingly, the A2 domain with the paired vicinal cysteines is resistant to ADAMTS-13 cleavage, whereas the absence of this bond increases the susceptibility to cleavage (Luken *et al.,* 2010). This could contribute to the mechanism regulating the VWF cleavage susceptibility by ADAMTS-13. Fig. 31 illustrates the configuration of disulfide bonds in the crystal structure of A1 and A2 domains of VWF.

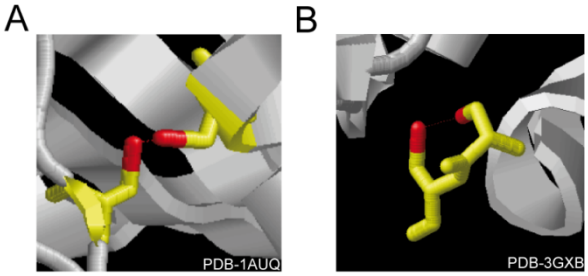

Fig. 31. Configuration of intramolecular disulfide bonds within VWF-A1 and A2 domains. (A) Spiral configuration of the disulfide bond forming the A1-domain loop. (PDB-1AUQ). (B) Hook configuration of the vicinal disulfide bond in the A2 domain. (PDB-3GXB). Three dimensional structures were depicted using RasWin software, cysteine residues are shown in yellow, and sulphur atoms in red**.**

The conformation and disulfide bond pairing of the residual, cysteine-rich, VWF domains was established using homology data by Zhou et al., (2012). Of particular interests is the proposed VWF C-domain conformation which - according to the authors - shares homology with the C domain of crossveinless 2. Fig. 32C and D show similar conformation of the crystal structure of crossveinless 2 and the three dimensional structure of VWF C3 (UniProt C2) domain predicted by I-TASSER. Interestingly, the ten cysteine residues within the C-domains are highly conserved between species and are linked according to Fig. 33B. The C-like domains lack one disulfide bond between Cys3-Cys5. This Cys3-Cys5 disulfide bond has a staple conformation and links adjacent strands within the same antiparallel β-sheet. Moreover this bond is exposed to solvent (Schmidt *et al.,* 2006) and it has been proposed to be involved in the *C*-terminal VWF self-association (Ganderton *et al.,* 2011).

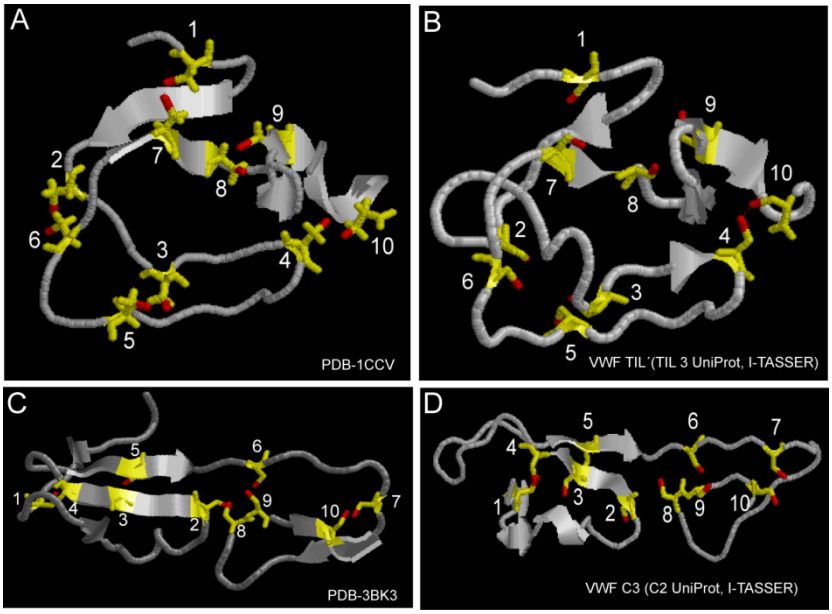

Fig. 32. Comparison between crystal structures of homologous proteins, and prediction of the three dimensional structures of VWF domains using the I-TASSER server. All structures were depicted using RasWin software. Cysteine residues are coloured yellow and numbered, and sulphur atoms are red. **(**A) Crystal structure of AMCI-1 (PDB-1CCV), all cysteines are disulfide bonded; (B) VWF TIL`(TIL3 UniProt) domain residues: Ser^{764}-Cys^{827} predicted by I-TASSER; only one disulfide bond between Cys1-Cys10 predicted; (C) Crystal structure of crossveinless 2 (PDB-1CCV), all cysteines are paired in disulfide bonds; (D) VWF C3 (C2 UniProt) domain residues: Lys^{2429}-Leu^{2496} predicted by I-TASSER; only one disulfide bond between Cys1-Cys4 predicted.

The *N*-terminus of the protein has been characterized in part by chemical analysis of the disulfide linkages and partly by evaluation of homology data. The crystal structure of the TIL domain is available from *Apis mellifera* chymotrypsin/cathepsin G inhibitor-1 (AMCI-1) and the structure of TIL domain of VWF, when predicted by I-TASSER (Fig. 32A, B), shows high level of similarity with the AMCI-1 structure. Moreover this similarity is confirmed by the chemically defined disulfide bonds. The configuration of five disulfide bonds in this domain is as follows: Cys1-Cys7: -LH Spiral; Cys2-Cys6: -/+ LHHook, Cys3-Cys5: -RHSpiral, Cys4-

Cys10: -RHHook, Cys8-Cys9: -LHSpiral. However in the neighbouring domains data determined from chemical analysis of disulfide bonds do not agree with the homology data. For example the three bonds: Cys^{1126}-Cys^{1130}, Cys^{1206}-Cys^{1199}, Cys^{1234}-Cys^{1237} between closely spaced cysteines (Marti *et al.,* 1987) were not predicted by homology. Interestingly, three cysteines (Cys^{1222}, Cys^{1225}, Cys^{1227}) near the A1 domain (Fig. 33A, green boxes in the E3 motif) were shown to form intermolecular VWF A1-domain dimer between *N*-termini of different VWF monomers. This A1 domain dimer has been analyzed repeatedly by limited proteolysis experiments (Andrews *et al.,* 1989a; Fujimura *et al.,* 1991), and expression experiments (Azuma *et al.,* 1991; Azuma *et al.,* 1993). The A1 domain dimer was identified as an additional structure not required for multimer assembly (Dong *et al.,* 1994). In contrast to experimental data, analysis of homology data indicates intramolecular linkages forming the E3 motif (Fig. 33A, orange disulfide bonds in the E3 motif).

Fig. 33A summarizes all identified unpaired cysteine residues identified in this study and their distribution within VWF domains. The cleavage sites of proteolytic enzymes applied in the present study are also depicted. The *N*-terminal region contains seven reduced cysteine residues. Two reduced cysteines, probably involved in the same disulfide bond, were detected in the D4 domain. The highest amount of eleven unpaired cysteine residues was found to be located in the *C*-terminal C-domains. The relative amount of four unpaired cysteine residues was reduced after collagen type III binding and the disulfide bonds, in which those cysteines are predicted to be involved, are marked red in the Fig. 33A. Furthermore, the configuration of those disulfide bonds is depicted in Fig. 33B and C on the basis of the homologous domain of crossveinless 2. The three reduced cysteine residues, which are contained in the CGXC sequences, are depicted in Fig. 33D.

In summary, the detailed analysis of disulfide bond configuration within the VWF monomer allowed identification of functionally significant disulfide bonds. Reduced cysteine residue derived from a disulfide bond with an allosteric configuration indicates functional role. However, the crystal structures of VWF monomer are available for the A-domains only and the residual, rich in cysteine fragments, analyzed by sequence homology show only partial agreement with chemically confirmed disulfide bonds.

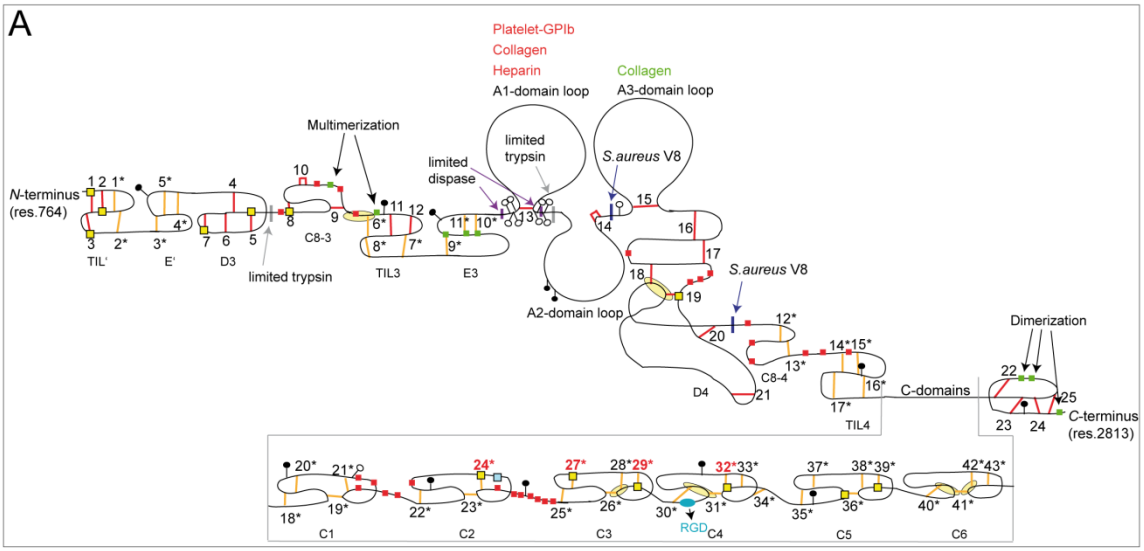

disulfide bond	$\chi_1,\chi_2,\chi_3,\chi_2',\chi_1'$	Cα-Cα (Å)	conformation
1-4	+,+,+,+,-	6.05	+/-RHSpiral
2-8	+,+,+,-,-	4.88	-/+RHHook
3-5	-,-,+,-,-	3.97	-RHStaple
6-9	-,-,-,-,-	5.39	-LHSpiral
7-10	-,+,-,-,-	6.03	-LHHook

Fig. 33. Location of identified unpaired cysteine residues in VWF. (A) VWF disulfide pairing as in Fig. 2; additionally sites of limited trypsin, dispase-I and *S.aureus* V8 protease digestion are depicted. Identified free cysteine residues are shown as yellow boxes on the protein chain. One of the two possible cysteine residues, highlighted with a yellow ellipse, is unpaired. Disulfide bond numbers coloured red (24*, 27*, 29* and 32*) represent bonds involving unpaired cysteine residues whose abundance in the sample decreased after collagen type III-binding. One cysteine residue, only found after SDS solubilisation of the VWF sample, and not in the VWF derivatized in buffer, is shown as blue box on the protein chain. (B) Conserved cysteine pairing in the C domain of crossveinless 2. Conserved cysteine residues are numbered from 1 to 10, disulfide bonds are shown as yellow lines. The 3D structure of crossveinless 2 C-domain homologous to VWF C-domains was depicted using RasWin software, cysteine residues are shown in yellow, and sulphur atoms in red. The two strands of antiparallel β-sheet are connected with the 3-5 allosteric disulfide bond. The disulfide bonds coloured red in A are assigned to the defined by homology structures. (C) Conformation of disulfide bonds in the C domain of crossveinless 2; Torsional angles, as well as Cα distances were measured for each bond using RasWin software. Each of the five torsional angles is positive or negative and based on this, conformation according to (Schmidt *et al.*, 2006) is assigned. (D) Sequences, encompassing the CGXC consensus sequence, in which free cysteine residues were identified (coloured red) are depicted; the position in the sequence is indicated by the possible disulfide bond connection of each cysteine.

5 Discussion

VWF mediates platelet adhesion to injured blood vessels under high physiological shear stress conditions. It fulfils a unique role in primary haemostasis since only the interaction between VWF and platelet-GPIb receptor is able to assure contact between injured endothelium and platelets under rapid blood flow in arterial circulation. Platelet clot formation at the site of vessel injury is regulated amongst other mechanisms by redox reactions. Plasmatic VWF exposes a high number of free thiol groups on its surface, which specifies VWF as a possible substrate for plasma oxidoreductases and suggests its possible involvement in further redox reactions at the site of clot formation. The significance of free thiol groups on VWF with regard to platelet adhesion was previously investigated using a cone-and-plate viscometer as a shear stress simulating device by Choi *et al*. (2007). The platelet clotting could be significantly inhibited by the blockade of free thiol groups in this setup. Moreover, the very high physiological and pathological shear stress applied in this experiment provoked thiol-disulfide reorganisation in the VWF molecule. However, the significance of this process under close-to-physiological conditions and the impact of free thiol groups on the interaction with collagen have not been investigated so far. The present study aimed to explore the function of free thiol groups and their exact location on the surface of plasma VWF. Furthermore, the modulation of interactions with collagen and GPIb receptor by thiol group derivatization, as well as the involvement of thiol-disulfide reorganisation in conformational changes in VWF induced by collagen binding were investigated. Since VWF conformation and function are regulated by both, binding to exposed ECM and by hydrodynamic shear stress, functional experiments were performed using its natural ligand, collagen type III, and were conducted under high physiological shear stress conditions.

The application of a flow chamber model which mimics the *in vivo* situation in human arterial circulation, allowed to measure the modulation of platelet adhesion to collagen type III provoked by free thiol group blocking in VWF. Furthermore, SPR-based analysis of both, collagen type III and platelet-GPIb receptor binding revealed the substantial involvement of free thiol groups in both functional interactions. Detailed analysis of both, NEM and MPB derivatization products was performed. Finally, the influence of the derivatization specifically on the VWF A1-domain structure and function was analyzed.

NEM-derivatization of VWF did not allow mass spectrometric-based identification of modified cysteine residues. The signal intensities of NEM-derivatized peptides were to low relative to the strong signals originating from the non-derivatized VWF peptides. Therefore the derivatized cysteine residue-containing peptides had to be enriched prior to MS analysis. This was accomplished by using a biotinylated maleimide reagent (MPB) for the analytical part of

the study. Using this setup it was possible to enrich 21 peptides modified with MPB by taking advantage of the high-affinity biotin-streptavidin interaction. The peptide-attached MPB was further confirmed by the presence of a specific fragmentation pattern of the reagent in the respective MALDI-MS/MS spectra. The MPB derivatization was performed under non-reducing conditions. Consequently, the peptides carrying the label have been primarily present in reduced state in plasma VWF. Conversely, all cysteine residues derivatized with iodoacetamide were originally involved in disulfide bonds and reduced during sample processing. Earlier studies also confirmed presence of partially reduced cysteine residues with different methods. Choi *et al*. (2007) identified seven peptides after binding of plasma VWF to thiol-active sepharose, on-bead trypsin digestion and subsequent MS analysis. Ganderton *et al*. (2011) identified 20 peptides containing reduced cysteine residue in the recombinant VWF C1-CK domains, by using differential labelling with carboxyamidomethyl and methyldisulfide for unpaired and disulfide bonded cysteine residues respectively. Despite the application of different methods, partially the same peptides, or in some cases the exactly defined cysteine residues shown to be accessible in reduced state in this and previous studies.

Half-cystines, which form disulfide bonds in mature proteins are highly evolutionarily conserved, in contrast to reactive free thiol groups of cysteine residues not involved in disulfide bond formation (Wong *et al.,* 2011). Unpaired cysteine residues identified in VWF in this and previous studies (Choi *et al.,* 2007; Ganderton *et al.,* 2011) have been either predicted to be involved in disulfide bonds, or the bond was chemically confirmed (Fig. 30A). In agreement with this, VWF peptides containing reduced, MPB-labelled cysteines required enrichment on streptavidin sepharose beads prior to mass spectrometry. Additionally, these cysteine residues were found to be involved in disulfide bonds to a higher extent than being present in the unpaired state. Taken together, those findings indicate that unpaired cysteine residues exposed on the VWF found in present and previous studies are partially involved in disulfide bonds, and may be reduced by plasma-oxidoreductases. The flexibility of their redox state suggests that they probably do not essentially contribute to stabilizing, structural functions but participate in redox reactions in plasma during primary haemostasis.

The *in silico*-analysis of the conformation of homologous domain yielded important information about the possible nature of disulfide bonds in the VWF C-domain. For example, one cysteine residue predicted to be involved in a potentially allosteric Cys3-Cys5 linkage by *in silico* analysis was identified in present study to be reduced to some extent (Cys^{2468}) (Fig. **33**B). Cys6-Cys9, Cys7-Cys10 and most probably Cys2-Cys8 bonds were found to be partly reduced as well. Each C-domain, contrary to the C-like domain, contains a CGXC motif. C1, C3 and C4 domains contain CGLC, CGRC and CGRC sequences respectively. In both CGRC sequences one cysteine residue was identified to be in a reduced state (Cys^{2494} and Cys^{2644}).

Cysteines forming the CGLC motif were not found in reduced state, as well as cysteines forming the second CGLC motif in the D3 domain. The fifth CGXC motif in the VWF mature chain resides in the D4 domain and displays CGIC sequence. Disulfide bond involving this sequence (Fig. 33A, bond no. 19) is also partly reduced as Cys^{1950} as well as most probably Cys^{2085} were found in reduced state. CGXC sequences, known as redox-active motifs, are often comprised in the thioredoxin fold and are present in members of the protein disulphide isomerase (PDI) family. PDI is a highly abundant ER luminal protein. Cysteines in the tetrapeptide CGXC motif which represent the active site of PDI, cycle between reduced and oxidized form and catalyze formation, isomerisation and reduction of disulfide bonds (Ferrari and Soling, 1999). An endogenous thiol isomerase activity has been also identified in several proteins, which do not possess any other sequence similarities with PDI, except for the CGXC motif. For example gonadotropic hormones leutropin and folliotropin (Boniface and Reichert, Jr., 1990), platelet integrin GPIIbIIIa (O'Neill *et al.,* 2000) or VWF propeptide (Mayadas and Wagner, 1992). Therefore, the reduced state of three cysteines in the CGXC consensus sequences in VWF mature subunit suggests intrinsic isomerase activity, and requires further investigation.

Seven unpaired cysteine residues were identified in the *N*-terminal region. The majority was previously predicted to be involved in disulfide bonds. The three unpaired cysteine residues identified in the TIL´ (TIL3 UniProt) domain, were all previously defined to be involved in disulfide bonds by chemical analysis. In the homologous AMCI-1 crystal structure, two of these disulfide bonds have -LHSpiral conformation and one exhibits a -/+LHHook conformation. Assuming that the conformation of disulfide bonds in the VWF TIL-domain structure is similar to AMCI-1, at least the two disulfide bonds exhibiting a spiral conformation should not appear in reduced state, as they were shown to represent mostly structural disulfides. The same applies for the Cys6-Cys9 bond in the C-domains of VWF also possessing –LHSpiral conformation, but was identified to be reduced in at least two C-domains. This discrepancy might be explained by a slightly different conformation of those disulfide bonds in VWF than in the homologous proteins. Despite VWF A-domains, the exact conformation of disulfide bonds in VWF is not possible to determine yet, because the crystal structures are not available and because the cysteines in the three dimensional structures predicted by I-TASSER are predominantly unpaired.

The VWF multimer and triplet structure was not affected by NEM derivatization. VWF did not aggregate nor was disruption of secondary structure elements detected, as shown by FTIR. The recognition of the derivatized sample by a polyclonal anti-VWF antibody was identical compared to the non-derivatized sample. Moreover, the enzymatic cleavage by *S. aureus* V8 protease under non-denaturating and non-reducing conditions showed the same

cleavage pattern for both, the derivatized and the non-derivatized sample. This is critical, because NEM attachment on the surface of the protein may alter the structural and functional properties of molecule. However, applied controls exclude, that observed effects are caused by unspecific secondary effects on the molecule conformation.

The analysis of the derivatized VWF molecule revealed, that the maleimide reagent attached to the *N*-terminal α-amino group as well. This modification could potentially influence VWF function and this aspect remains to be investigated. However, all common reagents used for e.g. fluorescent labelling, coupling to matrices or biotinylation, use amine coupling chemistry, which also binds to the α-amino group; do usually not provoke any substantial loss of protein activity. Examples of studies performed with directly labelled VWF support this assumption (Schneider *et al.,* 2007; Dayananda *et al.,* 2010).

Another aspect to consider is the presence of fibronectin in the VWF sample. In fact fibronectin is known to support VWF interaction with platelets. However, this occurs only under lower shear stress conditions than applied in the flow chamber experiments (Houdijk *et al.,* 1985). Therefore, effect of fibronectin on the flow chamber experiments can be excluded. However, the shear stress applied in the SPR studies, is comparably low and fibronectin might potentially bind to collagen type III, thereby influencing the obtained binding curves. Considering the significantly lower concentration of fibronectin compared to VWF in the evaluated samples, the minimal influence can be neglected. It remains unclear, whether the single unpaired cysteine detected in fibronectin subsequent to collagen binding may be involved in the process of primary haemostasis under lower shear stress conditions.

An important part of present study is represented by MALDI-MS measurements. The mass spectrometric data has been evaluated not only in a qualitative manner, but also by relative quantification of observed peaks. MALDI-MS analysis is considered to be a semi-quantitative method, as peak intensities cannot be directly compared as the signal intensity depends not only on the concentration but also on the sequence of a given peptide, formulation of the sample and several other factors. However, for a repeated measurement of a given sample, the relative signal intensities within the mass spectrum are constant (Duncan *et al.,* 2008), so that comparison between relative intensities of the same peptide peaks between samples processed identically is reasonable.

The blockade of free thiol groups markedly decreased the main physiological function of VWF, namely the mediation of platelet adhesion to collagen. This could be provoked by the inhibition of either the initial collagen type III binding and/or platelet adhesion to collagen-bound VWF. An interesting observation was that derivatized VWF induced the formation of platelet clots which were similarly large, but rarely distributed (Fig. 11). This fact, leads to the

assumption, that the NEM-derivatization impairs the first initial tethering of platelets mediated by the GPIb receptor and not the second firm adhesion mediated by the GPIIbIIIa receptor. In summary, functional studies suggested an impact of free thiol group blocking on either one or both important functions of VWF required for maintaining primary haemostasis. Consequently, the two interactions; collagen binding and GPIb receptor binding were investigated by additional assays.

The derivatization of VWF with 1 mM NEM decreased the platelet adhesion to a minimum of 13 %. Higher derivatization level did not provoke further decrease with respect to mediation of platelet adhesion. These findings were in contrast to results obtained by measuring collagen type III- and GPIb receptor binding by SPR, where only the higher level of derivatization provoked a significant decrease in activity with a dissociation affinity constant drop of factor 1.7 and 3.4 respectively (Fig. 13 and Fig. 15). These findings reflect the sensitivity of the flow chamber assay, which measures the combined effect of both functional interactions and therefore reflect the *in vivo* situation most closely. With the higher level of derivatization the effect of thiol group derivatization could be significantly demonstrated for the single interactions as well.

The blockade of unpaired cysteine residues in pdVWF impaired VWF collagen type III-binding under physiological shear stress conditions in flow chamber experiments. Furthermore, SPR studies revealed, that the inhibition was a result of a decreased association rate constant (k_a drop from 1.3×10^{-5} to 0.4×10^{-5}), and that it was provoked by the impairment of the A3 domain function. This could be concluded from the VWF A1-collagen type III binding inhibition by heparin, where the inhibitory effect of NEM-derivatization still persisted. Further studies with the TA1 fragment confirmed this result, as the derivatized TA1 fragment was equally active in collagen type III binding as the non-derivatized TA1 fragment. The VWF A3-domain alone, apart from the disulfide loop forming two cysteines, does not contain any further cysteine residues. The closest derivatized cysteines were found in the D4 domain. The VWF interaction with collagen has not been analyzed with regard to free thiol group content so far, nevertheless, it is difficult to distinguish between the actual VWF-collagen type III interaction and the possibly following self-association of VWF molecules. However, stable covalent thiol-disulfide exchange reactions were observed solely after application of very high shear stress (Choi *et al.,* 2007), or when involving ULVWF molecules (Li *et al.,* 2008). Collagen binding measurements performed in this study in the SPR system did not provide high shear stress conditions required for this interaction to occur, which enables to exclude the possibility of VWF self-association. VWF binding to collagen does not require any activation of the VWF molecule and occurs under both, static and high shear stress conditions. This indicates, that (i) the collagen binding site in the A3 domain is exposed in the tertiary and quaternary structure of the protein; and

moreover (ii) that this interaction has to be very fast and sufficiently strong to assure VWF adhesion under rapid blood flow conditions. Both assumptions are confirmed by the very low dissociation affinity constant of 3 nM. As the collagen binding domain is presented on the surface of VWF and the NEM-derivatization occurs on the surface of the coiled protein as shown by the MPB incorporation experiments, the decreased association rate after NEM derivatization may indicate steric hindrance of attached NEM groups to the neighbouring D4 domain. However such indirect inhibition of VWF A3-collagen interaction by the D4 domain has not been described so far.

A second or additional reasonable inhibition mechanism of VWF-collagen binding may be provoked by the derivatization of C-terminal domains. Although the A3- and C-domains do not seem to exist in spatial proximity in the VWF in solution, binding of a synthetic peptide to the VWF C-domain results in impaired VWF-collagen interaction (Szanto *et al.,* 2009). However the mechanism of this inhibition has not been understood so far. The conformation of VWF after binding to collagen changes and it is possible, that this conformational change involves some thiol-disulfide exchange reactions. The conformational change upon collagen binding may bring the C-domains and the functional A-domains in close proximity, which could explain the inhibitory effect on collagen binding after C-domain blocking observed by Szanto *et al.* (2009) In fact, the MALDI-MS-based comparison between free thiol group content in a VWF sample derivatized in solution *versus* a VWF sample derivatized after binding to collagen type III revealed some changes in the relative quantity of the unpaired cysteine residues. Moreover, these changes were observed in the C-domains (Fig. 33A, B; cysteine residues predicted to be involved in red marked bond), with the most prominent change in abundance of the reduced Cys^{2468}, which is predicted to be involved in the Cys3-Cys5 allosteric bond. It is most likely, that inhibition of the formation of disulfide bond by Cys^{2468} hinders rearrangement of VWF molecule. These findings indicate that disulfide bond reorganization occurs after collagen binding especially in the C-domain of VWF, and that this rearrangement may have an impact on the function of the A3 domain with respect to collagen binding.

Additionally to decreased activity in the flow chamber assay, the derivatized VWF sample exhibited diminished affinity to platelet GOF-GPIb receptor in SPR. This assay utilizes the platelet GPIb receptor, with two point mutations in the A1 domain. GOF-GPIb receptor binds VWF in its non-activated plasma form. Although VWF does not have to be activated by binding to ECM, shear stress or artificial modulators to bind GOF-GPIb receptor, this fragment is sensitive towards VWD type 2 mutants (Schneppenheim *et al.,* 2010; Flood *et al.,* 2011), indicating, that it binds only functional VWF molecules. Moreover, it has been shown, that the GOF-GPIb based assay is comparable to the VWF:RCo assay, where ristocetin ‘activates’ VWF for GPIb binding. The decreased affinity of NEM-VWF towards GOF-GPIb may therefore

indicate the inability of the A1 domain to form an active binding conformation. On the other hand, it cannot be excluded, that the inhibition was caused by steric hindrance resulting from the attachment of NEM molecules to the *N*-terminal part of the protein, being in close proximity to the A1 domain. However the modulation of GPIb interaction by NEM-derivatization is supported by the experiment with full length VWF precoated on the collagen surface, where the derivatized sample mediates platelet adhesion to a significantly lower extent than the underivatized sample.

Apart from the experiments using the entire VWF molecule, fragments derived from limited dispase and trypsin digestion yielded important information regarding VWF A1-domain structure and function. Firstly, the controversial thesis, that VWF A1-domain binds collagen type III, and moreover, can mediate platelet adhesion to collagen type III by itself (Bonnefoy *et al.,* 2006; Morales *et al.,* 2006) has been confirmed. Secondly the monomeric DA1 fragment has been shown to be less effective in collagen type III binding as well as in mediation of platelet adhesion to collagen type III under flow. These findings suggest that *N*-terminal multimer formation is important not only because it increases VWF size, but also because it enables the A1 domain to form intermolecular dimers which are more effective in collagen binding and mediation of platelet adhesion to collagen. Additionally, observations from a previous study, describing non-covalent association of *N*-terminal D3 domain and A1 domain, so called 'shielding effect', were confirmed as well (Ulrichts *et al.,* 2006). The TA1 fragment was associated with the *N*-terminus of the protein during the proteolytic digestion and subsequent purification procedure. In the *N*-terminal fragment five free cysteine residues were identified, and two in the actual TA1 fragment. Derivatization of those cysteines had, as discussed earlier, no effect on collagen type III binding, but increased the activity of TA1 fragment with regard to mediation of platelet adhesion to collagen type III. This effect was unexpected, since the derivatization of full length VWF in the same assay significantly decreased platelet adhesion to collagen type III. Moreover, in order to exclude the effect of NEM on decreased collagen affinity of VWF, full length samples were also coated on the collagen type III slide using saturating concentration assuring an equal level of bound VWF from both the NEM-derivatized and control sample. Nevertheless the effect was similar to the original flow chamber assay (Fig. 11 and Fig. 19), where samples were spiked to the perfusion mixture. These findings suggest two distinct regulation mechanisms for TA1 fragment and for the full length VWF. The adhesion of the TA1 fragment in complex with the *N*-terminus is probably regulated by the *N*-terminal shielding effect; i.e. the binding site in the A1 domain is cryptic, because it is non-covalently associated with the D3 domain. After collagen binding, the conformation of the protein *N*-terminus changes and the shielding effect of the D3 domain on the A1 domain is abrogated. The conformational change in the *N*-terminus upon collagen type III binding is also confirmed by previous study (Bendetowicz *et al.,* 1999); i.e. after binding of VWF to collagen,

affinity of FVIII to its binding site located in the D3 domain was lowered. The effect of increasing mediation of platelet adhesion by the TA1 fragment after free thiol group blocking can be explained by the observation of Ulrichts *et al.* (2006), that after binding of a specific antibody to the protein *N*-terminus, the shielding effect is abolished. It is possible, that NEM-derivatization of the cysteines in TIL and D3 domains causes a similar effect. These findings support the shielding theory. However the whole VWF mature subunit contains additional, different regulatory mechanisms, which involve thiol-disulfide reorganisation. These redox-based mechanisms most likely involve the VWF C-domains.

The VWF molecule released from endothelial cells is hyperactive and the activity, i.e. ability to bind platelets, is regulated in blood. One regulation mechanism is represented by the decrease of multimeric size through proteolytic cleavage of the ULVWF multimers by ADAMTS-13. There are also reports suggesting the regulation on the level of a single monomer. Each monomer of the hyperactive ULVWF multimer spontaneously binding platelets posses an active conformation after synthesis and prior to ADAMTS-13 cleavage, because it binds the platelet GPIb receptor spontaneously on the level of a single monomer (Arya *et al.,* 2002; Dong, 2005). The active conformation of ULVWF exposing A1 domain, may also favour the ADAMTS-13 binding and subsequent cleavage. In fact, the cleavage of ULVWF has been shown to occur already at very low shear stress (Dong *et al.,* 2002; Dong, 2005). Interestingly, ADAMTS-13 was shown to posses also reducing activity next to the proteolytic activity on disulfide bonds in the VWF C-domain (Yeh *et al.,* 2010). After cleavage by ADAMTS-13, VWF multimers are circulating in blood and do not bind platelets until they bind to exposed extracellular matrix. Different activity states of VWF also differ in the free cysteine group content and/or accessibility. The ULVWF newly released form endothelial cells was shown not to posses free sulfhydryl groups (Wagner and Marder, 1984) or to posses free cysteine residues, but buried within the quaternary protein structure (Li *et al.,* 2008), whereas plasma VWF exposes free cysteine residues on the surface. Plasmatic VWF, does not expose free cysteine residues on the surface any more upon activation with very high shear stress. The primarily free thiol groups build disulfide bonds subsequent to shear activation (Choi *et al.,* 2007). These findings suggest, that the conformational change in the VWF molecule, which allows the platelet-GPIb receptor binding to occur on the level of a single monomer may involve thiol-disulfide reorganization. The observation, that collagen type III binding induces disulfide bond forming by free cysteine residues present on the surface of plasmatic VWF and that the inhibition of this reorganisation by NEM impairs the ability to mediate platelet adhesion, support this thesis. Cysteines present in the C-domains of VWF play major regulatory role in this regard; originally involved in disulfide bonds, and cleaved by oxidoreductases after release into plasma. One disulfide bond, which links strands of the same antiparallel β-sheet (disulfide bond no. 27*) in VWF molecule seems to be most important in this regulation as it is partially

reduced in plasma VWF and forms a new disulfide bond after collagen type III-binding of VWF. Within the group of identified unpaired cysteine residues, which abundance decrease after collagen type III binding one cysteine is comprised within a CGRC sequence (disulfide bond no. 29*). This may hint to an involvement of CGXC sequences in the regulation of VWF activity. However, this aspect remains to be investigated as the oxidoreductase activity of those sequences has not been proven so far.

Experiments in the present study were conducted partly at high physiological shear stress, but partly at low shear stress in the SPR instrument or under static conditions. Blockade of free cysteine thiols in the VWF molecule caused decreased binding to collagen type III and decrease in binding to the GPIb receptor. Moreover, the collagen type III pre-coated VWF, derivatized with NEM exhibited reduced activity with respect to mediation of platelet adhesion. These findings allow formulating the thesis, that VWF activity is regulated by thiol-disulfide exchange and that this regulation is distinct from VWF self-association.

The function and position of cysteine residues, crucial for VWF activity regulation were identified in this study. Still the exact redox mechanism, i.e. the catalytic activity triggering thiol-disulfide rearrangements, as well as the involved proteins, and plasma oxidoreductases which reduce VWF, thereby modulating its activity remains to be investigated.

6 Summary

Willebrand factor (VWF) is a large, multimeric plasma glycoprotein, which is essential in the primary haemostasis process under high arterial shear stress conditions. VWF binds to exposed extracellular matrix (ECM) constituents at the site of vessel injury and recruits platelets from flowing blood. During synthesis, VWF undergoes a multimerization process via intermolecular disulfide bond bridging between cysteine-rich domains located at the VWF *N*- and *C*-terminus. The multimerization process results in VWF multimers ranging in size from a dimer to ultra large multimers (ULVWF), which are hyperactive in function. Therefore the activity of blood-stream released VWF is tightly regulated. The regulation mechanism is represented by the cleavage of the ULVWF by a specific protease called ADAMTS-13. Additionally, *in vitro* studies show susceptibility of VWF multimers to rapid reduction by low molecular weight thiols present in plasma as well as by plasma protein-thrombospondin 1. Primary haemostasis, especially platelet function, is partly redox-regulated by oxidoreductases present on the surface of the platelet membrane and released by endothelial cells. VWF circulates in blood as an inactive, coiled protein and becomes active in terms of platelets binding only after interaction with exposed ECM and subsequent shear force action. The transition from soluble to ECM-bound VWF and the high shear forces induce conformational changes in VWF, leading to exposure of the GPIb binding site on the VWF A1 domain. However, the mechanism and the exact molecular mode of this transition is unclear.

VWF is rich in cysteine, and its structure is highly determined by disulfide linkages. VWF is exposing reduced cysteine thiols on its surface. This indicates the presence of labile disulfides which in turn implies functional importance. The importance of those reduced cysteines has been largely attributed to the so-called self-association phenomenon, which was shown to occur at pathologically high shear stress conditions or to involve ULVWF molecules. However, the function of reduced cysteine thiols present on plasma VWF in regular primary haemostasis mediated by VWF under physiological shear stress conditions has not been investigated so far. The present study therefore focuses on the analysis of disulfide linkages in VWF, identification of unpaired cysteine residues, and finally the attempt to understand the origin of those unpaired cysteines and clarification of their function in plasma VWF, using several functional assays.

The results clearly demonstrate the high importance of unpaired cysteine residues on the surface of VWF. The blockade of those cysteines provoked substantial decrease in VWF function under physiological flow conditions in a flow chamber assay. The observed effect resulted from a combined action of several mechanisms, which inhibited both, VWF-collagen type III interaction and VWF-GPIb receptor interaction. Moreover, the identification of

unpaired cysteine residues enabled first insights into the possible inhibition mode. The analysis of the bond conformation in which the unpaired cysteines were originally involved enabled the identification of those cysteines which are potentially involved in redox regulation of VWF activity. Additionally, analysis and comparison of free cysteine residues on VWF either in solution or bound to collagen type III indicated thiol-disulfide reorganization upon binding to collagen. The impaired functionality of VWF upon blockade of free thiol groups, in assays conducted under low shear stress using surface plasmon resonance, allow distinguishing observed results from the previously described self-association. Furthermore, this distinction is supported by the perfusion experiments conducted using VWF pre-coated on collagen type III. Finally, additional experiments performed with functional VWF A1-domain fragments obtained by limited proteolysis yielded important information about A1 domain structure and function.

7 Zusammenfassung

Die primäre Hämostase wird unter sehr hohen arteriellen Scherraten durch den von Willebrand Faktor (VWF) vermittelt. VWF ist ein großes, multimeres Plasmaprotein, welches nach der Verletzung des Endothels an exponierte Komponenten der extrazellulären Matrix (ECM) bindet und zirkulierende Thrombozyten einfängt. Die Synthese des VWFs beinhaltet einen Multimerisierungsprozess, welcher *N*- und *C*- Termini der VWF Monomere mittels Disulfidbrücken verbindet. Der neu synthetisierte VWF ist reich an ultra-hochmolekularen Multimeren (ULVWF), die spontan mit Thrombozyten interagieren. Deswegen wird die Aktivität des frisch freigesetzten VWF streng reguliert, indem es durch eine spezifische Protease, ADAMTS-13, gespalten wird. *In vitro* Studien zeigen, dass VWF Multimere bereits durch geringe Mengen niedermolekularer Thiole, als auch durch das Plasmaprotein, Thrombospondin 1, reduziert werden können. Die primäre Hämostase, insbesondere die Funktion der Thrombozyten, wird ebenfalls zum Teil redox-reguliert. Zu den redox-Regulatoren der primären Hämostase tragen Oxidoreduktasen, die auf der Außenmembran der Thrombozyten lokalisiert sind oder durch Endothelzellen freigesetzt werden, bei. Infolge der regulatorischen Prozesse bindet der zirkulierende VWF nicht spontan an Thrombozyten und wird erst durch die Adhäsion an die ECM und Einwirkung von Scherstress aktiviert. Der Aktivierungsprozess beinhaltet eine Konformationsänderung des VWFs, wodurch die GPIb Bindungstelle exponiert und die Bindung an Thrombozyten ermöglicht wird. Der genaue Mechanismus der Umfaltung ist jedoch bis jetzt noch nicht aufgeklärt.

Der VWF ist reich an Cystein und seine Struktur wird stark von der Anordnung der Disulfidbrücken bestimmt. Der VWF exponiert auf der Oberfläche freie Sulfhydrylgruppen, was auf die Existenz von labilen Disulfidbrücken, mit funktioneller Rolle hindeutet. Die Funktion der freien Sulfhydrylgruppen wird weitgehend dem Phänomen der sogenannten VWF-Selbst-Assoziation zugeschrieben, welches allerdings bisher ausschließlich unter pathologischem Scherstress oder unter Beteiligung des ULVWFs gezeigt werden konnte. Die Funktion der freien Sulfhydrylgruppen des plasmatischen VWFs im Prozess der Primären Hämostase unter physiologischem Scherstress wurde noch nicht untersucht. Ziel dieser Arbeit war daher die Identifizierung der freien Sulfhydrylgruppen und die Ermittlung deren Funktion mit Hilfe mehrerer funktioneller Untersuchungen, sowie durch die Analyse der Konfiguration der Disulfidbrücken im funktionellen Zusammenhang.

Die Ergebnisse deuten darauf hin, dass die freien Sulfhydrylgruppen eine wichtige Funktion an der Oberfläche des VWFs erfüllen. Die Blockierung dieser Gruppen verursachte eine signifikante Beeinträchtigung der VWF-Funktion unter physiologischen Strömungsbedingungen in einem *in vitro* Flusskammersystem. Dieser Effekt konnte einer

Kombination mehrerer Inhibitionsmechanismen, die die VWF-Kollagen III und VWF-Thrombozyten GPIb Rezeptor Bindung hemmten, zugeschrieben werden. Darüber hinaus ermöglichte die Identifizierung der freien Sulfhydrylgruppen teilweise die Erkennung des zu Grunde liegenden Inhibierungsmechanismus. Die Analyse der Disulfidbrückenkonfiguration der labilen Disulfidbrücken, deren Reduktion die identifizierten freien Sulfhydrylgruppen generierte, ermöglichte die Identifizierung der funktionell wichtigen Cysteine, die potentiell an der Regulation der VWF-Aktivität beteiligt sind. Darüber hinaus, deuten die Analyse und der Vergleich der freien Sulfhyrdylgruppen von VWF in Lösung und Kollagen III-gebundenem VWF, auf Thiol-Disulfid-Reorganisation nach der Bindung des VWFs an Kollagen III hin. Die beeinträchtigte Vermittlung der Thrombozytenadhäsion durch VWF mit blockierten Sulfhydrylgruppen, in den Experimenten, wo VWF auf Kollagen III vor-inkubiert wurde, als auch Bindungsexperimente, die unter niedrigen Scherstress-Bedingungen durchgeführt wurden unterscheiden die beobachteten Effekte von VWF-Selbst-Assoziation. Die zusätzlichen Experimente mit den VWF A1 Domäne Fragmenten, lieferten wichtige Informationen zur Aufklärung der Struktur und Funktion der A1 Domäne.

Reference List

Andrews, R. K., Booth, W. J., Gorman, J. J., Castaldi, P. A., Berndt, M. C. (1989a) Purification of botrocetin from Bothrops jararaca venom. Analysis of the botrocetin-mediated interaction between von Willebrand factor and the human platelet membrane glycoprotein Ib-IX complex. Biochemistry 28:8317-8326.

Andrews, R. K., Gorman, J. J., Booth, W. J., Corino, G. L., Castaldi, P. A., Berndt, M. C. (1989b) Cross-linking of a monomeric 39/34-kDa dispase fragment of von Willebrand factor (Leu-480/Val-481-Gly-718) to the N-terminal region of the alpha-chain of membrane glycoprotein Ib on intact platelets with bis(sulfosuccinimidyl) suberate. Biochemistry 28:8326-8336.

Arya, M., Anvari, B., Romo, G. M., Cruz, M. A., Dong, J. F., McIntire, L. V., Moake, J. L., Lopez, J. A. (2002) Ultralarge multimers of von Willebrand factor form spontaneous high-strength bonds with the platelet glycoprotein Ib-IX complex: studies using optical tweezers. Blood 99:3971-3977.

Azimi, I., Wong, J. W., Hogg, P. J. (2011) Control of mature protein function by allosteric disulfide bonds. Antioxid.Redox.Signal. 14:113-126.

Azuma, H., Dent, J. A., Sugimoto, M., Ruggeri, Z. M., Ware, J. (1991) Independent assembly and secretion of a dimeric adhesive domain of von Willebrand factor containing the glycoprotein Ib-binding site. J Biol.Chem. 266:12342-12347.

Azuma, H., Hayashi, T., Dent, J. A., Ruggeri, Z. M., Ware, J. (1993) Disulfide bond requirements for assembly of the platelet glycoprotein Ib-binding domain of von Willebrand factor. J Biol.Chem. 268:2821-2827.

Barg, A., Ossig, R., Goerge, T., Schneider, M. F., Schillers, H., Oberleithner, H., Schneider, S. W. (2007) Soluble plasma-derived von Willebrand factor assembles to a haemostatically active filamentous network. Thromb.Haemost. 97:514-526.

Baronciani, L., Federici, A. B., Beretta, M., Cozzi, G., Canciani, M. T., Mannucci, P. M. (2005) Expression studies on a novel type 2B variant of the von Willebrand factor gene (R1308L) characterized by defective collagen binding. J.Thromb.Haemost. 3:2689-2694.

Bendetowicz, A. V., Wise, R. J., Gilbert, G. E. (1999) Collagen-bound von Willebrand factor has reduced affinity for factor VIII. J Biol.Chem. 274:12300-12307.

Bienkowska, J., Cruz, M., Atiemo, A., Handin, R., Liddington, R. (1997) The von willebrand factor A3 domain does not contain a metal ion-dependent adhesion site motif. J.Biol.Chem. 272:25162-25167.

Bockenstedt, P., Greenberg, J. M., Handin, R. I. (1986) Structural basis of von Willebrand factor binding to platelet glycoprotein Ib and collagen. Effects of disulfide reduction and limited proteolysis of polymeric von Willebrand factor. J.Clin.Invest 77:743-749.

Boniface, J. J., Reichert, L. E., Jr. (1990) Evidence for a novel thioredoxin-like catalytic property of gonadotropic hormones. Science 247:61-64.

Bonnefoy, A., Romijn, R. A., Vandervoort, P. A., VAN, R., I, Vermylen, J., Hoylaerts, M. F. (2006) von Willebrand factor A1 domain can adequately substitute for A3 domain in recruitment of flowing platelets to collagen. J.Thromb.Haemost. 4:2151-2161.

Budde, U., Pieconka, A., Will, K., Schneppenheim, R. (2006) Laboratory testing for von Willebrand disease: contribution of multimer analysis to diagnosis and classification. Semin.Thromb.Hemost. 32:514-521.

Burgess, J. K., Hotchkiss, K. A., Suter, C., Dudman, N. P., Szollosi, J., Chesterman, C. N., Chong, B. H., Hogg, P. J. (2000) Physical proximity and functional association of glycoprotein 1balpha and protein-disulfide isomerase on the platelet plasma membrane. J.Biol.Chem. 275:9758-9766.

Chen, K., Detwiler, T. C., Essex, D. W. (1995) Characterization of protein disulphide isomerase released from activated platelets. Br.J Haematol. 90:425-431.

Choi, H., Aboulfatova, K., Pownall, H. J., Cook, R., Dong, J. F. (2007) Shear-induced disulfide bond formation regulates adhesion activity of von Willebrand factor. J.Biol.Chem. 282:35604-35611.

Cierpicki, T., Bania, J., Otlewski, J. (2000) NMR solution structure of Apis mellifera chymotrypsin/cathepsin G inhibitor-1 (AMCI-1): structural similarity with Ascaris protease inhibitors. Protein Sci. 9:976-984.

Colombatti, A., Bonaldo, P., Doliana, R. (1993) Type A modules: interacting domains found in several non-fibrillar collagens and in other extracellular matrix proteins. Matrix 13:297-306.

Cruz, M. A., Handin, R. I., Wise, R. J. (1993) The interaction of the von Willebrand factor-A1 domain with platelet glycoprotein Ib/IX. The role of glycosylation and disulfide bonding in a monomeric recombinant A1 domain protein. J.Biol.Chem. 268:21238-21245.

Daopin, S., Piez, K. A., Ogawa, Y., Davies, D. R. (1992) Crystal structure of transforming growth factor-beta 2: an unusual fold for the superfamily. Science 257:369-373.

Dayananda, K. M., Singh, I., Mondal, N., Neelamegham, S. (2010) von Willebrand factor self-association on platelet GpIbalpha under hydrodynamic shear: effect on shear-induced platelet activation. Blood 116:3990-3998.

de Mol, N. J., Fisher, M. J. Surface Plasmon Resonance. Methods and Protocols. Springer-Verlag GmbH, Heidelberg, (2010), pp. 91-100.

Dong, J. F. (2005) Cleavage of ultra-large von Willebrand factor by ADAMTS-13 under flow conditions. J.Thromb.Haemost. 3:1710-1716.

Dong, J. F., Moake, J. L., Nolasco, L., Bernardo, A., Arceneaux, W., Shrimpton, C. N., Schade, A. J., McIntire, L. V., Fujikawa, K., Lopez, J. A. (2002) ADAMTS-13 rapidly cleaves newly secreted ultralarge von Willebrand factor multimers on the endothelial surface under flowing conditions. Blood 100:4033-4039.

Dong, Z., Thoma, R. S., Crimmins, D. L., McCourt, D. W., Tuley, E. A., Sadler, J. E. (1994) Disulfide bonds required to assemble functional von Willebrand factor multimers. J Biol.Chem. 269:6753-6758.

Dorum, S., Arntzen, M. O., Qiao, S. W., Holm, A., Koehler, C. J., Thiede, B., Sollid, L. M., Fleckenstein, B. (2010) The preferred substrates for transglutaminase 2 in a complex wheat gluten digest are Peptide fragments harboring celiac disease T-cell epitopes. PLoS.One. 5:e14056.

Duncan, M. W., Roder, H., Hunsucker, S. W. (2008) Quantitative matrix-assisted laser desorption/ionization mass spectrometry. Brief.Funct.Genomic.Proteomic. 7:355-370.

Emsley, J., Cruz, M., Handin, R., Liddington, R. (1998) Crystal structure of the von Willebrand Factor A1 domain and implications for the binding of platelet glycoprotein Ib. J Biol.Chem. 273:10396-10401.

Essex, D. W. (2009) Redox control of platelet function. Antioxid.Redox.Signal. 11:1191-1225.

Essex, D. W., Chen, K., Swiatkowska, M. (1995) Localization of protein disulfide isomerase to the external surface of the platelet plasma membrane. Blood 86:2168-2173.

Ferrari, D. M., Soling, H. D. (1999) The protein disulphide-isomerase family: unravelling a string of folds. Biochem.J. 339 (Pt 1):1-10.

Fischer, B. E., Thomas, K. B., Schlokat, U., Dorner, F. (1998) Triplet structure of human von Willebrand factor. Biochem.J. 331 (Pt 2):483-488.

Flood, V. H., Gill, J. C., Morateck, P. A., Christopherson, P. A., Friedman, K. D., Haberichter, S. L., Hoffmann, R. G., Montgomery, R. R. (2011) Gain-of-function GPIb ELISA assay for VWF activity in the Zimmerman Program for the Molecular and Clinical Biology of VWD. Blood 117:e67-e74.

Foster, P. A., Fulcher, C. A., Marti, T., Titani, K., Zimmerman, T. S. (1987) A major factor VIII binding domain resides within the amino-terminal 272 amino acid residues of von Willebrand factor. J.Biol.Chem. 262:8443-8446.

Fowler, W. E., Fretto, L. J., Hamilton, K. K., Erickson, H. P., McKee, P. A. (1985) Substructure of human von Willebrand factor. J.Clin.Invest 76:1491-1500.

Fretto, L. J., Fowler, W. E., McCaslin, D. R., Erickson, H. P., McKee, P. A. (1986) Substructure of human von Willebrand factor. Proteolysis by V8 and characterization of two functional domains. J.Biol.Chem. 261:15679-15689.

Fuchs, B., Budde, U., Schulz, A., Kessler, C. M., Fisseau, C., Kannicht, C. (2010) Flow-based measurements of von Willebrand factor (VWF) function: binding to collagen and platelet adhesion under physiological shear rate. Thromb Res. 125:239-245.

Fujimura, Y., Usami, Y., Titani, K., Niinomi, K., Nishio, K., Takase, T., Yoshioka, A., Fukui, H. (1991) Studies on anti-von Willebrand factor (vWF) monoclonal antibody NMC-4, which inhibits both ristocetin- and botrocetin-induced vWF binding to platelet glycoprotein Ib. Blood 77:113-120.

Furlan, M., Robles, R., Affolter, D., Meyer, D., Baillod, P., Lammle, B. (1993) Triplet structure of von Willebrand factor reflects proteolytic degradation of high molecular weight multimers. Proc.Natl.Acad.Sci.U.S.A 90:7503-7507.

Ganderton, T., Wong, J. W., Schroeder, C., Hogg, P. J. (2011) Lateral self-association of VWF involves the Cys2431-Cys2453 disulfide/dithiol in the C2 domain. Blood 118:5312-5318.

Girma, J. P., Chopek, M. W., Titani, K., Davie, E. W. (1986) Limited proteolysis of human von Willebrand factor by Staphylococcus aureus V-8 protease: isolation and partial characterization of a platelet-binding domain. Biochemistry 25:3156-3163.

Hill, B. G., Reily, C., Oh, J. Y., Johnson, M. S., Landar, A. (2009) Methods for the determination and quantification of the reactive thiol proteome. Free Radic.Biol.Med. 47:675-683.

Houdijk, W. P., Sakariassen, K. S., Nievelstein, P. F., Sixma, J. J. (1985) Role of factor VIII-von Willebrand factor and fibronectin in the interaction of platelets in flowing blood with monomeric and fibrillar human collagen types I and III. J.Clin.Invest 75:531-540.

Huizinga, E. G., van der Plas, R. M., Kroon, J., Sixma, J. J., Gros, P. (1997) Crystal structure of the A3 domain of human von Willebrand factor: implications for collagen binding. Structure. 5:1147-1156.

Hulstein, J. J., de Groot, P. G., Silence, K., Veyradier, A., Fijnheer, R., Lenting, P. J. (2005) A novel nanobody that detects the gain-of-function phenotype of von Willebrand factor in ADAMTS13 deficiency and von Willebrand disease type 2B. Blood 106:3035-3042.

Jasuja, R., Furie, B., Furie, B. C. (2010) Endothelium-derived but not platelet-derived protein disulfide isomerase is required for thrombus formation in vivo. Blood 116:4665-4674.

Kang, I., Raghavachari, M., Hofmann, C. M., Marchant, R. E. (2007) Surface-dependent expression in the platelet GPIb binding domain within human von Willebrand factor studied by atomic force microscopy. Thromb.Res. 119:731-740.

Katsumi, A., Tuley, E. A., Bodo, I., Sadler, J. E. (2000) Localization of disulfide bonds in the cystine knot domain of human von Willebrand factor. J.Biol.Chem. 275:25585-25594.

Kessler, C. M. (2007) Diagnosis and treatment of von Willebrand disease: new perspectives and nuances. Haemophilia. 13 Suppl 5:3-14.

Koedam, J. A., Hamer, R. J., Beeser-Visser, N. H., Bouma, B. N., Sixma, J. J. (1990) The effect of von Willebrand factor on activation of factor VIII by factor Xa. Eur.J Biochem. 189:229-234.

Koedam, J. A., Meijers, J. C., Sixma, J. J., Bouma, B. N. (1988) Inactivation of human factor VIII by activated protein C. Cofactor activity of protein S and protective effect of von Willebrand factor. J Clin.Invest 82:1236-1243.

Kong, J., Yu, S. (2007) Fourier transform infrared spectroscopic analysis of protein secondary structures. Acta Biochim.Biophys.Sin.(Shanghai) 39:549-559.

Koppelman, S. J., Koedam, J. A., van, W. M., Stern, D. M., Nawroth, P. P., Sixma, J. J., Bouma, B. N. (1994) von Willebrand factor as a regulator of intrinsic factor X activation. J Lab Clin.Med. 123:585-593.

Lacey, D. J., Wellner, N., Beaudoin, F., Napier, J. A., Shewry, P. R. (1998) Secondary structure of oleosins in oil bodies isolated from seeds of safflower (Carthamus tinctorius L.) and sunflower (Helianthus annuus L.). Biochem.J 334 (Pt 2):469-477.

Lankhof, H., van, H. M., Schiphorst, M. E., Bracke, M., Wu, Y. P., Ijsseldijk, M. J., Vink, T., de Groot, P. G., Sixma, J. J. (1996) A3 domain is essential for interaction of von Willebrand factor with collagen type III. Thromb.Haemost. 75:950-958.

Lankhof, H., Wu, Y. P., Vink, T., Schiphorst, M. E., Zerwes, H. G., de Groot, P. G., Sixma, J. J. (1995) Role of the glycoprotein Ib-binding A1 repeat and the RGD sequence in platelet adhesion to human recombinant von Willebrand factor. Blood 86:1035-1042.

Lemmon, C. A., Ohashi, T., Erickson, H. P. (2011) Probing the folded state of fibronectin type III domains in stretched fibrils by measuring buried cysteine accessibility. J Biol.Chem. 286:26375-26382.

Li, F., Moake, J. L., McIntire, L. V. (2002) Characterization of von Willebrand factor interaction with collagens in real time using surface plasmon resonance. Ann.Biomed.Eng 30:1107-1116.

Li, Y., Choi, H., Zhou, Z., Nolasco, L., Pownall, H. J., Voorberg, J., Moake, J. L., Dong, J. F. (2008) Covalent regulation of ULVWF string formation and elongation on endothelial cells under flow conditions. J.Thromb.Haemost. 6:1135-1143.

Luken, B. M., Winn, L. Y., Emsley, J., Lane, D. A., Crawley, J. T. (2010) The importance of vicinal cysteines, C1669 and C1670, for von Willebrand factor A2 domain function. Blood 115:4910-4913.

Majima, E., Goto, S., Hori, H., Shinohara, Y., Hong, Y. M., Terada, H. (1995) Stabilities of the fluorescent SH-reagent eosin-5-maleimide and its adducts with sulfhydryl compounds. Biochim.Biophys.Acta 1243:336-342.

Marti, T., Rosselet, S. J., Titani, K., Walsh, K. A. (1987) Identification of disulfide-bridged substructures within human von Willebrand factor. Biochemistry 26:8099-8109.

Mayadas, T. N., Wagner, D. D. (1989) In vitro multimerization of von Willebrand factor is triggered by low pH. Importance of the propolypeptide and free sulfhydryls. J.Biol.Chem. 264:13497-13503.

Mayadas, T. N., Wagner, D. D. (1992) Vicinal cysteines in the prosequence play a role in von Willebrand factor multimer assembly. Proc.Natl.Acad.Sci.U.S.A 89:3531-3535.

Metcalf, D. J., Nightingale, T. D., Zenner, H. L., Lui-Roberts, W. W., Cutler, D. F. (2008) Formation and function of Weibel-Palade bodies. J Cell Sci. 121:19-27.

Miseta, A., Csutora, P. (2000) Relationship between the occurrence of cysteine in proteins and the complexity of organisms. Mol.Biol.Evol. 17:1232-1239.

Morales, L. D., Martin, C., Cruz, M. A. (2006) The interaction of von Willebrand factor-A1 domain with collagen: mutation G1324S (type 2M von Willebrand disease) impairs the conformational change in A1 domain induced by collagen. J.Thromb.Haemost. 4:417-425.

O'Neill, S., Robinson, A., Deering, A., Ryan, M., Fitzgerald, D. J., Moran, N. (2000) The platelet integrin alpha IIbbeta 3 has an endogenous thiol isomerase activity. J.Biol.Chem. 275:36984-36990.

Obert, B., Houllier, A., Meyer, D., Girma, J. P. (1999) Conformational changes in the A3 domain of von Willebrand factor modulate the interaction of the A1 domain with platelet glycoprotein Ib. Blood 93:1959-1968.

Pareti, F. I., Niiya, K., McPherson, J. M., Ruggeri, Z. M. (1987) Isolation and characterization of two domains of human von Willebrand factor that interact with fibrillar collagen types I and III. J.Biol.Chem. 262:13835-13841.

Pimanda, J. E., Ganderton, T., Maekawa, A., Yap, C. L., Lawler, J., Kershaw, G., Chesterman, C. N., Hogg, P. J. (2004) Role of thrombospondin-1 in control of von Willebrand factor multimer size in mice. J.Biol.Chem. 279:21439-21448.

Purvis, A. R., GROSS, J., Dang, L. T., Huang, R. H., Kapadia, M., Townsend, R. R., Sadler, J. E. (2007) Two Cys residues essential for von Willebrand factor multimer assembly in the Golgi. Proc.Natl.Acad.Sci.U.S.A 104:15647-15652.

Rogers, L. K., Leinweber, B. L., Smith, C. V. (2006) Detection of reversible protein thiol modifications in tissues. Anal.Biochem. 358:171-184.

Romijn, R. A., Westein, E., Bouma, B., Schiphorst, M. E., Sixma, J. J., Lenting, P. J., Huizinga, E. G. (2003) Mapping the collagen-binding site in the von Willebrand factor-A3 domain. J.Biol.Chem. 278:15035-15039.

Ruggeri, Z. M. (2002) Platelets in atherothrombosis. Nat.Med. 8:1227-1234.

Ruggeri, Z. M., Mendolicchio, G. L. (2007) Adhesion mechanisms in platelet function. Circ.Res. 100:1673-1685.

Ruggeri, Z. M., Zimmerman, T. S. (1980) Variant von Willebrand's disease: characterization of two subtypes by analysis of multimeric composition of factor VIII/von Willebrand factor in plasma and platelets. J Clin.Invest 65:1318-1325.

Sadler, J. E. (1998) Biochemistry and genetics of von Willebrand factor. Annu.Rev.Biochem. 67:395-424.

Savage, B., Sixma, J. J., Ruggeri, Z. M. (2002) Functional self-association of von Willebrand factor during platelet adhesion under flow. Proc.Natl.Acad.Sci.U.S.A 99:425-430.

Schlunegger, M. P., Grutter, M. G. (1992) An unusual feature revealed by the crystal structure at 2.2 A resolution of human transforming growth factor-beta 2. Nature 358:430-434.

Schmidt, B., Ho, L., Hogg, P. J. (2006) Allosteric disulfide bonds. Biochemistry 45:7429-7433.

Schmugge, M., Rand, M. L., Freedman, J. (2003) Platelets and von Willebrand factor. Transfus Apher.Sci. 28:269-277.

Schneider, S. W., Nuschele, S., Wixforth, A., Gorzelanny, C., exander-Katz, A., Netz, R. R., Schneider, M. F. (2007) Shear-induced unfolding triggers adhesion of von Willebrand factor fibers. Proc.Natl.Acad.Sci.U.S.A 104:7899-7903.

Schneppenheim, R., Obser, T., Budde, U., Patzke, J. Development of a new functional assay for von Willebrand factor binding to platelet GpIba that does not require Ristocetin. GTH 2010, Nürnberg. HAEMD2.| 30[1], A28. 2010. Schattauer-Verlag.
Ref Type: Conference Proceeding

Schooten, C. J., Tjernberg, P., Westein, E., Terraube, V., Castaman, G., Mourik, J. A., Hollestelle, M. J., Vos, H. L., Bertina, R. M., Berg, H. M., Eikenboom, J. C., Lenting, P. J., Denis, C. V. (2005) Cysteine-mutations in von Willebrand factor associated with increased clearance. J Thromb.Haemost. 3:2228-2237.

Shankaran, H., Alexandridis, P., Neelamegham, S. (2003) Aspects of hydrodynamic shear regulating shear-induced platelet activation and self-association of von Willebrand factor in suspension. Blood 101:2637-2645.

Sixma, J. J., van Zanten, G. H., Saelman, E. U., Verkleij, M., Lankhof, H., Nieuwenhuis, H. K., de Groot, P. G. (1995) Platelet adhesion to collagen. Thromb.Haemost. 74:454-459.

Smith, M. L., Gourdon, D., Little, W. C., Kubow, K. E., Eguiluz, R. A., Luna-Morris, S., Vogel, V. (2007) Force-induced unfolding of fibronectin in the extracellular matrix of living cells. PLoS.Biol. 5:e268.

Strohalm, M., Kavan, D., Novak, P., Volny, M., Havlicek, V. (2010) mMass 3: a cross-platform software environment for precise analysis of mass spectrometric data. Anal.Chem. 82:4648-4651.

Stryer, L. Biochemie. Spektrum der Wissenschaft Verlagesgesellschaft mbH, Heidelberg, (1990), pp. 44-44.

Szanto, T., Vanhoorelbeke, K., Toth, G., Vandenbulcke, A., Toth, J., Noppe, W., Deckmyn, H., Harsfalvi, J. (2009) Identification of a VWF peptide antagonist that blocks platelet adhesion under high shear conditions by selectively inhibiting the VWF-collagen interaction. J.Thromb.Haemost. 7:1680-1687.

Thomas, G., Skrinska, V. A., Lucas, F. V. (1986) The influence of glutathione and other thiols on human platelet aggregation. Thromb.Res. 44:859-866.

Tsai, H. M. (1996) Physiologic cleavage of von Willebrand factor by a plasma protease is dependent on its conformation and requires calcium ion. Blood 87:4235-4244.

Ulrichts, H., Udvardy, M., Lenting, P. J., Pareyn, I., Vandeputte, N., Vanhoorelbeke, K., Deckmyn, H. (2006) Shielding of the A1 domain by the D'D3 domains of von Willebrand factor modulates its interaction with platelet glycoprotein Ib-IX-V. J.Biol.Chem. 281:4699-4707.

Ulrichts, H., Vanhoorelbeke, K., Girma, J. P., Lenting, P. J., Vauterin, S., Deckmyn, H. (2005) The von Willebrand factor self-association is modulated by a multiple domain interaction. J.Thromb.Haemost. 3:552-561.

Veyradier, A., Obert, B., Houllier, A., Meyer, D., Girma, J. P. (2001) Specific von Willebrand factor-cleaving protease in thrombotic microangiopathies: a study of 111 cases. Blood 98:1765-1772.

Vollmar, B., Slotta, J. E., Nickels, R. M., Wenzel, E., Menger, M. D. (2003) Comparative analysis of platelet isolation techniques for the in vivo study of the microcirculation. Microcirculation. 10:143-152.

Wagner, D. D., Marder, V. J. (1984) Biosynthesis of von Willebrand protein by human endothelial cells: processing steps and their intracellular localization. J.Cell Biol. 99:2123-2130.

Walkowiak, B., Kesy, A., Michalec, L. (1997) Microplate reader--a convenient tool in studies of blood coagulation. Thromb.Res. 87:95-103.

Wong, J. W., Ho, S. Y., Hogg, P. J. (2011) Disulfide bond acquisition through eukaryotic protein evolution. Mol.Biol.Evol. 28:327-334.

Xie, L., Chesterman, C. N., Hogg, P. J. (2001) Control of von Willebrand factor multimer size by thrombospondin-1. J.Exp.Med. 193:1341-1349.

Xie, L., Chesterman, C. N., Hogg, P. J. (2000) Reduction of von Willebrand factor by endothelial cells. Thromb.Haemost. 84:506-513.

Yan, B., Smith, J. W. (2000) A redox site involved in integrin activation. J Biol.Chem. 275:39964-39972.

Yeh, H. C., Zhou, Z., Choi, H., Tekeoglu, S., May, W., III, Wang, C., Turner, N., Scheiflinger, F., Moake, J. L., Dong, J. F. (2010) Disulfide bond reduction of von Willebrand factor by ADAMTS-13. J.Thromb.Haemost. 8:2778-2788.

Zhang, J. L., Qiu, L. Y., Kotzsch, A., Weidauer, S., Patterson, L., Hammerschmidt, M., Sebald, W., Mueller, T. D. (2008) Crystal structure analysis reveals how the Chordin family member crossveinless 2 blocks BMP-2 receptor binding. Dev.Cell 14:739-750.

Zhang, Q., Zhou, Y. F., Zhang, C. Z., Zhang, X., Lu, C., Springer, T. A. (2009) Structural specializations of A2, a force-sensing domain in the ultralarge vascular protein von Willebrand factor. Proc.Natl.Acad.Sci.U.S.A 106:9226-9231.

Zhou, Y. F., Eng, E. T., Zhu, J., Lu, C., Walz, T., Springer, T. A. (2012) Sequence and structure relationships within von Willebrand factor. Blood 120:449-458.

8 Theses

1. Plasma von Willebrand factor (VWF) contains a high number of unpaired cysteine residues. A total of nineteen free thiol groups in VWF mature subunit were identified on the surface of the protein. Seven were placed in the *N*-terminal TIL- and D3-domain, two in the D4-domain and ten in the *C*-terminal C-domains. SDS-unfolding gains access to one additional free thiol in one of the C-domains.

2. Binding of VWF to collagen type III results in decreased abundance of four unpaired cysteine residues in the C-domains, indicating thiol-disulfide reorganisation upon collagen binding.

3. *In silico* modelling of VWF domains as well as evaluation of the disulfide bond configuration in homologous domains allowed identification of one potentially allosteric disulfide bond. The presence of a reduced cysteine residue primarily involved in this allosteric bond confirms its functional importance. Additionally, three cysteine residues, comprised in potentially redox active tetrapeptide CGXC sequences were identified in reduced state.

4. The blockade of unpaired cysteine residues with N-ethylmaleimide (NEM) results in substantial loss of the physiological VWF activity. The ability to mediate platelet adhesion under high physiological shear stress conditions is decreased from 25 % platelet surface coverage for the control sample to 13 % platelet coverage. This effect is caused by both, inhibition of VWF-collagen type III binding and VWF-platelet-GPIb receptor binding.

5. The collagen type III-binding is significantly decreased after free thiol group blockade and results in an increase in the dissociation affinity constant from 3.8 nM to 5.2 nM. The inhibition is predominantly caused by decreased association rate constant (drop in k_a from 2.1×10^5 to 1.1×10^5 $M^{-1}s^{-1}$). The lower binding affinity is provoked by the inhibition of VWF A3-domain interaction with collagen.

6. The interaction with the platelet GPIb receptor is inhibited by free thiol group blockade, and results in an increase in dissociation affinity constant from 4.8 to 16.2 nM. The inhibition of GPIb binding by thiol group blocking is also confirmed by a decreased mediation of platelet adhesion by pre-coated VWF adhered to collagen type III. Here, the platelet surface coverage dropped from 68 % to 57 % upon NEM derivatization.

7. The dimeric form of the VWF A1-domain is more effective in collagen type III binding as well as in mediation of platelet adhesion than its monomeric form.

8. The A1 domain is non-covalently associated with the VWF *N*-terminus which confirms the functional shielding theory. Upon derivatization of cysteine residues in the isolated A1 domain complexed with the *N*-terminus, the ability of mediation of platelet adhesion by the A1 domain increases. This effect is probably provoked by the unshielding of the functional A1 domain by derivatized *N*-terminus. However, the same derivatizatized fragment, binds equally affine to the collagen type III as its underivatized counterpart.

Curriculum vitae

Date of birth:	28.11.1984
Place of birth:	Szprotawa, Poland
2009-2012	Dissertation, Prof. Dr. Rüdiger Horstkorte, at The Medical Faculty of Martin-Luther-University Halle-Wittenberg, Germany In cooperation with Dr. Christoph Kannicht, Octapharma R&D, Molecular Biochemistry Department, Berlin, Germany
05/2009	Master of Science Degree accomplished at University of Applied Sciences (Beuth Hochschule für Technik) in Berlin/Germany in cooperation with Octapharma R&D, Berlin. Title of Mater Thesis: “Flow-based investigation of mechanisms in primary haemostasis”
03/2009 – 10/2009	Participation in ExzellenzTandem Project at University of Applied Sciences (Beuth Hochschule für Technik) Berlin/Germany
03/2008 – 08/2008	Internship at Octapharma R&D in Berlin, accomplishment of the research project - “Investigation of the structure-function relationship of the von Willebrand factor (VWF)”
2007-2009	Biotechnology student at the University of Applied Sciences (Beuth Hochschule für Technik) Berlin/ Germany
06/2006	Bachelor of Science Degree. Title of Bachelor Thesis: “Human Genome Project”.
2003-2006	Biotechnology student at the University of Szczecin/Poland
05/2003	High School Graduation in Zielona Góra, Poland

Selbstständigkeitserklärung

Ich erkläre hiermit, dass ich die vorliegende Arbeit ohne unzulässige Hilfe Dritter und ohne Benutzung anderer als der angegebenen Hilfsmittel angefertigt habe. Die aus anderen Quellen direkt oder indirekt übernommenen Daten und Konzepte sind unter Angabe der Quelle gekennzeichnet.

Ich versichere, dass ich für die inhaltliche Erstellung der vorliegenden Arbeit nicht die entgeltliche Hilfe von Vermittlungs- und Beratungsdiensten (Promotionsberater oder anderer Personen) in Anspruch genommen habe. Niemand hat von mir unmittelbar oder mittelbar geldwerte Leistungen für die Arbeit erhalten, die in Zusammenhang mit dem Inhalt der vorliegenden Dissertation stehen.

Erklärung über frühere Promotionsversuche

Die Arbeit wurde weder im Inland noch im Ausland in gleicher oder ähnlicher Form einer anderen Prüfungsbehörde vorgelegt.

Berlin, den 04.10.2012

Barbara Solecka

B. Solecka

Acknowledgement

First of all I wish to express my sincere gratitude to Dr. Christoph Kannicht for the opportunity to accomplish this thesis at Octapharma R&D Berlin, as well as for his constant support, motivation, inspiring discussions and critical review of this manuscript.

I am deeply grateful to my supervisor Prof. Dr. Rüdiger Horstkorte, for his assistance and support in preparing this thesis as well as his disposition to review.

I express my gratitude to Dr. Christoph Weise from the department of Chemistry and Biochemistry, FU Berlin, for his assistance in MALDI-MS measurements as well as invaluable help in interpretation of the data.

I thank all the members of the Octapharma R&D Berlin for their support and a great working atmosphere. I am deeply grateful to Dr. Birte Fuchs for her support and critical review.

Finally, I would like to express my deepest gratitude for the support and encouragement that I received from my family and friends.